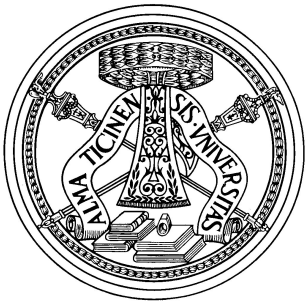

Universitá degli Studi di Pavia

Facoltá di Ingegneria

Dipartimento di Bioingegneria

Biomechianics of popliteal stenting

Biomeccanica dello stenting popliteo

Supervisor:
Dott. Michele Conti
Co-supervisor:
Prof. Ferdinando Auricchio

Author:
Francesco Flain
UIN **404779**

Academic year 2013/2014

Alla mia mamma

Ringraziamenti

Ringrazio anzitutto il Dottor Conti, mio relatore, senza il cui supporto, la guida sapiente e soprattutto la pazienza, non sarei riuscito a completare questa tesi.

Un ringraziamento particolare va poi ai miei “lettori”, Simone, Carlotta, Giovanni e Diego, che mi hanno aiutato con la stesura del lavoro in inglese, e che hanno speso il loro tempo per rileggere e correggere il mio elaborato.

Vorrei infine ringraziare le persone a me piú care, papá, nonne, zii, per essermi state sempre vicine in tutto il percorso di studio.

Infine la mia mamma, alla quale questo lavoro é dedicato.

Abstract

From the anatomical point of view, the popliteal artery is the vessel that connects the superficial femoral artery with the tibial arteries. This vessel, being located behind the knee, is particularly exposed to biomechanical stresses. In fact the popliteal artery is characterized by complex kinematics, composed of shortening, torsion and bending during knee flexion. Furthermore, as other peripheral arteries, this vessel is affected by cardiovascular diseases, such as stenoses and aneurysms. The gold standard treatment for these pathologies is surgery, with the application of a bypass, because alternative endovascular procedures, based on stent insertion, have limited effectiveness because of the cited biomechanical stresses. Particularly the durability of the stent still has not reached acceptable levels: after few years the stent usually breaks down due to excessive wearing.

Starting from these considerations, it is evident that a deeper understanding of popliteal biomechanics, that would allow to better analyze and quantify the stresses acting on the stent, is needed in order to design a new product able to maximize the long term efficacy of the therapy.

The present work of thesis has been conceived within this perspective. The whole project consists of three macro topics analyzed in detail through the different chapters. The first part introduces the clinical problem and the guidelines for angioplasty procedures and it is followed by a review of the major study works present in the literature about the topic.

The second part, instead, concerns the methods used for the measurement and elaboration of the data. The procedure for the isolation of a 3D object, which is the reconstruction of the popliteal artery based on CT images, is presented in this section. The data obtained in this way will then be used in order to build a more regular 3D model than the one produced by a standard CT-based 3D reconstruction. The other object that will be presented in this chapter is the stent chosen for the study: it consists in a modified Viabahn model of Gore. Finally the third part is devoted to the presentation of the results of the simulations carried out on the object introduced in the second part. Clarifying pictures are added at the end of each section that analyzes a specific problem.

Sommario

La poplitea é l'arteria della gamba che dal punto di vista anatomico, si colloca tra l'arteria femorale superficiale e le arterie tibiali. L'arteria, passante dietro il ginocchio, é particolarmente esposta a sollecitazioni biomeccaniche; la poplitea é infatti caratterizzata da una cinematica complessa, composta da accorciamento, torsione e piegamento durante la flessione della gamba. La poplitea, come altre arterie periferiche é soggetta a malattie cardiovascolari, quali stenosi e aneurismi. Il trattamento di routine per tali patologie rimane ancora la chirurgia con impianto di bypass, perché le tecniche endovascolari alternative, basate sull'impianto di stent, hanno ancora esiti limitati perché soffrono le sollecitazioni biomeccaniche. In particolare, la durabilitá dello stent non ha ancora raggiunto livelli accettabili; dopo pochi anni l'impianto spesso fallisce per rottura a fatica. Da queste considerazioni emerge la necessitá di una profonda comprensione della biomeccanica della poplitea, capace di analizzare e quantificare le sollecitazioni imposte all'impianto, con l'obiettivo finale di progettare uno stent in grado di massimizzare la longevitá della terapia. Il presente lavoro di tesi si colloca in questo contesto. L'elaborato si compone di tre macro argomenti distribuiti rispettivamente su piú capitoli. La prima parte ha carattere introduttivo; viene definito il problema clinico e lo stato dell'arte esistente per la procedura di angioplastica, e vengono presentati una serie di lavori a riguardo di questo argomento presenti in letteratura. La seconda parte della tesi invece riguarda il design degli oggetti studiati: verrá descritta la procedura tramite il quale viene isolato un oggetto 3D, che é la ricostruzione dell'arteria poplitea sotto studio, ricavata dalle TC inviateci dal partner medico. Spiegheremo poi un metodo per ricostruire l'oggetto in 3D e ottenere un profilo molto piú regolare di quello ricavabile dalle TC. L'altro oggetto che verrá presentato in questo capitolo é lo stent da noi scelto. Si tratta di una nostra rivisitazione del Viabahn della Gore. La terza parte infine é dedicata alla presentazione dei risultati, di alcune simulazioni da noi svolte, sugli oggetti che vengono presentati nella seconda parte. Al termine di ogni sezione descrittiva di un problema saranno presentate immagini chiarificatrici.

Contents

List of Figures

List of Tables

Chapter 1

Introduction and Aims

Vascular diseases are a group of pathologies that affect the heart and the blood vessels. In this work of thesis we focus our efforts in the treatment of those pathologies that affect the popliteal artery, that is the vessel that connects the femoral and tibial arteries. Regarding this anatomical area, two main pathologies are most commonly found: the stenosis and the aneurism. The term "stenosis" encompasses all those pathologies that result into an abnormal narrowing of the vessel. The aneurysm, instead, generated by a loss of elasticity of the vessel, is a localized blood-filled ballon-like bulge of the wall, that causes a change in the normal vessel shape and hemodynamics. This first chapter has the purpose of presenting to the reader the essential features of the anatomy of the popliteal artery and its correct position in the body; it is aimed also at introducing in a deeper way the two pathologies cited above and to describe the most common interventions that are made to solve these problems; the description will be correlated with some explicative images to make the description clearer. Finally, the chapter will end with the summary of the goals of this work of thesis that are going to be further analyzed in the following chapters. In the conclusive part we will also give a first explanation of the organization of all the paper.

1.1 Anatomy of the Popliteal and the Femoral Artery

The femoral artery is the terminal branch of the external iliac artery; it is the most important vessel, about the arterial circuit, of the inferior art. It begins behind the inguinal ligament, between the lacuna of the vessels and ends in the channel of the adductor muscles. After this area it continues as the popliteal artery and it goes down in the antero-medial region of the thigh. At the beginning the femoral artery occupies the lateral angle of the lacuna of the vessels, just behind the inguinal ligament and it is anterior to the insertion of the pectineal muscle. It then divides in two branches, the superior one - the femoral branch - and the inferior one, the genito-femoral branch. It then passes through the Scarpa's triangle in its first part and as it exits the triangle it becomes posterior to the sartorius muscle. The femoral vein is placed just behind the artery. As introduced above, below the articulation of the knee, there is the poplipeal artery. This artery goes from the adductor channel to the arch tendon of the soleus muscle. Past this point it branches into two vessels, called the tibial anterior and the tibial posterior arteries. We can identify several segments of the popliteal artery, as showed in Figure 1.1 and as reported by Scheinert (2013), that are defined as follows: P1 segment, from intercondylar fossa to proximal edge of patella; P2 segment, from the proximal part of the patella to the center of knee joint; P3 segment, from center of the knee joint to the origin of the anterior tibial artery. In this area the course of the vessel is quite straight and there are not many branches. However, the incidence of vascular pathologies is quite

relevant; this means that the mechanical factors are very important to be understood, because, although the high frequency of pathologies in this area, the treatment possibilities are numerous; in the next section some of them will be reported.

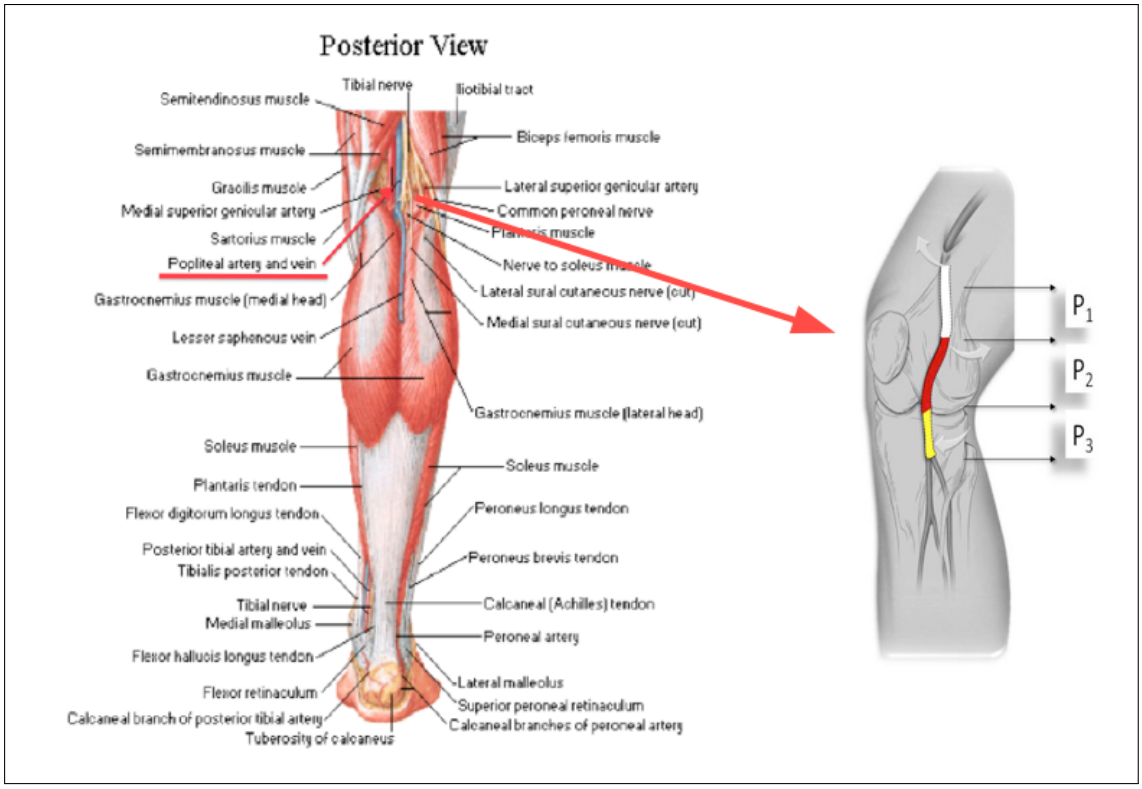

Figure 1.1: In the left part of the figure the musculoskeletal anatomy of the leg from the posterior view (Netter (2014)); in the right one a magnification of the popliteal artery that shows the three parts (P1, P2, P3) that compose it (courtesy of doctor G. Piffaretti).

1.2 Popliteal Diseases

The pathologies that directly affect the popliteal artery are the more diverse. However, in our work, we have decided to focus our attention on the ones that most frequently affect this anatomical area: the stenosis and the aneurysm (Underwood (2009)). The definition of these two pathologies has been given in the introduction, but it is interesting to examine in depth their description; a clarifying image is fundamental to figure out the problem we are facing. Below this section, and also in the next pages, two examples of the problems that we are talking about are reported: in the first one (Figure 1.2) is reported an example of stenosis. It is very easy to understand that this kind of situation could cause very dangerous problems to the entire leg if it is not treated in the best possible way. The main cause of stenosis is certainly atherosclerosis, that is a result of the accumulation of fat in the arterial vessel wall; its consequence is the impairment of the blood flow through the artery. However also other factors are often relevant for the development of this pathology. It is usually the best way to evaluate the degree of stenosis the utilization of imaging techniques, such as MRI or CT scan. The degree of stenosis is expressed as the percentage of reduction of the radius of the vessel compared to its normal values.

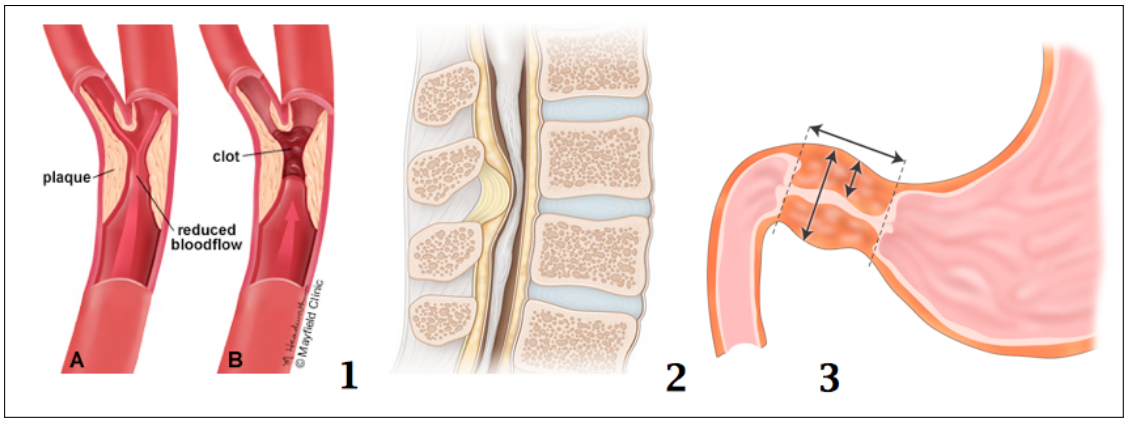

Figure 1.2: Representation of stenosis examples that affect three different components of the human body, in order: a typical blood vessel (1), a cervical spinal stenosis (2), and an example of a pyloric stenosis (3).

The aneurysm, reported in Figure 1.3 in the next page, is a localized, blood-filled balloon-like bulge in the wall of the blood vessel. This pathology has to be treated surgically as soon as possible, because its growth directly correlates with a higher risk of vessel rupture, that in turn leads to bleeding and eventually to a hypotensive shock, caused by a dramatic reduction of the blood pressure. The classification of aneurysms can be made in different ways: by site of presentation, by type or by morphology. Classification by site simply takes into consideration the anatomical area that the aneurysm affects. It is not interesting for our work, because we are focusing only on femoro-popliteal aneurysms. However the other two classifications need to be introduced in order to understand a bit more the problem. The type differentiates between "true" and "false" aneurysms. The true type involves all three layers of the arterial wall, that are the intima, the media and the adventitia. On the contrary the false one, also called pseudo-aneurysm, is a collection of blood leaking outside the artery, that is contained by the surrounding tissue. The last interesting classification is the morphological one. It takes into consideration the shape and the size of the aneurysm. According to it, aneurysms can be classified into saccular and fusiform. The saccular is almost spherical in shape and involves only a portion of the vessel wall. On the other side, the fusiform one is highly variable in both diameter and length, and often it involves a large portion of the vessel.
Both these diseases can be caused by a huge variety of factors, including those at the basis of the most common vascular wall pathologies, such as diet, smoking habit or else. However in this anatomical area kinematic forces play a big role, as we can understand if only we think at the stress that walking alone exercises on the knees. So, these forces can cause several problems in combination with the degeneration associated to the age of the subject. As we will see in the next chapters, actually all the patients we considered in our study are quite old.

1.3 Mini-Invasive Solutions

The presence of a stenosis or an aneurysm is easy to be diagnosed with clinical procedures. It is detectable with non-invasive procedures that are able to document the localization and the severity of the pathology. Indeed stenosis and aneurysms are often associated with unusual blood sounds resulting from turbulent flow over the affected area and are easily audible by any doctor with a stethoscope. However, to confirm the diagnosis, medical imaging is needed. An example of these exams is the Doppler ultrasound that is also the most commonly used procedure. Furthermore,

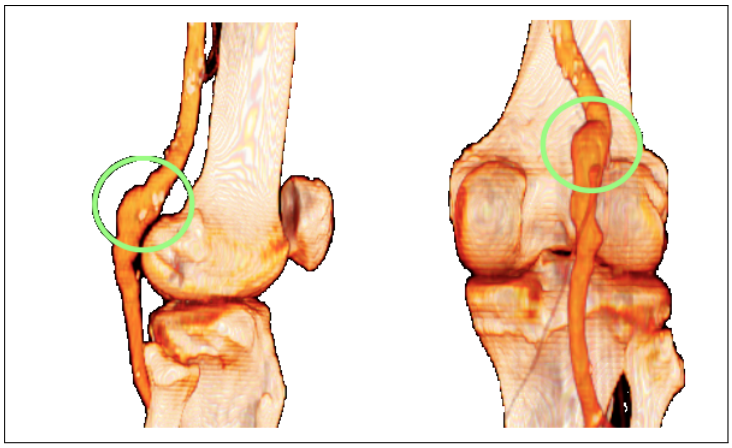

Figure 1.3: 3D reconstruction done with OsiriX, that shows the unnatural shape of the vessel in case of an aneurysm (green circle). In the figure both the lateral and posterior view of the knee area of a patient we treated are reported.

taking as example stenosis and general occlusions, they can be easily detected with a velocity detector, such as the Doppler probe. The color Doppler signal shows the direction of the flow. Moving on, the fastest method to evaluate the blood flow in the inferior limbs is to compare the systolic blood pressure at the level of the ankle with the one at the wrist level. In normal conditions, the pressure at the ankle level is 90% that measured at the wrist. If this value is lower, we are facing arterial insufficiency. The lower is the percentage value, the more severe is the insufficiency. After the detection of the presence of an obstruction it is necessary to localize it in the vessel; for this reason, unfortunately, invasive diagnostic tests are needed. The most common is the angiography, which can give details about the localization and the extension of the lesions.
Once completed the analysis of the disease, it is appropriate to plan the repair. The goal of an intervention is always to get the best result in the less invasive way possible. This is the main reason of all the imaging tests and measures that are made. The more information the surgeon has for the intervention, the easier will be the choice of the correct procedure.
Now we are going to describe the gold standard technique in case of stenosis and aneurysms. It might not be the best one in terms of effectiveness, but it is valid for both the diseases that we are going to talk about in this chapter and with some little differences, that we are going to discuss in the text that follows, the intervention is applicable to both.
In the previous century ('900), the most common way to treat those diseases was the bypass technique. It consists in the placement of a new piece of vessel, that can be either biological or artificial, in the proximity of the damage. After that, the vessel flow is diverted in the new channel that makes a sort of bridge over the damaged area. In the last years, though, this technique has been mostly replaced by angioplasty and stenting, but it is still used to treat this kind of diseases in some specific areas of the vascular network. Angioplasty with the application of an uncovered stent, as shown in Figure 1.3, is not very useful in case of aneurysms, but it is fundamental in presence of a stenosis. It consists of a mechanical widening of narrowing or obstruction of an artery, typically caused by atherosclerosis. An empty closed balloon is inserted, by a guided probe, the so-called "balloon catheter", and it is directed through a flexible wire all the way to the stenosis (Diggery (2012)). When it is positioned over the narrowed area it is inflated up to a fixed size using water pressure, with an inflating pressure that is around 100 times the normal blood pressure. The expansion of the balloon pulls the calcium and the fatty deposits into the wall of the vessel, restoring the normal blood flow.

This operation of ballon inflation has to be made several times to get good results. In general, and in particular for the popliteal area, this procedure is not enough to produce long-lasting results. Indeed, after a variable period of time, the calcium and the fatty deposits start to narrow down the vessel again. For this reason a stenting procedure becomes necessary. This procedure consists in the placement of a stent, over the area of the vessel affected by the two pathologies we are talking about.

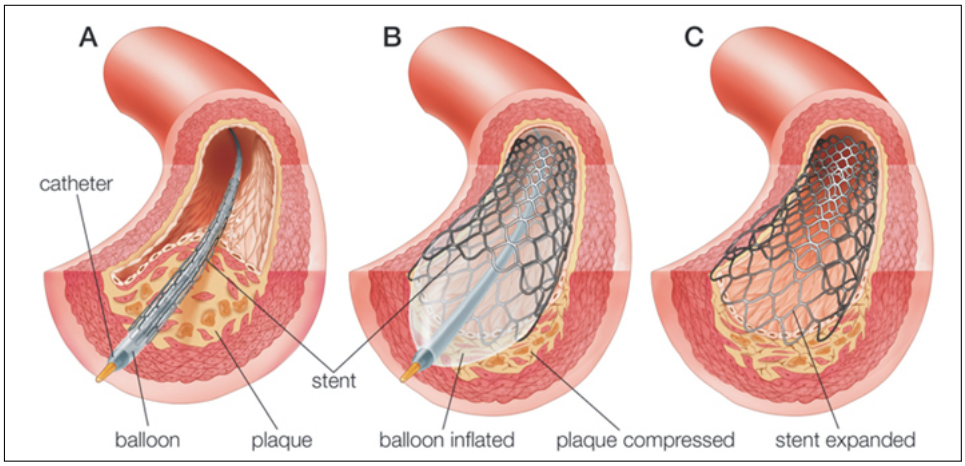

Figure 1.4: The three steps of an angioplasty procedure: step (A), the stent is moved along the vessel until the point of application; step (B), the ballon is inflated and the stent increases in radial dimension to reach the vessel walls diameter; step (C) the deflated balloon is pulled out from the vessel and the stent maintains its final open configuration.

Here, the choice of the type of the stent is very wide. In Figure 1.5 are shown just a few examples of different applicable stents. The choice between covered and not covered stent is fundamental. For the aneurysm covered stents are worldwide preferred over the uncovered ones. In fact, the aneurysm causes vortices in the blood flow of the vessel, and more in general a variable turbulence. With a covered stent it is possible to restore the normal direction of the flow, because the cover of the stent is impermeable, so it does not allow blood going into the aneurysm anymore, that remains isolated out of the structure. On the contrary in case of stenosis the choice between covered and not covered stent is very difficult. Unfortunately both choices can have complications or side-effects. In case of a deep and fast proliferation of the atherosclerotic plaque, a covered stent, that isolates the calcium and the fatty deposits from the blood flow, is preferred. It has to be taken into consideration though that a covered stent has a less stability compared to the uncovered one. Indeed, because of the continuous movement and bending of the leg, the stent could move away from its initial position. This problem is best avoided by using the uncovered stent, because it guarantees a greater long-lasting stability in terms of holding its initial position, but, as said before, it is not able to guarantee a good proliferation coverture.
The technique just described is valid for a great variety of vessels, of course including the poplitea. However the kinematic forces play a fundamental role after the application of the stent. The problem of stent durability that leads to stent rupture is still an unsolved problem in this anatomical area. Indeed after a few years femoro-popliteal stents undergo rupture and/or loss of the initial shape. Considering these problems further biomechanical investigations have still to be performed.
Moving on in the discussion, we are now presenting the results that we found. The application of a covered stent in case of aneurysms has to first achieve the most important result, that is the restoring of a normal blood flow in the vessel. The results of stent applications must be very clear

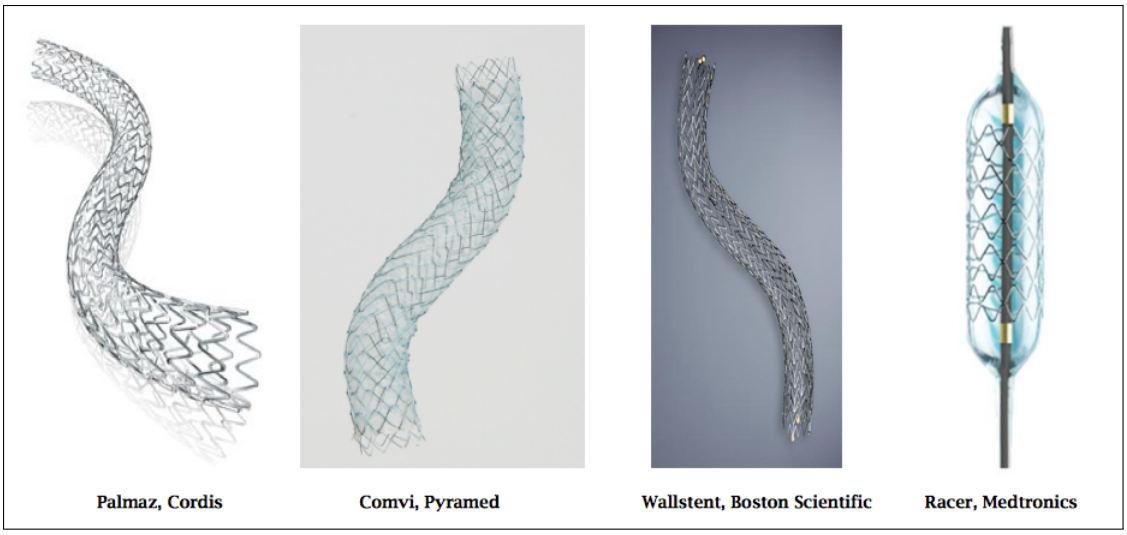

Figure 1.5: Examples of worldwide-known commercial stents. The Racer by Medtronics is an example of the new generation of drug-eluting covered stents.

when we speak about flow direction. As we said before, an aneurysm causes swirling blood flow in the vessel and the stent implantation has to eliminate this problem. The comparison between the vessel blood flow before and after the application of the stent is proposed in Figure 1.6. In the upper part of the figure the situation before the implantation in three different steps of the blood flow is reported; in the lower one we show the three steps after the placement of the stent. The aneurysm is localized in the P1 portion of the popliteal artery.

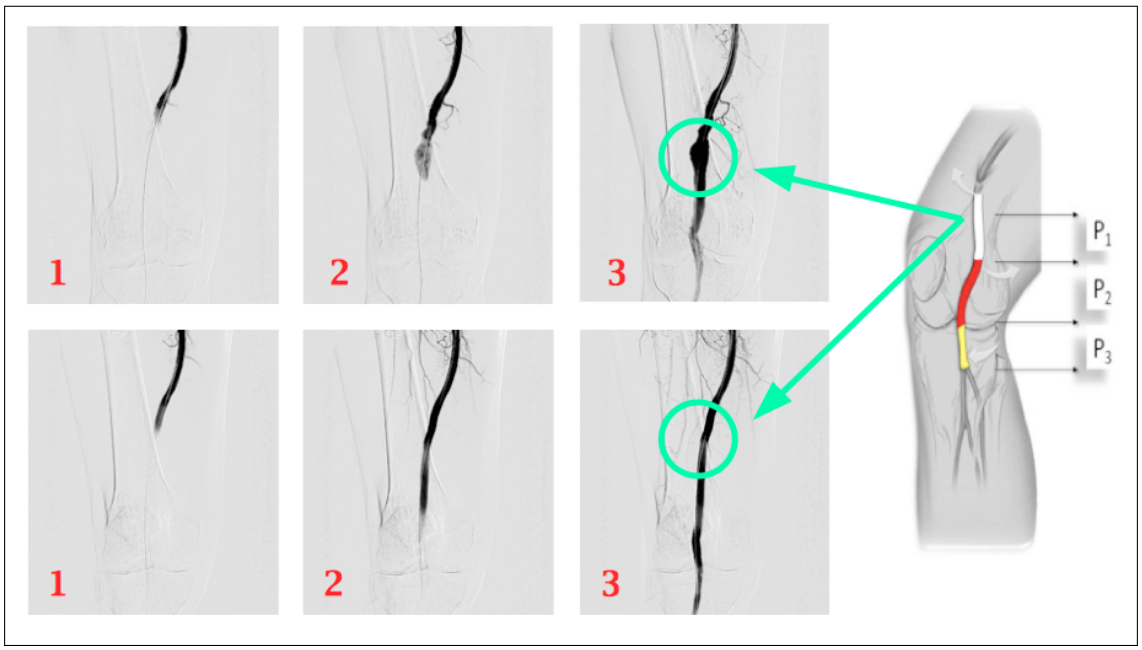

Figure 1.6: The figures show the differences between the blood flow before and after the stent application. Steps from 1 to 3 show different frames where the blood flow is at different consecutive levels. We can see that the aneurysm is localized in the P1 portion of the popliteal artery, just below the point where the vessel comes out of the adductor canal.

1.3.1 Stent rupture

An important aspect that has to be taken into account for the choice of the stent, is its performance concerning durability. Obviously we consider that the uncovered stent would not change its placement position in time. Independently from the age of the patient, the device has to stay in the body for, at least, several years. The principal enemy of durability is stent rupture, that is the breaking of its mesh; the rupture in femoro-popliteal stents is unfortunately still an unsolved problem. Because of this, the durability of a stent is no longer than few years. After this period, the device has to be replaced. Researchers are looking for materials that support better the wear caused by the continuous movement of the leg during daily activities. Indeed the wear is considered the main cause of stent failure. As a result of this first introduction to the problem, we report in Figure 1.7, two examples of stent rupture caused by wear and of stent anomalies in different parts of the body.

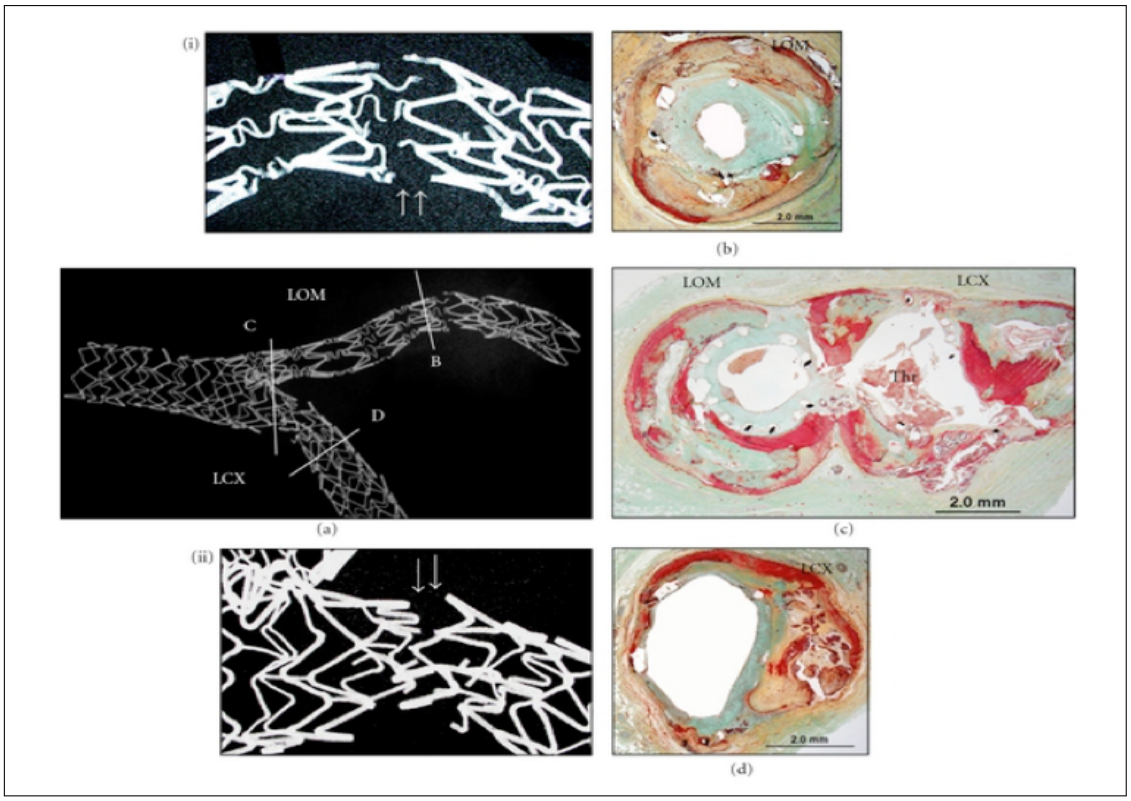

Figure 1.7: This is a great example of stent rupture, probably cause by fatigue in different points of the vessel. The carotid stent is reported in subfigure (a) in the center. It has three fractures, showed with letters (B,C,D). The focus about fractures B and D are above and below the main subfigure. In the right part of the figure, the three images of the real ill vessel are presented.

1.4 Goals of the work and its organization

The main goal of the thesis is the complete understanding of the kinematics behavior of the vessel through the creation of a FE model of it in different configurations. The organization of the chapters of this work is the following:

- 2 - *literature review* → to introduce the reader to the topic, the first paragraph after the

introduction is dedicated to the literature review of the works regarding popliteal kinematics or in general aspects of the popliteal artery. We consider only works published in the last twenty years;

- 3 - *study workflow* → this chapter describes all the steps we do to get to the final FE results that we treat in Chapter 7;
- 4 - *medical image analysis* → the chapter is divided into three main sections: image acquisition, where all the steps before the data acquisition are described; image treatment where the results of the analysis of the vessel geometrical features are proposed; centerline analysis where the geometrical features of the vessel are evaluated;
- 5 - *kinematics analysis* → all the steps of the design from the CT collection to the vessel FEA are proposed;
- 6 - *stent model* → parallel to the vessel design, a method of stent FE design with the software MatLab is proposed. The stent follows the design of the world know Viabahn of the Gore;
- 7 - *simulation* → it is the final chapter of the work, where the results of the FE designs are evaluated together. The first part of the chapter is dedicated to the stent mechanical behavior tests; the second one is dedicated to the contact analysis between the two objects.

At the end of all this chapter the reader will understand completely the procedure we propose. We want to stress that the work is automatized as much as possible to be repetitive for lots of cases of study in the future. All the sections are correlated with explanatory figures.

Chapter 2

Literature review of popliteal biomechanics

In this chapter a review of the current scientific literature, regarding popliteal biomechanics, is proposed. The scheme of reading is the following: each section starts with the introduction of the work with the citation of the authors and the title of the article. We always report also the typology of the patients involved and the technique of imaging used. Furthermore there are proposed the measurements taken by the authors with the results found according to the goals. At the end of each paragraph there is a brief conclusion with possible qualitative considerations. After the description of the work, when useful, there is an image that describes something interesting about the methodology of the authors.

Wensing 1995

The article, written by Wensing et al. (1995), is probably the first work regarding the analysis of the kinematics of the superficial femoral artery (SFA) during the bending of the knee. The study is conduced on a group of 22 people of different ages, between 23 and 68 years old; both male and females. Magnetic resonance angiography (MRI) is the technique of images performed on the patients. Wensing and Scholten create for the first time a 2D model of the SFA configuration during bending, as depicted in Figure 2.1. They notice that the vessel raise, at the complete bending, to a typical configuration that they named: S shape. Besides this main curve, all subjects show 3 or more smaller curves in the femoral and popliteal artery proximal to the knee joint. This strong changing in configuration is the cause of the increasing of tortuosity in the vessel, that they deeply investigate with a series of geometric calculations not reported here in the paragraph. It is interesting now to understand how they do to get this conclusion. In every of the 22 patients they ask them to bend the knee and the hip of 90° to simulate the sitting position. During this, they analyze the results of the bending, as said above, with the MRI. Indeed they notice that there is a length excess in the vessel during the flexion. This excess is corrected with 2 physiological techniques: the compensation made, that ends with the S shape configuration and the elasticity of the vessel. From the measure of the radius R of the curve in sagittal plane of the S, they get with some steps an estimation of the arterial elasticity.
The main interest of the authors is to investigate the way in which the femoral artery copes with length excess as a result of knee flexion. The main conclusions of this study are the following: i) they understand that vessel tortuosity developing during the knee flexion is age dependent. Besides, S angle decreases with age due to the stiffness increase of the vessel; ii) the tortuosity is

mainly caused by elasticity, that has a strong negative correlation with age (this last aspect might need a deeper investigation, because it disagrees with other author's results).

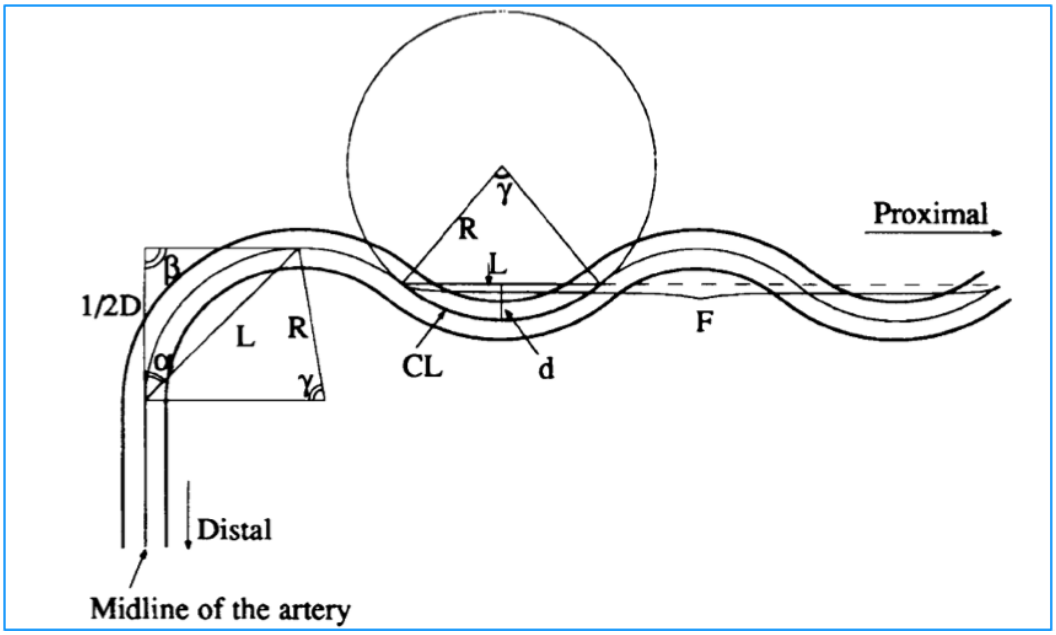

Figure 2.1: Wensing's model showing the first model in literature than describes the kinematics of the popliteal area in case of a 90° bending of the knee.

Smouse 2005

Smouse et al. (2005) publish their work, ten years later, in 2005. They make a great step forward with respect to Wensing et al. (1995). They choose as case of study cadavers. So they are able to make some simplifications; indeed there are not any muscoskeletal forces, that, on the contrary, are present in an alive patient. They introduce for the first time the stent into the vessel during the analysis in order to study its interaction. The number of patient in their study is not so high, only 7 people. However, they make an intelligent choice: they decide to analyze both legs to discover if there is any intra-patient difference, and also to have more available data. This solution is good especially in case of lack of cases to study. The imaging technique is a pretty particular choice for the authors, instead of using MRI or CT, as the most common solution, they use angiography, for getting more detailed images of the vessels.
They perform the measurements simulating 2 different situation: the walking one, with the hip bent of 20° and the knee of 70°, and on the other hand the sitting position, with the two angles of bending both of 90°. They measure mainly arterial changing of dimensions, such as shortening and bending angle, and at the end axial rigidity of the vessel. The work ends with the table of all the found results. In their data table, that we do not report in this work of thesis, it is easy to see that the shortening of the vessel is much less consistent in presence of the stent into the vessel. The shortening is even smaller with shorter devices. For example the shortening with a 70°/20° bending without any device in the poplitea is calculated as 9% from the length in straight configuration. However, the shortening with a stent is approximately 4%. This phenomenon is due to the opposition of the stent to the bending forces. Furthermore, with longer and more rigid stents, the ability of the artery to axial compression is severely compromised. Once axial com-

pression is maximized, the entire arterial segment bends or undulate to accommodate the shorter distance between the hip and the calf. They even discover that the bending is the main cause of stent fracture at least concerning the ones they investigated. Another problem is shown in the left subfigure below depicted in Figure 2.2. Adjacent stents separated by bare artery may shift out of the plane during joint bending. The conclusion of the work gives another interesting contribute that needs to be studied deeper. They define a kind of *"ideal stent"*, that should be made up of a series of independent flexible rings without any longitudinal connectors.

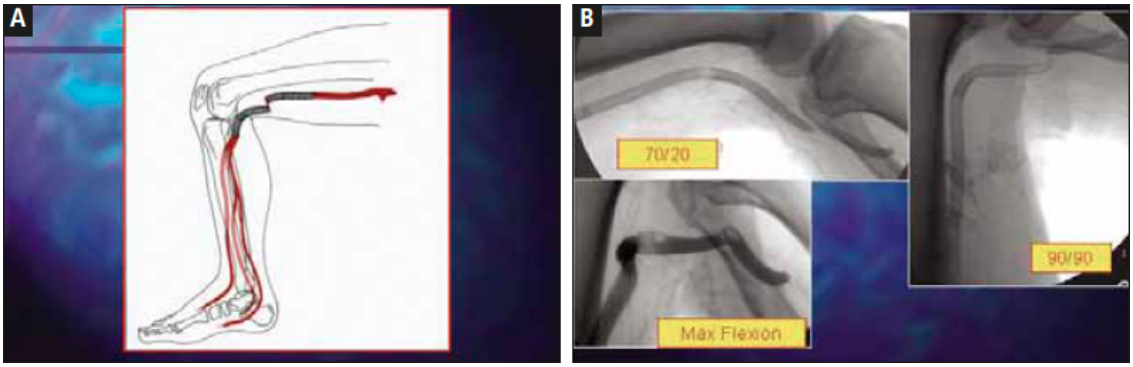

Figure 2.2: Left subfigure: a realistic simulation of the configuration of the vessel during knee bending. Right one: the MRI images of what effectively happens into the vessel.

Cheng 2006

The first aspect that needs to be evaluated about Cheng et al. (2006)'s study, is the age of the eight volunteers, between 20 and 36 years old, therefore people who do not need the implantation of a stent, that is the final goal of the study. However, this work contains some interesting results that merit to be reported in the paragraph. As done by other authors, they evaluate both the left and the right vessel of the patients to get more information. To quantify in vivo deformations of the superficial femoral artery, during maximum knee and hip flexion, that they proposed as the goal of their study, this team use as technique of imaging a common MRI machine.
They limite the study of the vessel between two important anatomical points: the profunda femoris (PF) to the descending genicular (DG), the natural limits of the superficial femoral artery (SFA). The main measured made are three: the SFA length in supine position, resulted as 22 ± 3.1cm, with a maximum value of 26.7 cm and a minimum of 16.8 cm, depending on the height of the case, that is between 155 cm and 180 cm; the SFA length in fetal position, 19.5 ± 2.2cm. Those two measurement are introduced in order to compare the difference in value between fetal and supine position. The third data acquired is the angle of twist of the vessel, estimated as $60\pm34°$. All the measures are made both for the left and the right vessel, with the purpose to understand if there is any intra-patient difference. From the last measurement they finally understand that the transition from supine to fetal position causes a significant SFA twisting that could give rise to several future problems for the stenting. Furthermore the vessel in fetal position results more compressed than in all other positions. This compression is probably a great cause of stent fracture.
Another interesting operation that they make is the comparison of the data taken in relation with the height of the patients. It is important to notice that once the measures of the vessels increase, the height increases too. The last important result that Cheng et al. (2006) found is that SFA deformation cannot be assumed similar in different people; in other words it is not possible to assume similarity intra-people.

The other conclusion reported in this article, that fits very well to our goals and ideas of the problem is that the high rate of stent fracture in the SFA is related to mechanical fatigue as a result of dramatic, repetitive, nonpulsatile SFA deformations.

Nikanorov 2009

This is the second of three works made from the collaboration between Nikanorov A. (2009) and doctor Smouse. This work has two main purposes: to characterize the types and ranges of stent distortion theoretically produced by extremity movement, and as second one to use these ranges as parameters for in vitro long-term fatigue testing of commercially available self-expanding nitinol stents. Also in this case cadavers are used for the study. The idea is to measure the shortening and the bending of the stents and use the devices for in vitro fatigue testing. 5 commercial self expanding stent are used. The main result is the comparison between value of compression and distortion of unstented arteries and stented ones. The results are reported below the Table 2.1. The angles are about the bending of the knee and the hip. The first line corresponds to the value of shortening in case of unstened artery, the second line refers to the case of stented vessels.

Popliteal Artery	**Middle SFA**	**Distal SFA**
14%	9%	23%
11%	3%	6%

Table 2.1: Results in terms of shortening found by the authors after a 90° bending of the knee.

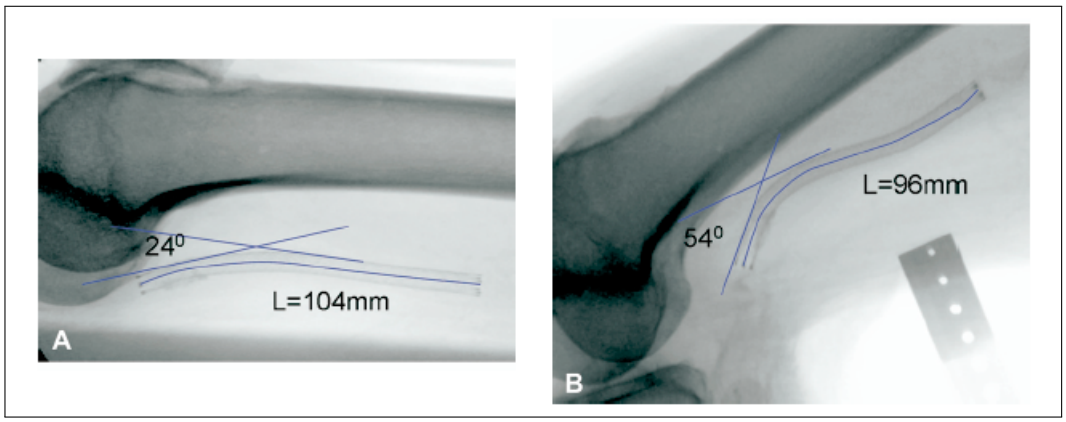

Figure 2.3: Evaluation of the length of popliteal stent in case of straight leg (A) and bent leg (B).

To make this analysis more concrete, because as we said before they have worked with cadavers, phosphate - buffered saline (37±2°) is circulated through the closed system for all the duration of the experiment, to reproduce natural conditions into the vessels. As it is easy to read from the table the results are that nitinol self-expanding stents undergo both axial and bending deformation when implanted into the superficial femoral, middle and distal, and popliteal arteries. Furthermore, commercially available stents exhibit a variable ability to withstand chronic deformation in vitro, and their response is highly dependent on the type of deformation applied. We report above in Figure 2.3 the comparison in length found with the bending of the knee in the vessel. In the figure are also reported the exact measures found with the MRI.

Choi 2009

The next work that appears in the literature through the years is the article of Choi et al. (2009). In this paper the first thing that comes clear as strange to the eye of the reader is that the age of the eight volunteers (20-36 years old) is not coherent with the profile of a people who usually need a SFA/popliteal stent implantation, as we previous saw with the article described in the section above of Cheng et al. Anywhere, differently from the all other works, that focus the attention specifically on the SFA and the popliteal artery, the goal of this work is not to analyze specific solution for a femoral stent but to aid the developing of more durable endovascular devices in general; including stent and stent grafts. All the images are taken with both MRI and Computed Tomography. With the first, the team gets the principal images of the area, with the second method they make the measurements, after the elaboration of the images. We do not take into account the other anatomical areas that they investigate. The measure the superior femoral artery (SFA) shortening, comparing the length between supine position and bent one, simulating sitting position, 8.8±4.4%. Another information that they get is the maximum curvature of the vessel, approximatively evaluated as 0.14mm^{-1}.
As a result they notice that their method is valid for a lot of different types of vessels and it is able to quantify deformations in examples of different various vessels, such as abdominal aorta, common iliac artery, SFA and LAD.

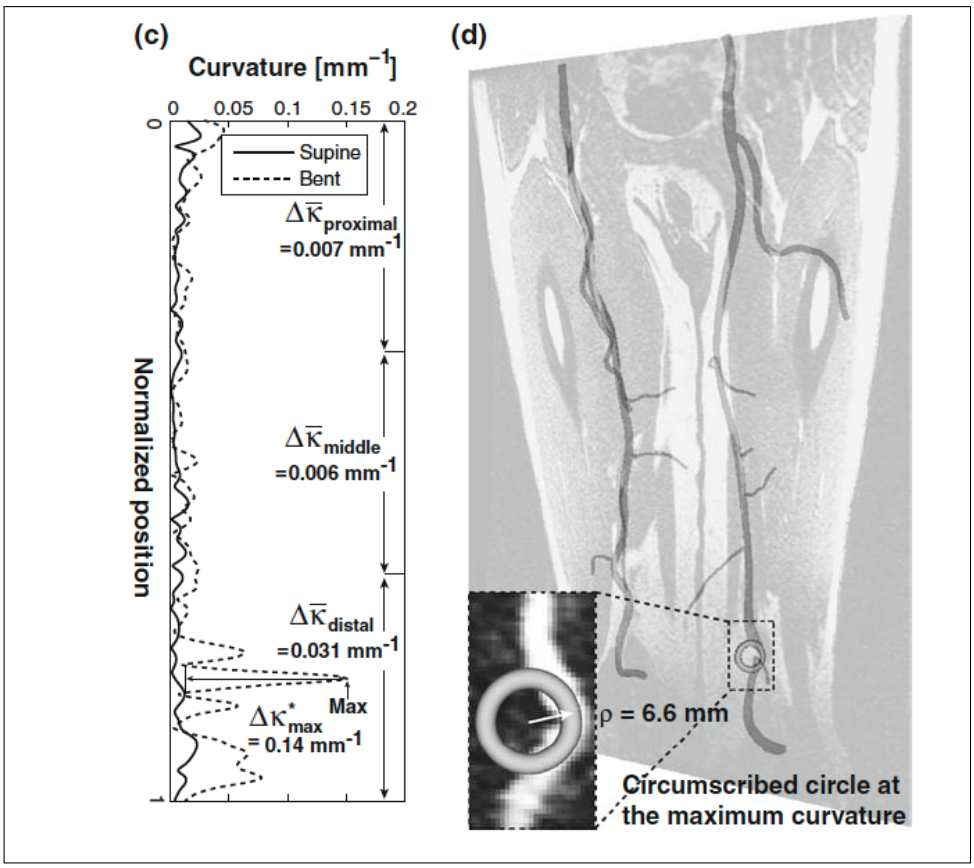

Figure 2.4: Analysis of the variation of the curvature of the whole superficial femoral artery, comparing the straight position with the bent position.

Jonker 2009

The first thing to say about the work of Jonker et al. (2008) is that those authors do not make a proper analysis of the kinematics of the SFA or the poplitea, but they just make such a literature review of past works of the topic. They do this research to evaluate stent durability and design, by reporting the results reached by others authors in a unique paper. However, they find lots of interesting results: first of all they understood that for the prevention from stent fracture and distortion, stents should change in length and contour, similar to the corresponding arterial changes during extremity movement. This shrewdness is also useful to improve stent patency; secondly they quantify the percentage of fracture of Nitinol stent, that occurs between 8% and 28% of the cases. Other interesting results found are that fracture is more common in patients who walk more than 5000 step a day, caused by fatigue, and that long stent and overlapped ones, used in case of atherosclerosis have an higher fracture rate.

Cheng 2010

As we saw until now about literature the work made by Cheng et al. (2010) is very innovative if compared to the others. For the first time the investigation is made considering only the most probable patients, according to the age, that could need a SFA stent implantation. However, also here images are taken from 7 healthy volunteers, that is not such a satisfactory sample, with MRI. The main goal of this job is to describe geometric changes of the superficial femoral artery (SFA) resulting from hip and knee flexion, expressly in old people. To reach this point Cheng and his team make a series of measurement, concentrating on the shortening. They measure: the shortening of the top part of the SFA, evaluated as $5.9\pm3.0\%$; its twisting, as $1.3\pm0.8°/cm$; the shortening of the middle part of the SFA, as $6.7\pm2.1\%$, and its twisting as $1.8\pm1.1°/cm$. After that they measure also the deformations of the third and bottom part of the SFA and they notice that there, the deformation and the curvature are more significant than in the other two areas. The cause is probably the less musculoskeletal constraint in that area compared to the one in others.

Ganguly 2011

The work of the team of Ganguly et al. (2011), is a natural consecution of the article of Cheng et al. (2010), already commented in the previous paragraph. As the others they concentrate the analysis into old patients. In particular, the volunteers are aged 67 as mean value with a standard deviation of 8.5 years. The technique of analysis is different in comparing to other works; indeed Ganguly et al. (2011), in stead of other authors that use MRI, decide to use computed tomography (CT). However, this is not the unique innovation of this work. For the first time somebody study what happen during the bending of the knee with the presence of a stent, in the femoral artery, into an alive patient. This is an improvement to the work of Smouse et al. (2005). Indeed in the work they actually study for the first time the influence of a stent during the bending of the vessel, but with cadavers. A problem that emerges from this paper is that the stents is not the same in sizes and lengths and, in many cases, multiple stents from different manufacturers are implanted during the treatment. Unfortunately it is not yet immediate to compare the results of different samples.
To get the information that they need they make two images of the leg of the patients, one with the leg in extended position and the other with the knee bent of 90°. About the bent position they perform 2 interesting measurements: i) the stent length compression during bending, that

they quantified as 4± 3% of the total length; ii) the stent curvature, quantified between 27±22%, with a maximum value of 0.054, that corresponds to a bend angle of 100.9°. The torsion values are not calculated for the human subject data because, in many cases, there are multiple points under torsion. According to Jonker et al. (2008) they get as a result that chronic fatigue is still the main cause of stent fracture.

Young 2012

Either the work of Young et al. (2012) presents some important differences from the others that are interesting to stress. The anatomic area of study of course is the same, but the approach of analysis is slightly different. The goal of these scientists is to model the key physical characteristics of the vessel, focusing on the arterial length changing during activity.
The innovation in this work is the technique of imaging used to get the information: is stead of MRI, CT or arteriography, they use a motion capturing system, a kind of gait analysis system. As a great assumption they decide not to consider mechanical properties of the vessel. The analysis is performed in three different levels. They measure the shortening of the femoral artery with the system, during three different activities: gait, with a result in shortening of 8.3±0.6%; stair climbing, 11.9±2.2%; sitting motion at 90°, 14.7±3.8%. The main result is an equation to get the percentage of shortening with a known angle of flexion of the knee.

$$\%F_{shortening} = (0.0016) * \theta HF_{max} - 0.0289 \tag{2.1}$$

Another result that they find is very interesting and need a deeper investigation because it is in contrast with the results of another work. They get as a results, in contrast with Wensing et al. (1995) demonstrate, that age factor does not influence shortening or elongation.

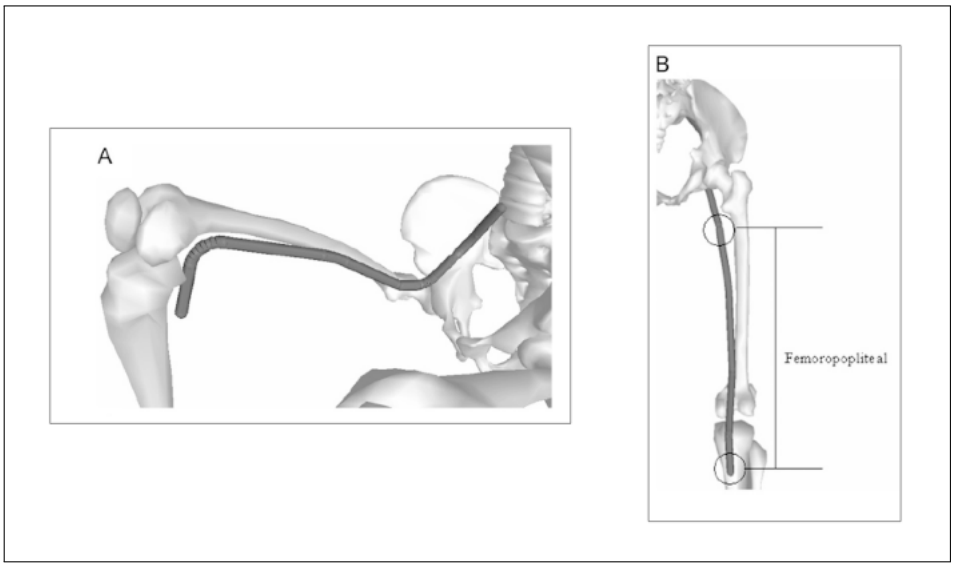

Figure 2.5: Figures A and B report the model of the vessel in the two configurations described in the paragraph.

Shulte 2012

The next work presented here is performed by Shulte and Kralj (2012). The analysis is made considering the principal properties of a world know stent, the Misago peripheral stent from Terumo EMEA. The team makes an evaluation of the outcomes of the device after one year from the implantation, on 744 patients. The patients have different risk factor in their clinic history, such as smoking, cholesterol, diabetes mellitus and others. They evaluate situations of re-stenonis or occlusion into the vessels of the patients, comparing the actual situation to the one before the implantation of the stent with a CT scan. After that they study other factors after three years from the implantation. They find stent fracture and some calcified stenosis after some years to the implantation. The conclusions agree with ones found by other authors: long stenosis requires overlapping stents; arterial motion segments is difficult to analyze. Furthermore, Misago is a valuable treatment option compared to other devices on the market such as Resilient (Leipzig) and Zilver PTX (CookMedical).

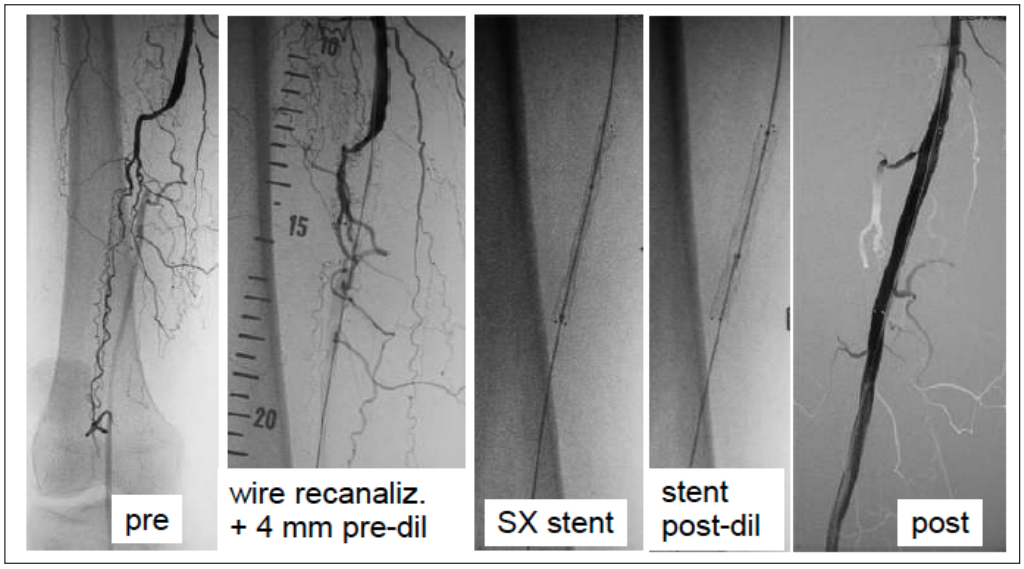

Figure 2.6: Angiographic reconstructions of the leg in different configurations: the pre operative situation (A), during the stent implantation (B,C), just after the implantation (D), and at the end of the follow up (E).

Ghiriallais 2013

The work performed by Ghriallais and Bruzzi (2013) is a brilliant solution of the problem of the lack of volunteers. They create a finite element (FE) model capable of capturing loading condition and deformation characteristics of femoropopliteal artery during knee flexion, from the images of a leg of a single volunteer. Specific deformations of length change, curvature change, and axial twist are measured and used to validate the deformed artery of the model presented here by comparing these measurements and the vessel shape to similar experimental studies that investigate arterial deformations through angiographic images. They do not put any stents into the model. Any diseases are not simulated either.
As technique of imaging they use computed tomography (CT), that is a quite common technique, as we saw in previous works. As said in the introduction of the section, from the images get from a single leg of a volunteer, in extended position, they create the FE model. From the model in the

extended position of it, they simulate the bending of the knee, trying to imitate in-vivo conditions. The next step is the measurement of the principal features of the vessel: i) the femoropopliteal shortening, that they quantify as 1.82 cm (8.23%); ii) the mean curvature of the vessel, measured in cm^{-1}, as 0.294±0.26, with a maximum of 0.601 cm^{-1}, in proximity of the knee joint; iii) the stress on the wall of 61.17 kPa. The radial compression and distortion of the vessel lumen cross section area (CSA), that is evaluated in the region of the vessel behind the knee. The twist angle for the entire vessel, from the straight to flexed knee configurations, is calculated to be 32.71°.
The problem of this work is that they do not compare the results found after the bending of the knee to the reality. However, there is an important result that is good to report: they understood that it is impossible to quantify the dynamic forces imposed to the stent by the surrounding muscles.

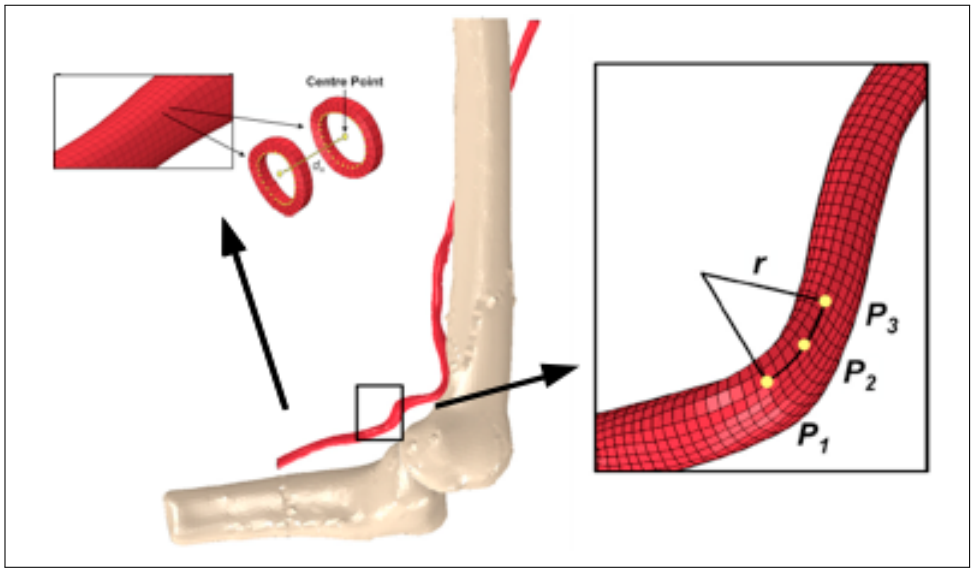

Figure 2.7: FEA reconstruction of the bones of the legs and of the popliteal artery. The mesh configuration can be appreciate in the two magnification boxes.

Nikanorov 2013

This is the third contribute about this topic of Nikanorov and Schillinger (2013). The first works is published in 2005, and the second in 2009; the works are both reported in previous pages. As they discuss, this is the first work in literature that examines the deformation of peripheal intravascular stents implanted in affected patients. It is a sort of continuation of the work of Smouse et al. (2005). Their analysis of the 19 cases is divided in three main anatomical cases: stents implanted in the SFA, in the SFA/proxial poplitea and into the poplitea. The goal of the investigation is to measure, as said, the deformation of the stent into the vessel. To perform this they place on the patients some markers to measure the differences between erect position, simulated ambulation and simulated sitting. To indirectly measure the deformation they draw the centerline of the vessel with multiple connecting points, along the curvature of the stent. The result is that the compression of the stent into the superior femoral artery (SFA) is much less severe than in the other parts of the vessel with an average of 1.7% in the simulated walking position and 3.1±1.8% during a 90° bending of both knee and hip. This second measure is very low if it is compared to the one found into the inferior part of the leg. The compression into the popliteal artery is estimated as 8.5±3.2%. However there are still some limitations to reach the real morphology of the vessels:

the patients bend the leg while standing, in order to simulate the sitting or ambulation position, but they are not actually sitting or working. Nevertheless the position and the morphology of the stent remain relatively constant during the follow up, that is a good news for us. So the degree of chronic deformation can largely be predicted by post procedure assessment.

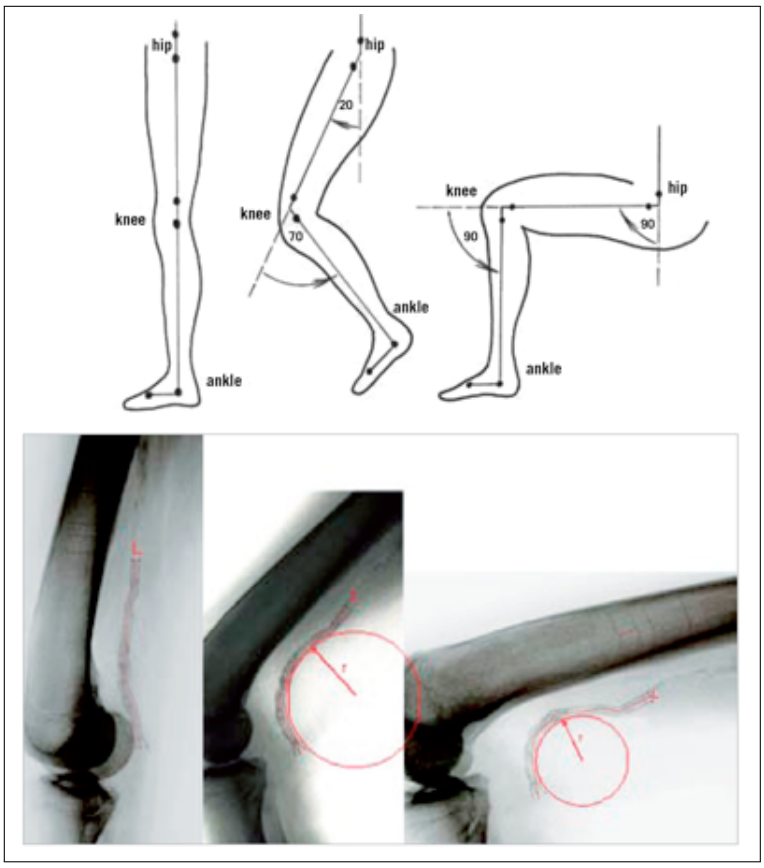

Figure 2.8: Comparison of the vessel structure in 3 different positions of the leg: straight (A), 70° bending of the knee and 20° bending of the hip (B), sitting position 90° bending of both structures (C).

Gökgöl 2013

The last work that is proposed in this chapter is the work of Gökgöl and Diehm (2013). It is the last work in time about the topic that we are investigating into. It is very recent, indeed it was published in December 2013 on the "Journal of Endovascular Therapy". This clarification is just to stress the attention on how the studying of femoropopliteal diseases is actual, in particular in the way to understand forces and kinematics that act in this area. The purpose of the article is to quantify in vivo deformations of the popliteal artery during leg flexion in subjects with clinically relevant peripheral artery diseases. To reach this goal five patients (4 males, aged 69±10 years old) with different calcification levels in the popliteal artery are investigated. The images are taken with a 3D rotational angiography. The images are taken in two different positions, with the leg straight and with it flexed of 70° as angle of bending of the knee, simulating the walking situation. To bend the leg they use a kind of big pillow to reproduce the needed angle. We do the same thing as they do with the pillow, to impose the bending of the knee. In Appendix D.1 is going to be described the preparation of our device. We use this article as a point of start and

we do some of the things described into; for example they isolate the centerlines of the vessel and they make a 3D reconstruction of the arteries; we do it too as is fully described in Chapter 5. The goal of this model is to quantify the axial deformation, the twisting and the curvature of the vessel in the innovative bent position of the knee. They find a value of 5.9%±2.5% in terms of average shortening of the popliteal artery. Also the value of maximal curvature in the two different position is calculated; however, we are not interested in this aspect. Doctor Gökgöl and his team end the work explaining that axial elongations and arterial twistings seem not to be affected by the calcification levels, at least in their patients.

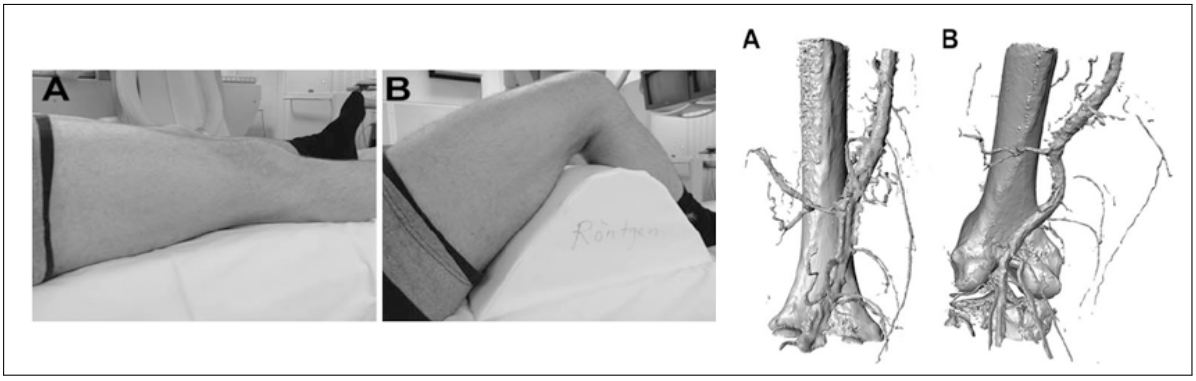

Figure 2.9: Comparison of the vessel path between straight (A) and bent (B) position. In the right part of the image it is shown a reconstruction of the popliteal area.

2.1 Conclusions

Now that we presented the most interesting articles about the topic of our study it is necessary to analyze all together the results found by the authors.
All the studies are performed with the goal of find different aspects that would help to understand completely the problems around femoropopliteal kinematics. However it is necessary to underline some aspect that are either interesting for our goals. The first article that we actually did not introduced before about the topic is written by Browse N. L. (1979). The methods of analysis that year were very backward considering the technology we own now. However it is the first work able to evaluate the femoropopliteal shortening, as the 20% of the total length, that is a realistic value compared to the results found by the other authors. Then 16 years later Wensing et al. (1995) explain the popliteal kinematics with the first computed method. Their idea is good but the problem is the difficulty of the calculation of the parameters used to evaluate the curvature of the different tracts of the poplitea depicted in Figure 2.1. A great improvement in this direction is the model applied by Ghriallais and Bruzzi (2013). It is necessary to remember that in this work it is not studied the comparison of the model to the post stenting implantation situation. However the approach of reconstruction of the model is similar to our workflow. The comparison of pre and post stenting configurations of the vessel is proposed by Shulte and Kralj (2012) but is limited to a simple fluoroscopy analysis of the changing of blood dynamics similar to the one proposed in Figure 1.6.
In our work we describe a method to calculate the curvature of the vessel to avoid the problem of the noise caused by rough data. The results are comparable to the ones of Choi et al. (2009). Indeed to make an easier comparation between the results we also use the graphical technique of plotting the curvature in vertical direction with the vessel next to the graph, proposed in Figure 2.4.

The last big topic that is proposed by some authors in literature is the evaluation of the vessel conditions after the stenting implantation. This is the central topic in some work, such as the ones proposed by Smouse et al. (2005) or by Ganguly et al. (2011). They compare the vessel kinematics in the two main cases, leg in straight configuration and in the bent one. However, the problem of these works is the absence of a comparison between the pre and the post operative situations and this is a point that we want to implement.

Chapter 3

Study workflow

In this chapter we illustrate to the reader the workflow, that we follow for the analysis of popliteal stenting and kinematics. The goal in the chapter is to clarify the ideas about all the actions and the steps we make for the realization of our work, from the beginning to the results. The first workflow, that describes the structure of this thesis in blocks, can be basically split in four main parts as shown by the illustrative scheme depicted in Figure 3.1. In the further pages, we are going to describe all the parts of the workflow, following the steps listed here below. The four steps are:

1. *medical image analysis*: the first step is schematized in Figure 3.2. We begin with some literature review about the topic, that has the goal to understand how is the situation in the common knowledge about femoro-popliteal stenting. After that, we reconstruct the 3D lumen profile through the data received by the medical partner. After the successful reconstruction of the vessel, we make a lumen centerline analysis for all the datasets we have (the reader should refer to Chapter 4 for the complete presentation of these aspects);

2. *reconstruction of the arterial kinematics*: from the centerline data, calculated in the previous step, we reconstruct the anatomy of the vessel in 3D, taking into account all its features of interest (refer to Chapter 5 for further details). The summarizing scheme of this step is proposed in Figure 3.3. It begins with the sweeping of the vessel surface down to the centerline and ends with the writing of the input model in the correct configuration for the FEA software;

3. *creation of stent model*: from design parameters defined by the user, we create a 3D mesh of the stent; the step of the realization are shown in Figure 3.4. The stent will interact with the vessel during the simulation of contact and deformation (in Chapter 6 further details about stent design);

4. *simulation of the implant*: the simulation of the contact between the two object we create is the target that we want to reach with our work. The simulation consists in the test of the contact between the stent and the vessel (refer to Chapter 7 for further details). The simulation includes also the mechanical tests on the stent model.

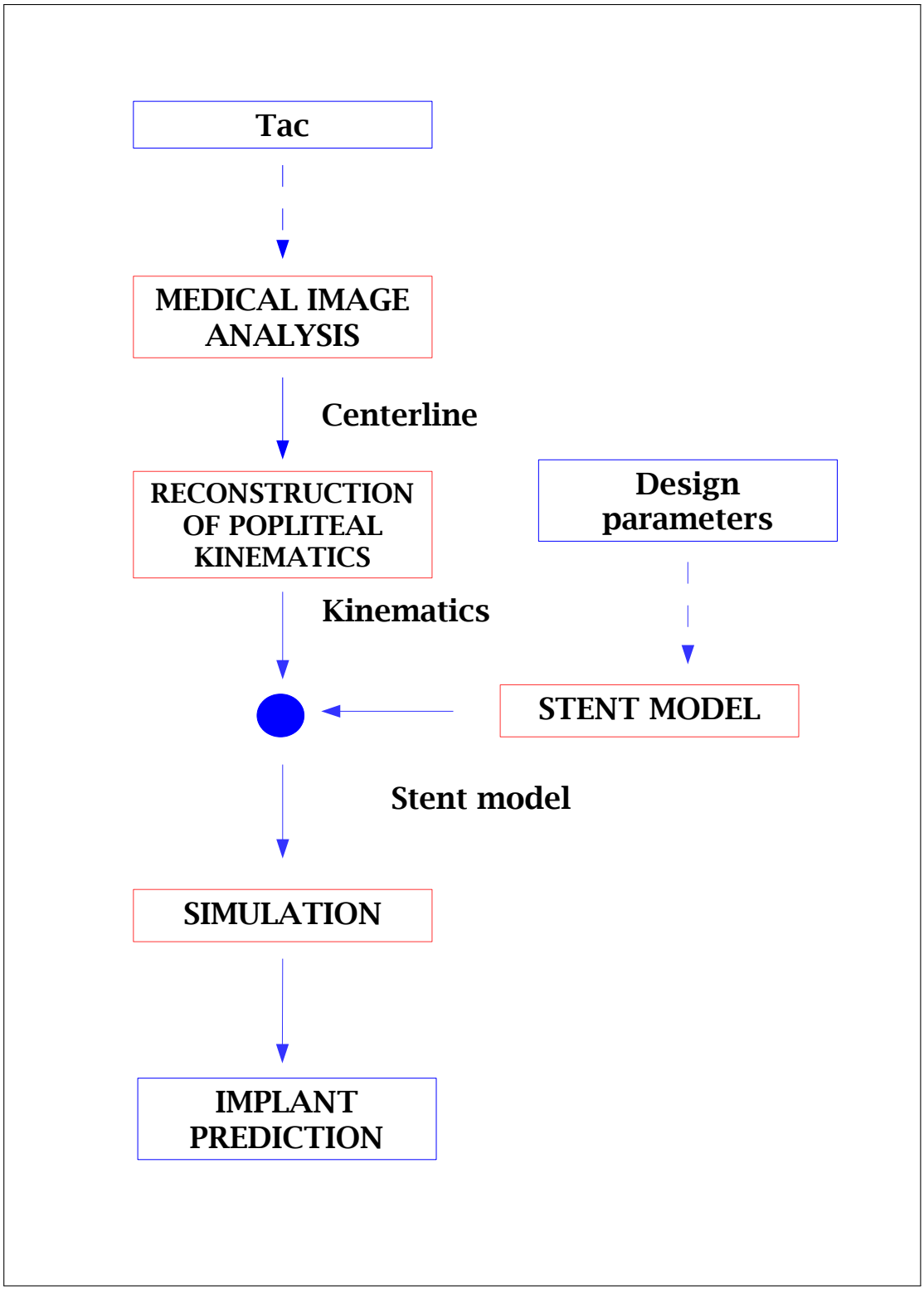

Figure 3.1: Basic workflow scheme: workflow summarizing all the topics that we are going to explain in the next chapters, every red block represents a diagram that will be presented in the further pages.

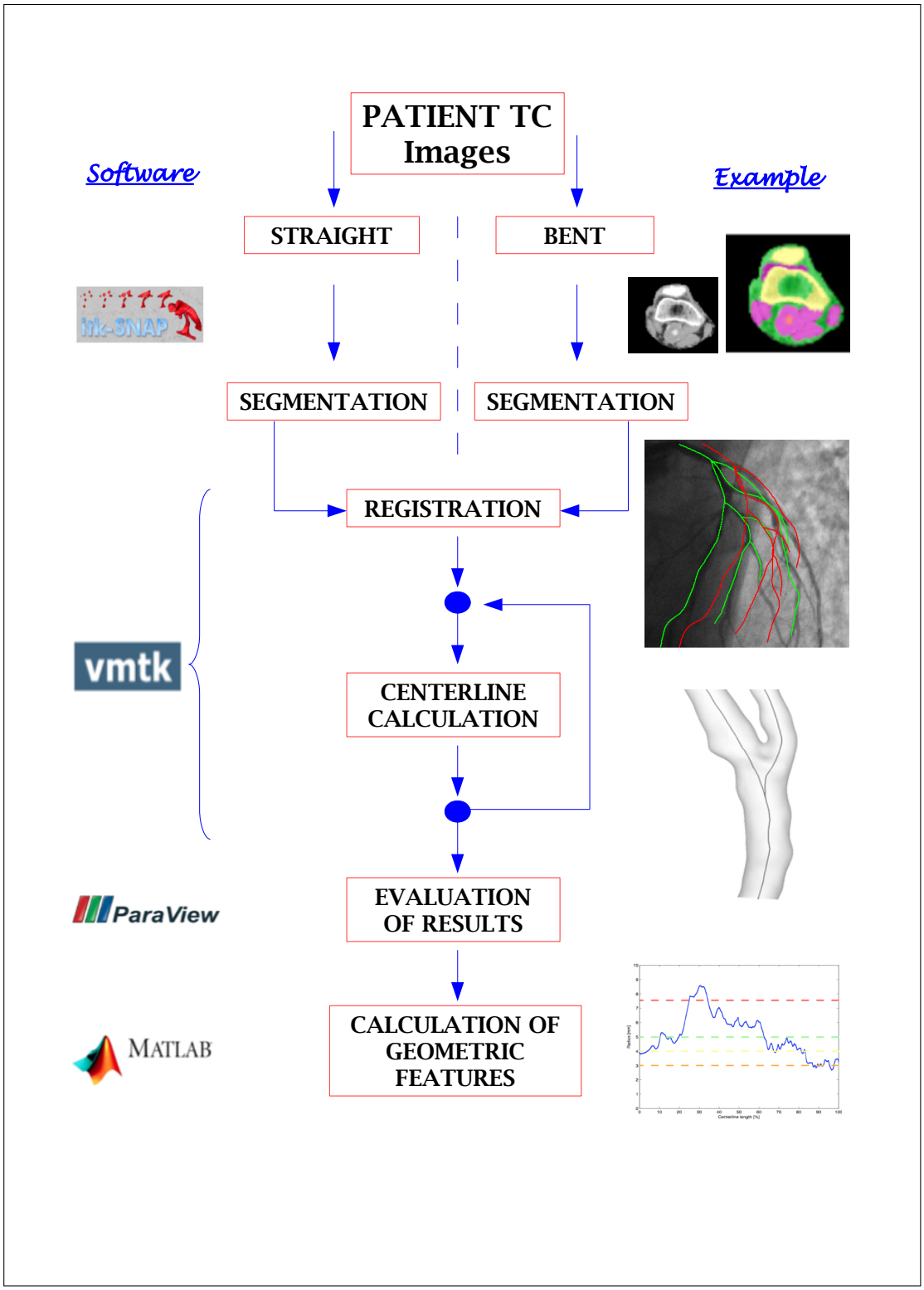

Figure 3.2: Medical image analysis: Workflow describing the operative steps performed to evaluate the centerline features with MatLab. The analysis starts from medical CT images and needs the registration of the data in order to compare the results.

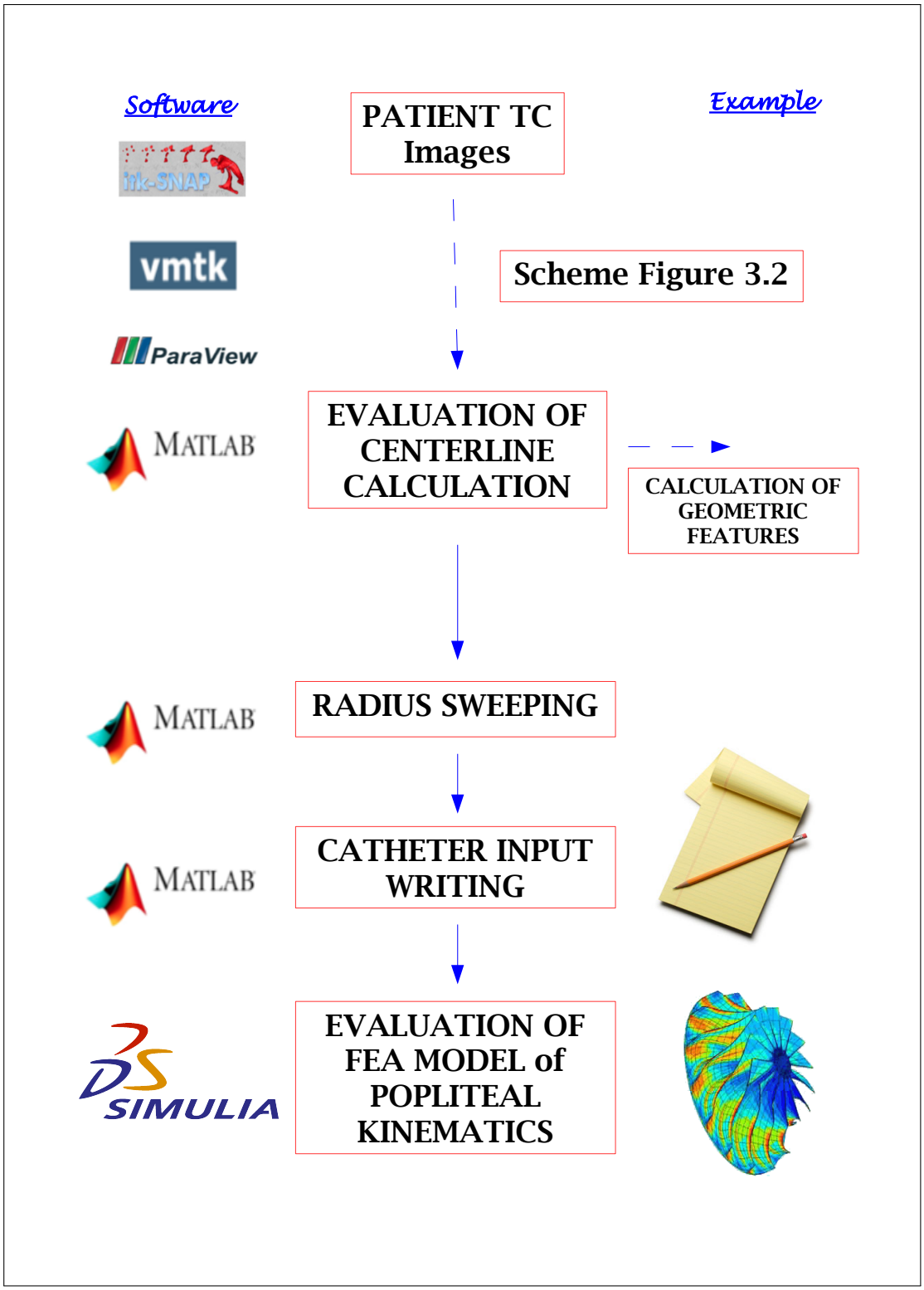

Figure 3.3: Reconstruction of the arterial kinematics: from the STL file of the centerline, with the application of the sweeping filter that works with the application of the radius values vector, we arrive to the writing of the input file of vessel, that is ready for the simulations.

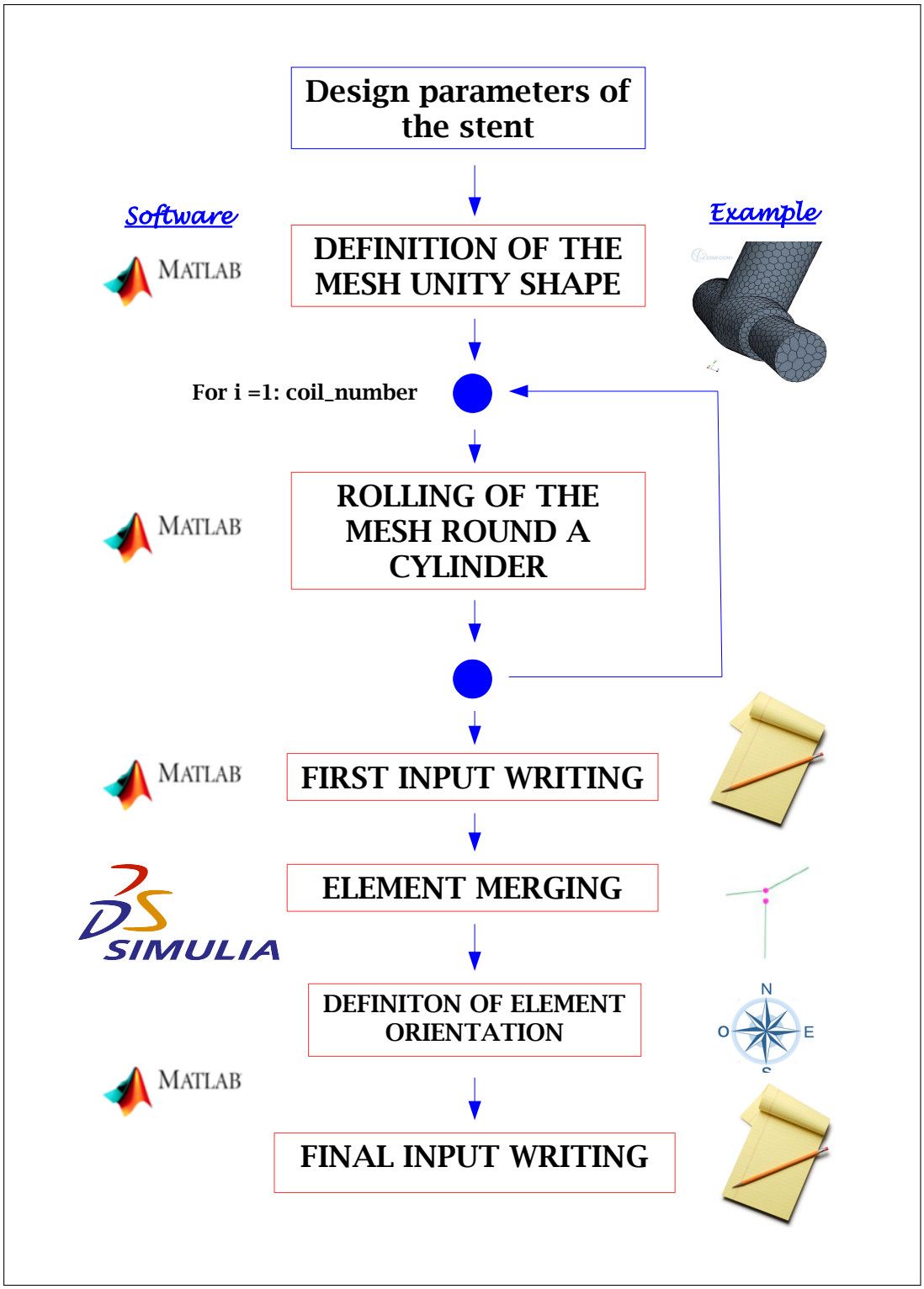

Figure 3.4: Creation of a stent model: with the application of the design parameters we create a first simple model of a ring of the stent that will be repeated for the desired length we decide to apply to our device. After the definition of the orientation of the beam elements that compose the stent the stent model is ready to be loaded in the FEA software for the simulations.

In this chapter we introduce all the parts that compose the scheme, but we do not describe the results we found such as the simulation ones. The results are reported in further chapters to make a complete summarize of the relative step.
Here in the following sections we try to describe in initial manner all the work we do. Every scheme have a proper section that describes it. For more detailed analysis the reader has to go to the proper chapter of the topic.

3.1 Medical image analysis

Since we receive the medical images from the clinical partner, we are ready to start with the elaboration of the rough data. Before to start with the segmentation, we have to divide the image archives between the two configurations of the leg, that are grouped in series of DICOM images. This step is easily achieved with the open source software "OsiriX" (Pixmeo SARL - Switzerland) version 5.8. With the software it is also possible to select the region of interest (ROI) reducing thus the size of the dataset. The elimination of useless DICOM is also a good procedure to reduce the size of the image dataset and to speed-up the medical image analysis.

3.1.1 Segmentation and registration

Now it is the time to concentrate the attention on what we are really interested into of the entire leg: the vessels, in particular the popliteal artery. The first thing to do is to isolate this tissue to the others, such as bones or soft ones. To get this point, we use another open source software, called "ITK-Snap" (Insight toolkit), version 2.4.0. This software permits to make a primary segmentation of the pixels of interest. With one of its tools, called "Snake ROI tool", it is possible to make a 3D automatic segmentation of what the user needs. If the result is not precise as the user wants it is possible to make manual corrections, to every slice, to get a better result. With some experience, it is also possible to detect directly the point of beginning and of ending of the poplitea. To remind the reader, the popliteal artery begins when the superior femoral artery comes out from the adductor channel, and ends when it branches into the two tibial arteries.
We make a 3D segmentation both to the vessel and bones to keep the idea of where exactly a certain point of the vessel is in anatomy. The segmentation of all the parts of the leg is useful to make interesting 3D reconstruction images. The bones are fundamental to reach the step of the registration of the two vessels, that is presented below. To distinguish between different kind of tissues it is possible to choose different segmentation colors. A great tool of ITK-Snap, connected to the segmentation colors, is the one that permits to save the labels, that refers to different colors, used for detecting different types of tissues, in a separate way. With ITK-Snap it is also possible to detect any calcifications in the vessel. They are visible in raw images, but they get more visible in the CT with the application of the intensity threshold, as depicted in Figure 3.5.
The next step is the registration of vessels. It is fundamental for the analysis of vessel kinematics. Registration consists in a rigid roto-translation of one instance, taking as a point of reference the other, as shown in the example in Figure 3.6.
It is performed by the open source software VMTK (Tcl & Tk) (vascular modeling toolkit) version 8.5.9. It gives a method called *"vmtkicpregistration"*, that is based on the iterative method of the closest point; for further details the reader should refer to Appendix A.1. The registration can be applied when two different configuration of images of the same anatomical area are available. We apply the registration in two different cases: with the images of the patient with the leg in straight and in bent position, and when the comparison is done between pre operation of stent implant and post implantation case. The registration needs the creation of a matrix of translation, using

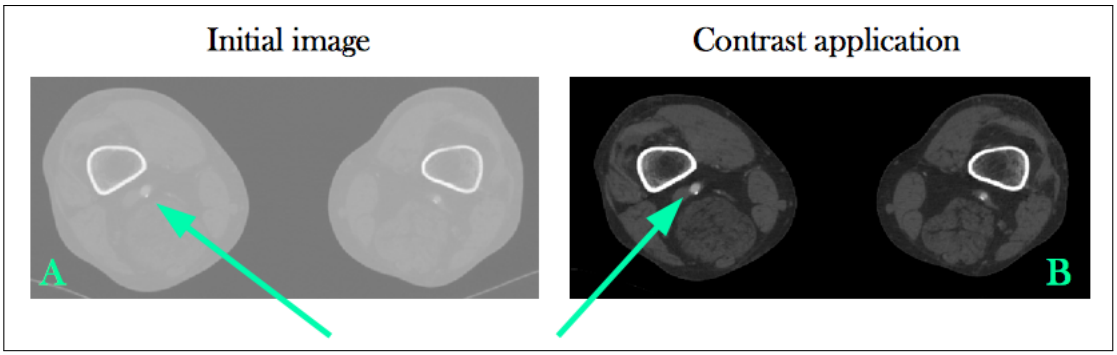

Figure 3.5: Comparison between a raw CT scan image (A) and the same image after the application of a simple intensity threshold filter (B).

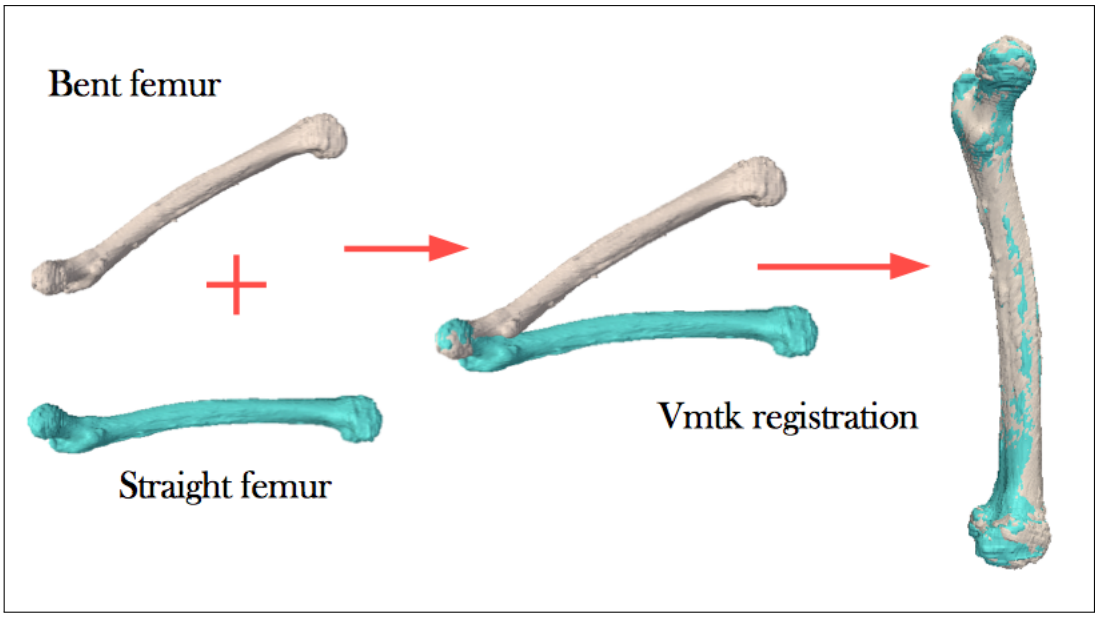

Figure 3.6: Example of registration of the femurs in different configurations: the result is shown in the right part.

as second reference instance the femur in the second (bent or post) configuration. The result is the object in an intermediate configuration that is very similar to the second (bent or post) one. We have to take as reference the bones because we consider them as rigid bodies and so we are able to apply a rigid roto-translation. Since we create the matrix of translation, we apply it also to all the other tissues including vessels. The result are STL files that contain registered objects. The registration is either applied with VMTK. With this software is also possible to smooth edges of the objects that we consider too much jagged. The smoothing filter of VMTK is a method applicable to discrete surface based on the Taubin's algorithm (explained in A.1). This algorithm consists in a low-pass filter that removes high curvature variations, and does not produce shrinkage (Taubin (1995)). Later in Chapter 5 we will submit a method of smoothing that is very good for the application of smooth to objects. However, smoothing filters are available also in the other softwares introduced until now ITK-Snap and Paraview.

3.1.2 Centerline evaluation

A big problem of the vessel analysis of geometrical features is often the presence of stenosis into the vessel. After the registration we make the calculation of the centerline. However, if the stenosis is severe, the centerline calculation tool of VMTK fails. In these cases we have to modify the real situation of the vessel manually, to get a more smooth internal profile and to eliminate those great discontinuities. This problem of discontinuity of the images can be caused also by low image quality. When we consider that the vessel is correctly meshed and registered, we can make the centerline calculation with VMTK. To be clear in the exposition we have to specify that the centerline is the line that connects two sections of the lumen, whose minimal distance from the boundary is maximal in some sense (Piccinelli et al. (2009)). Consequently, centerline computation can be formally described as a functional minimization problem. It is created by the connection of the centers of every horizontal sliced, with a predefined distance between each other of the tube that we are considering. The calculation of the centerline, with the VMTK filter *"vmtkcenterlines"*, is good to be combined to the calculation of some geometrical features that is made with the filter *"vmtkcenterlinegeometry"*. The centerline filter needs an input that has to be something shape as a tube or a channel, like for example a vessel, and it gives as result its centerline.

3.1.3 Inner radius

With the calculation of the centerline of the poplitea we achieve our first goal. Now that we have isolated the centerline of the vessel, in both the configurations, straight, bent and registered one, we can pass over the elaboration of the CT and go into some more mathematical analysis of the results. The analysis, that we describe in the next sections, is performed with another powerful software: MatLab, version 2013a of MathWorks. The file of the centerline contains lots of useful data, that we can analyze. The matrix data of the centerline files has a number of rows as the number of CT frames, used for the elaboration of the 3D model, and a number of column as the different types of data carried. Interesting measures that the file carries are values about: the radius of the maximum sphere that can be inscribed in the vessel section, the curvature, the torsion and the three coordinates of the nodes of the centerline. The analysis of the radius values along to the centerlines slices is very interesting because it permits to detect the presence of irregularity in the vessel profile. Indeed the vessel radius has to be quite regular down to the popliteal tract especially in the straight configuration. When we find an interruption of this continuity we are probably in presence of a stenosis or an aneurysm. An accurate measurement of the vessel radius, as function of the centerline position, can certainly support the detection of the vascular diseases by the physician, which is the end user of our tool. With the knowledge of the values of vessel inner diameter in the popliteal tract, it is possible to find unexpected values of radius that correspond to a stenosis if the values are too small or to an aneurysm if they are too high. As we know from the literature, the value of the inner radius of the popliteal artery should be between 4 mm and 6 mm (Gray (2009)). So when we find from the data values that are quite far from this range we are in presence of one of the illness that we have introduced. In particular the increasing in vessel radius is considered an aneurysm when the increasing is more that the 50% of the mean radius that is approximately 5 mm in every patient. So for values higher than 7.5 mm the presence of an aneurysm should be taken seriously into account. A similar discussion can be made also for the stenosis, but in general the stenosis is characterized by a number that expresses its percentage.

3.1.4 Length and shortening

The value of the radius is directly takable from the data matrix of the centerlines but some other features has to be calculated. The first one we immediately derivate is the centerline length. The

length is fundamental for the comparison of data of different patients. By the normalization of the data it is possible to compare directly different values. The length of the vessels is calculated by the sum of the 3D distance of each node to the one that follows it. The algorithm is based on the equation of the calculation of the distance between two nodes in the space:

$$length = \sum_{i=1}^{N-1} (x, y, z)_{N+1} - (x, y, z)_N \tag{3.1}$$

Where N is the total number of nodes, and every result of the sum, is the distance between two consecutive nodes. The measure of the length of the vessel is underestimated in comparison to the real situation, because it is a discrete measure, based on the equation of distance between two points in the space. The sum should be made with an infinite sum of distances between very close nodes, ideally with distance 0, that is the theoretical basis of an integral function. In reality, the connection between two nodes does not usually follow the shortest way. This underestimation can be limited as the minimal value by the diminution of the slice thickness during the CT scan; however, it would cost much more time for the computation. The calculation of the vessel length is also very interesting for another aspect. It permits to measure the percentage of shortening of vessels during the bending of the knee. To evaluate the robustness of our results, we compare the measures of length and shortening we find with the ones readable in literature and presented in Chapter 2. We report all the results here below in Table 3.1. It is necessary to make some notes about the data reported in the table because a few results presented seem not to be coherent with the others. Taking as example the first data, it is taken from a very old publication made by Browse N. L. (1979). As the reader can easily imagine, the techniques of measure were not so precise as in the last years, and the measure appears a little overestimated compared with the mean value of the other authors. However it is interesting to report the result to show that the first measure of the popliteal shortening was done in 1979. Another important clarification has to be made about the results of Smouse et al. (2005). As the reader remember from Chapter 2, the team make the measures on dead patients so the results are affected by the absence of muscular forces that behave on the vessels. The last measure that makes some doubt is the value found by Ghriallais and Bruzzi (2013). It is reported in the paragraph dedicated to this article, that the measures were not calculated directly on the patient, but on a model that they create from the patient images.
We now report below in the Table 3.1 the literature results about the shortening of the 90° popliteal artery bending. The last line of the table is dedicated to our result about the shortening.

Authors	**Year**	**% of Shortening**
Browse et al.	1979	20 %
Smouse et al.	2005	14 % (Cadavers)
Cheng et al.	2006	13 ± 11 %
Muller et al.	2010	15.8 %
Shulte et al.	2012	21 %
Ghriallais et al.	2013	8.23 % (Model)
Gökgöl et al.	2013	16.4 ± 8.4 %
Our Result	2014	17%

Table 3.1: Report of some results about popliteal shortening, expressed in percentage, after a bending of 90° of the knee.

As we can see from the table our result is quite consistent with the results found in the previous studies, using different techniques. The main problem of the shortening calculation is the

availability of both data regarding the vessel in straight configuration and in bent one.

3.1.5 Curvature problems

Another interesting data, as introduced above, is the vessel curvature. The curvature is a measure that expresses the displacement of an object from the flat shape. It is either a measurement of the tortuosity of the vessel. Curvature is very useful in the detection of the points where the stent probably is going to have a faster rupture in its mesh. Indeed the points of maximal curvature are the points of maximal stresses on the mesh. Unfortunately the curvature values, given us by VMTK, with the centerline calculation are very jagged. For this reason the data are not useful for the creation of a good curvature profile. In Appendix A.3 we are going to present an interesting method that we developed for the calculation of the curvature.

3.2 Reconstruction of the arterial kinematics

When the reader comes to this section should have understood the work that we have to do to generate good STL outputs of the vessel profile and of the vessel centerline. The centerline file is fundamental to perform the steps that are going to described in this section. The reconstruction of the arterial shape that is going to be evaluate to understand its kinematics is necessary in our case. Because the images that comes to us from the medical partner are not sufficient in high resolution, the vessel profile results sharp. For this reason we decide to redesign the vessel from the beginning. The reconstruction of the vessel, from the kinematics, allows the creation of intermediate states, between the straight and the bent configuration of the vessel anatomy. Those states will be fundamental when we will speak about simulation in Chapter 7.

3.2.1 Radius sweeping and catheter input writing

The first step of the artery reconstruction is the radius sweeping. With a MatLab script every centerline node is correlated with a circumference. The radius is evaluated from the sampling of the vector containing all the radius values of the real vessel, taken from the CT. The sweep consists in a unrolling of a circumference down to the centerline profile. The number of nodes that forms the centerline can be sampled to speed up the vessel reconstruction and to reduce the mesh dimension. When the radius is correctly swept down the centerline profile we are able to write our input of the vessel that will be evaluate with the FEA software Abaqus, Simulia, version 6.12 in Chapter 7. The script that creates the catheter input is structured to give multiple results when it is called. It creates two different input files of the vessel. The first one is a sort of tester of the vessel; an input file containing at least four steps. In all those steps the catheter changes in configuration. The steps of the catheter are described with more detailed in Chapter 5. The other input is a script readable as a part of a CAE model, that we are going to test in Chapter 7 with the contact analysis with the stent mesh.

3.3 Creation of a stent model

The design of the stent is the other model that we make for the realization of our goals. However, this time the design does not start from an existing model, such as the centerline. Giving some design parameters to the script, or to the interface we create for this step a new model, ex novo, but following the shape of the world know Viabahn of Gore. The creation follows some rules that we decided at the time of the planning such as the unit shape of the stent or the distance between the rings that composes the object. The script creates first of all a single ring of the mesh, and if

it is correct it reproduces that ring a number of times chosen by the user. After that it writes a primer input model of the object. We have to specify that the rings are made of beam elements that connect their nodes. On the contrary each ring is connected to the previous and the following with truss elements; the reader should refer to Appendix A.5 to understand the differences between those two element types. Now, we pass the input file to our FEA software Abaqus Simulia because it is the only one able to correctly merge the nodes that compose two different instances. These nodes in the design are effectively overlapped one to the other. When the merging is correctly done, we take back the data of the nodes and the elements to MatLab by the writing of an input and import the data tables. MatLab now calculates the orientation of the beam elements of the stent. All the procedures just introduced are going to be explained deeper in Chapter 6. When the stent is ready to be tested we write also for it an input file readable with the FEA solver.

3.4 Some further details about the workflows

This chapter of workflow wanted to introduce the reader to various problems that affect the project that leads to a simulation of contact between a vessel and a stent design. As said in the chapter the better explanation of the problems is postponed to further chapters.
Another important aspect that we want to stress to the reader is the strength of the software Paraview (parallel visualization application), version 4.0.1. We use this software to analyze all the results we performed during the work, because this software is able to read lots of different file format, and it is very useful to make comparison between different objects.

Chapter 4

Medical image analysis

This chapter is the first one where we show some of the results that we found during our analysis. Here, we are going to treat in a deeper way medical images and we try to get some interesting results from them. We start the chapter with the explanation of the technique we use to collect the images data from the patient in the correct way. After that, we are going to speak about the treatment we reserve to the images to elaborate the results we are interested into. All this results are present in the last part of the chapter with of course some clarifying images.

4.1 Image acquisition

The correct collection of the imaging data is fundamental to reach reliable results from the patient. For this reason the collection has to be made with extreme attention of all the details that could possible affects the data. Here in this section we propose all the shrewdnesses we use to keep the data collected in the correct way.

4.1.1 Set-up for leg bending: literature

After the introduction of the problem we are studying, we now explain the procedure we choose for the effective image acquisition. This chapter is closely connected to the previous one because here, in this fourth chapter, we describe all the steps of the acquisition of the images, that are introduced in the previous chapter with the relative scheme.
This acquisition section opens with the explaination of how others authors, found in literature, have overcome the problem of the positioning of the patient during the imaging acquisition. All their solution are reported in Table 4.1 in the next page. Into the table, the measurements regarding the angles, are considered as the angle of knee bending. They impose it from the horizontal plane, considering as positive the angle produced by the normal bending of the knee. The main goal of these studies, as said before, is to understand the differences in vessel shape from the supine position to a fixed angle of bending position. As it is easy to read into the table, not all the authors make the measurement for both the situations. Indeed, for example Wensing et al. (1995) and Ghriallais and Bruzzi (2013) perform the measurement in supine position and then they mathematically calculate the results, with a model, of the bending of the knee in stead of measuring its. The first team do it with a geometric model; on the other side and the second one with a finite element (FE) model.

Author	Year	Imaging Technique	Angle of Measure
Wensing, Scholten	1995	MRI	0° vs Model
Smouse, Ninkanorov	2005	Arteriography	0°, 70° vs 90°
Cheng, Wilson	2006	MRI	0°
Choi, Cheng	2009	CT	0° vs 90°
Cheng, Choi	2010	MRI	0° vs 41.6°
Ganguly, Simons	2011	CT	0° vs 90°
Young, Streicher	2012	Motion System	0° vs 90°
Ghriallais, Bruzzi	2013	CT	0° vs Model
Nikanorov, Schillinger	2013	Radiography	0° vs 90°
Gökgöl, Diehm	2013	3D Angiography	0° vs 70°

Table 4.1: The table wants to group all the different techniques used by literature authors, to avoid the problem of the knee bending.

After this last literature review, we propose our solution of the problem with the construction of a device in nylon. For a clarifying example of the utilization of the device and of the equations that characterize it, the reader should go to Appendix D.1. Concluded this initial part of preparation of the patients, we now are going to describe all the technique used for the acquisition.

4.1.2 Set-up for leg bending: our approach

The main problem that we have to solve is that the CT scan of the hospital Macchi Foundation of Varese, that we use for the measurements of some other cases has a closed gantry entrance. On the contrary the machine of Ganguly et al. (2011), is with a not completed closed ring of measure. The diameter of the gantry entrance of our machine is 67 cm. The first measurement, that is needed to get informations of the vessel in straight configuration is taken with the patients in supine position. We are interested in this step also the get some information about the length, of the bones, of the patients. Those data are going to be useful to fix the patients in the correct position, to reach the required angle of bending of the knee. It is easy to understand, that not all the patients have the same bone lengths. For this reason, we can not use the same static device, as a pillow for example, to bend the leg for all the patients.
In the anatomical sketch proposed in Figure 4.1 we identify three important points, that we use later in this paragraph for the primary analysis of the bending. These three points are the points of junction of the bones of the leg. They are:

- A - the beginning point of the femurs;
- B - the center of the knee;
- C - the malleolus;

As it is easy to understand simply from the image reported in Figure 4.1, it is not difficult to detect the correct position of these three points after the first elaboration of the computed tomography (CT) scan. The determination of these points would be much less detailed if we were not able to use computed tools as this proposed. The three letters in figure correspond to the relative element presented in the list just above.
The very simple sketch, made by hand, proposed in Figure 4.2, is useful to understand the problem in investigation. After we have taken some basic information from the CT images we should have those data to work with:

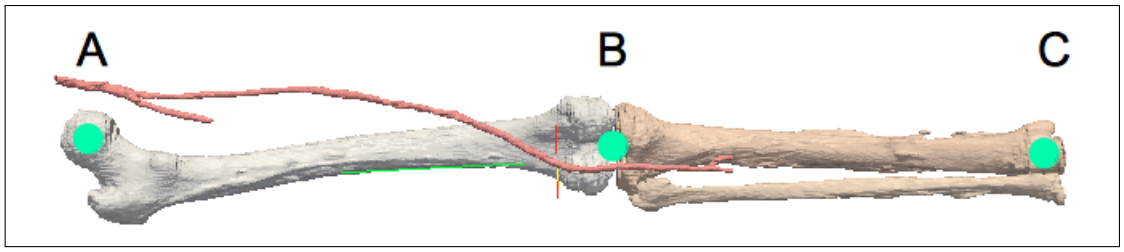

Figure 4.1: Anatomical view of the nodes of interest from the elaboration of the CT images. Nodes A,B,C correspond respectively to the beginning of the femur, the center of the knee and the malleolus.

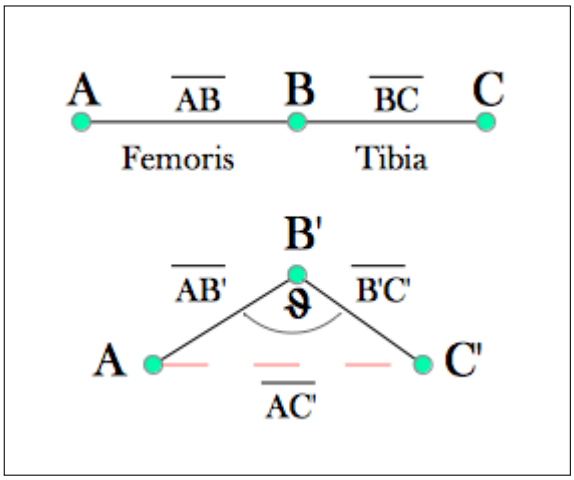

Figure 4.2: Schematic comparison of the configuration of the 3 nodes in extended/bent position, where the three letters correspond to the three joints introduced in Figure 4.1.

- $\overline{AB}$ = length of the superior part of the leg, above the knee, corresponding to the femur;
- $\overline{BC}$ = length of bones (fibula and tibia) of the inferior part of the leg, below the knee, until the feet joint;
- $\overline{AC} = \overline{AB} + \overline{BC}$ total length of the bones considered above;

Now that we get the measures, it is the time to set the angle of bending θ, shown in the sketch in Figure 4.2, to reach the position proposed in the inferior subfigure. This imposition have direct effect on the decreasing of length of $\overline{AC'}$. This decreasing is produced by the bending of the knee. By the increasing of the angle θ the value in centimeters of $\overline{AC'}$ decreases. Because the triangle A$\hat{B}$'C' is not a rectangular one, we can not use the Pitagora theorem. However, we could use in stead of it the Carnot formula, also called the law of cosines. We know that in case of bones, the length of the segments $\overline{AB}$ and $\overline{BC}$ would not change during the bending. Only the positions in the space of the nodes are different; that cause a variation of the segment $\overline{AC'}$ that is unknown a priori. All these consideration are reported in the system of equation proposed here below. To perform the calculation, of the segment $\overline{AC'}$, θ must be given:

$$\begin{aligned} \overline{AB} &= \overline{AB'} \\ \overline{BC} &= \overline{B'C'} \\ \overline{AC'} &= \sqrt{\overline{AB'}^2 + \overline{B'C'}^2 - 2\overline{AB'}\,\overline{B'C'}cos\theta} \end{aligned} \tag{4.1}$$

Now we have an equation useful to calculate the segment $\overline{AC'}$, that is a measure of the bending angle θ, that has to be imposed before starting the analysis. This formula is particularly interesting because we do not need nothing else in stead of the measure of the length of the bones for getting it. A clarifying example regarding this formula is reported in Appendix D.1. In that paragraph is reported also the device that helps the patient to position the leg in the correct angle configuration.

4.1.3 Acquisition protocol

The protocol of acquisition of the image groups all the details that need to be taken into account for the correct collection of medical data. The creation of a substantial protocol permits to compare results, found in different patients, together. For our study we get medical images from two different medical partners: the hospital Foundation Macchi of Varese and the Cisanello of Pisa. The main problem is that the acquisition protocol is decided in each hospital separately and it is not imposed by a common standard. Here below in Table 4.2 we describe some basic features of the protocol used in the Macchi Foundation of Varese. It contains some important aspects, that have to be followed to perform the data acquisition in the correct and repetitive way. After the table, we will qualify some other important aspects that are not reported into it.

Parameter of Acquisition	**Value**
Collimation	0.5x64 rad
Field of view	large
Period of rotation of the gantry	0.4 sec
Thickness of the layer	1 mm
Interval of reconstruction	0.8 mm

Table 4.2: Table including some of the parameters that have to be set for the correct images acquisitions (courtesy of Macchi Hospital, Varese, Italy).

A proposal of acquisition protocol from our clinical partner of Varese is the following: the exam has to include the study of the subrenal abdominal aorta, of the iliac axes and of the arterial vessels of the inferior limbs. The basal acquisition is necessary to evaluate eventual parietal vessel calcifications. Furthermore the basal acquisition is analyzed in combination with the others, with the applying of the mean of contrast. This parallel analysis in necessary to evaluate eventual thrombotic endoluminal appositions, like for example ulcers, dissections or crackings. Done the basal acquisition, immediately after the dispensing of 40 mL of physiologic solution with a flux of injection of 4 mL/sec the mean of contrast is injected. It is administered in a quantity of 120 mL, with the same flux of injection of 4 mL/sec of the physiological solution. The injections are made with an automatic injector double headed.
The arterial phase is obtained with the technique of the bolus tracking, that consists in the placement of the machine on a region of interest (ROI), that is the suprarenal abdominal aorta with a threshold of 100 HU (Hounsfield unity) higher than in the basal acquisition. When this threshold is reached, the arterial acquisition starts automatically. It has to be performed with the patient supine with the inferior limbs stopped in straight position. The venous phase is acquired 90 seconds after the ending of the mean of contrast injection. Between the arterial phase and the venous one, there are 50 seconds where the doctor can come into the CT room and place the device for the bending below the articulation of the knee. Therefore the venous acquisition is done with the patient with the leg bent at a fixed angle.

4.1.4 Technical Data

This section wants to summarize the technical data that characterize the CT scans that are used to get the images from the patients. The first important aspect that we need to stress on, is that all the images we used for the 3D reconstructions, are taken by Computed Tomography (CT) scans. Be able to work on the same data format is a good point of departure to make correct comparisons. The problematic aspect, that we have introduced above, is that the images comes from different hospitals and of course from different scan machines. As it is predictable the two hospital we collaborate use different CT machines. The hospital of Pisa works for the acquisition with a Discovery CT 750 from the General Electric Medical System. On the contrary, the structure of Varese uses a Siemens MedCom CT scan. Another difference is made by the contrast agent used for the images that is not the same.
However there are also a lot of similarities between the two procedures. For example, the dimensions of the images taken. In both cases the format is 512 x 512 pixels. Another similarity consists in the rotation direction of the CT scan that is in all the machines clock wise. Other technical aspects of the scans are reported here below in Tables 4.3 and 4.4. The tables include the most important technical aspects for the different hospitals.

ID Patient	Slice thickness	Dist. source-pat.	Pixel dimensions	Pixel spacing
0 Pre	2.5 mm	538.5 mm	512x512	0.78/0.78
1 Pre	2.5 mm	538.5 mm	512x512	0.78/0.78
2 Pre	3 mm	535 mm	512x512	1.96/1.96
2 Post	0.65 mm	535 mm	512x512	0.65/0.65

Table 4.3: Every line of the table corresponds to a patient dataset: patient 2 contains two datasets because the images were taken in two different moments, before the implantation of the stent and afterwards.

Machine CT	Hospital	Patient ID
Discovery CT 750 GEMS	Cisanello, Pisa	0, 1
Siemens MedCom	Macchi, Varese	2

Table 4.4: It is possible to appreciate the association between the patient ID, instrument used and the relative hospital.

4.1.5 Diagnostic Data

In the previous paragraph we stressed the attention on the technical aspects of the scan machines. Now it is the time to go a little bit deeper in what it is really interesting for us: the patients. In this small paragraph we summarize the principal diagnostic aspects of the cases that we analyze during this work. Those information that are presented in this part are regarding registry and medical data of the patients before the intervention, such the age of the cases, their number of calcifications and the percentage of the stenosis before the intervention. Some of these data are possible to find in the CT files. However, some other are not specified, and only some detailed inspections in the CT permit us to get. Unfortunately only the case with ID 1 carries in its dataset some data about the anamnesis of the patient, such as information about: number of stenosis and their percentages, number of calcifications, Fountain stage of the patient, dysplipidemia, arterial hypertension, smoke, cerebrovascular diseases and creatinine values in the blood. The presence of

these data is very interesting, in a project that wants to analyze the influence of this factors in the vascular diseases. All the data reported in this section should be findable into the dataset sent by the medical partner. In the next section we present some results that we find with the using of mathematical softwares, such as MatLab or Paraview.

4.2 Image treatment

In the previous chapter we introduced the workflow of the operations reported in this chapter. Now, in this section we report the results of the mathematical analysis of the data, performed by MatLab and Paraview. The explanation, as always, is correlated with some illustrative figure we made. During the presentation of the results we will follow the same order defined by the medical imaging analysis workflow.

4.2.1 Preliminary image analysis

In this section we resume the description reported in Chapter 3. It starts with the descriptions of the preliminary image elaboration to improve the quality of the images. We have to say that is preferable that images come from a CT scan than to an MRI or other image machines. This because CT images are surely more detailed, by a smaller pixel spacing. However, CT detection is more invasive because it requires the application of the contrast die. Taking as a point of departure the utilization of a CT we introduce deeper the type of data that we want to get from the scan.
As already fully described in the introduction, the first goal of this work is to analyze, in terms of deformations, the differences in configuration of the popliteal artery. To have a good idea of these differences, we need to get two different set of images from each patient. Two scenarios that can be studied are:

- 1 - evaluation of the differences between a leg vessel in straight configuration, compared to it in the bent one (straight versus bent);
- 2 - evaluation of the differences between a leg vessel before the implantation of a stent, to it during the follow up, after the implantation of the device (pre versus post);

Considering the patient IDs reported in Table 4.3, we have to specify that for patient 0 and 1, we can apply a straight/bent evaluation. On the contrary for patient 2 we are able to study in him only with a pre/post investigation. In this section we discuss mainly about the case straight versus bent because it is the first we collected and it is the one with the best quality images. However sometimes when it is necessary we spend some words also for the other case.
Now we are finally ready to describe completely the procedure of medical image analysis. For a general straight/bent case, the imposition of the leg, with a fixed angle of bending θ, is described in the previous paragraph. The primer step when we receive every dataset is to distinguish the two sets of images, that usually are given together in the same archive file. The resulting two datasets should be able to give a result like the one proposed here below in Figure 4.3. For a clear description, we decided to earmark a paragraph for every important action we do on the datasets. Images and tables are entered below the relative discussion to permit a faster comprehension.

4.2.2 Segmentation

The technique of segmentation permits to isolate the different tissues that compose the legs of the patient. Those tissues are: bones, muscles, vessels and other tissues, like skin. Because we are particularly interested in the vessels, we want to isolate it from the other just listed. This is

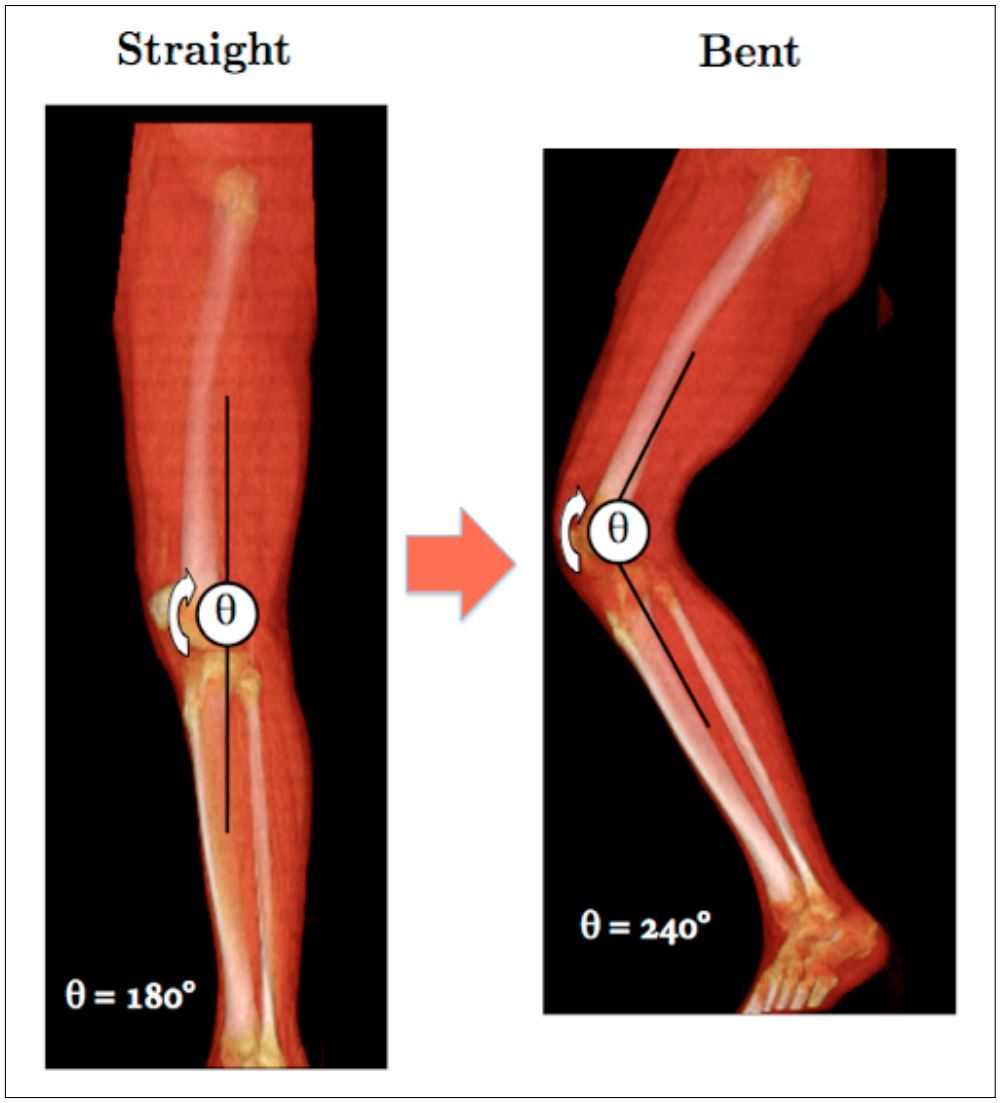

Figure 4.3: Initial comparison between two different positions of the leg: straight and bent (courtesy of Cisanello hospital, Pisa, Italy)

possible, by the elimination of the other tissues. ITK-Snap also in this case provides a specific tools to make it. The complete behavior of the coloring tool is exposed in Appendix A.4. With the tool, it is possible to isolate 3D reconstructions of the instance of interest, save them separately. The instances are saved in files with the extension "STL" (STereo Lithography representation) that can be opened with Paraview. We create an STL file for each of the six different parts of interest: femur, fibula, tibia, vessel and the muscles of the popliteal fossa, leg boundary; then we also create an STL file with all the parts together, used for the visualization of the patient situation.
In the Figure 4.4, we report an example of the result of a segmentation. The image shows the 3D reconstruction of the area around the knee junction. The data are from the Cisanello hospital, Pisa, Italy. Another segmentation example that we want to show is reported in Figure 4.5. This time the data are collected from a patient of the Macchi Hospital, Varese, Italy. The comparison has the goal to show that the registration operations is a repetitive procedure, and it does not to be made ad hoc for each particular case. Furthermore, the reader can see that the images in Figure 4.4 has better resolution compared to the resolution of the case depicted in Figure 4.5.

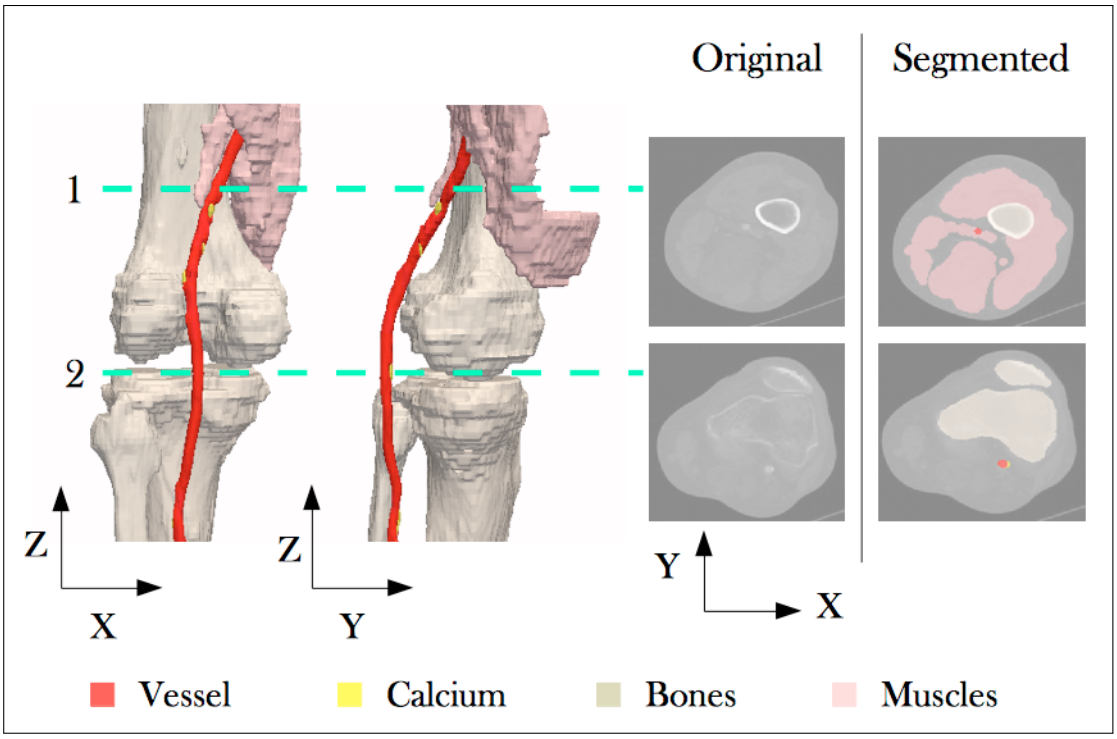

Figure 4.4: Results of the 3D segmentation of the images provided by Cisanello Hospital, Pisa, Italy. Together with the images of the 3D reconstruction of the knee joint area on two different planes, the figure shows the processing of the segmentation coloring filter applied with ITK-Snap.

4.2.3 Registration

The next stage of the analysis is the registration of the bones. It is fundamental to be able to compare data from the same patient acquired in different configurations. The registration consists in a rigid roto-translation of objects in the space, taking as a reference another feature it permits us to compare data of the poplitea, acquired in the two leg situations introduced before. The registration has to goal to treat together object in different configurations, such as the vessels. We know since Wensing et al. (1995) publication, that the popliteal artery changes dramatically its shape during the bending of the leg. The comparison of the data before and after the bending, by the registration, permit us to evaluate this change. In Figure 4.6 we try to show, in the best way, the help that the registration gives to the analysis.
The poplitea artery, that is situated behind the knee articulation, begins out from the adductor channel, of the tendon arch, of the soleum muscle, that is the anatomical part proposed in Figure 4.6 in pink in both the subfigures. In the figure we report in the left part of it, the leg in the straight configuration, with the poplitea colored in red. In the right part, we have the leg in the bent position, with the popliteal artery in blue. This choice was made to highlight the differences between the two vessels after the registration. The comparison is better proposed in the magnification box.

4.3 Centerline analysis

In the previous chapter we introduced the concept of centerline. We also introduced the information obtainable from the analysis of it. If the segmentation and the registration of the vessel is done in the correct way, we can go on through the further step of the workflow. The calculation of the

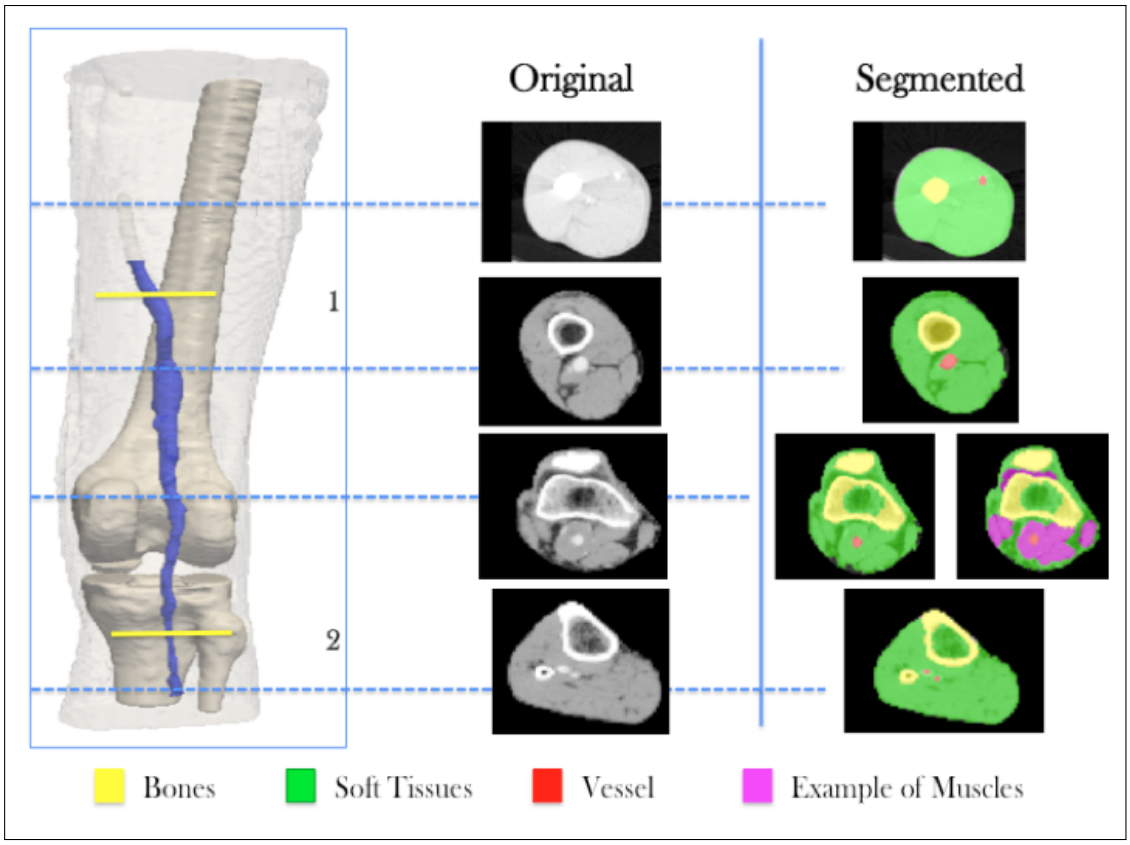

Figure 4.5: Results of the 3D segmentation for the images provided by Macchi Hospital, Varese, Italy. The procedure is the same described in Figure 4.4.

centerline can be performed with the software VMTK. All the code we use with the software are reported in the Appendix B. The centerline dataset, that we get with VMTK from the STL of the vessel has 20 columns of data. These columns contain different features of the centerline. For instance, there is a column recording the measurement of the curvature of the centerline; another containing the values of the radius of the maximal sphere, that can be inscribed into the vessel in that section. Other fundamental columns are the ones that contain the values of the three cartesian coordinates of the nodes, that compose the centerline in the space. These data are fully analyzed for different purposes in our discussion later.
The measures calculated on the centerlines were introduced in Chapter 3. To make the calculation of the measures faster, we design a very simple MatLab GUI (Graphical User Interface), that makes automatically the calculations and prints the results for a given patient dataset. For a full description of the GUI the reader has to go to Appendix C. The interface contains also the methods for the calculation of the data described in the next paragraphs.

4.3.1 Vessel radius analysis

As we introduced before, the radius of the centerline is already present into the dataset after the calculation of the centerline with VMTK. The only thing we have to do for the radius data is to plot them in the correct way to be able to compare the data from different sets. This is the idea of the results shown in Figure 4.7. The figure has the goal to evaluate the differences in the radius profiles before and after the implantation of a stent (pre/post configuration). The slice thickness of

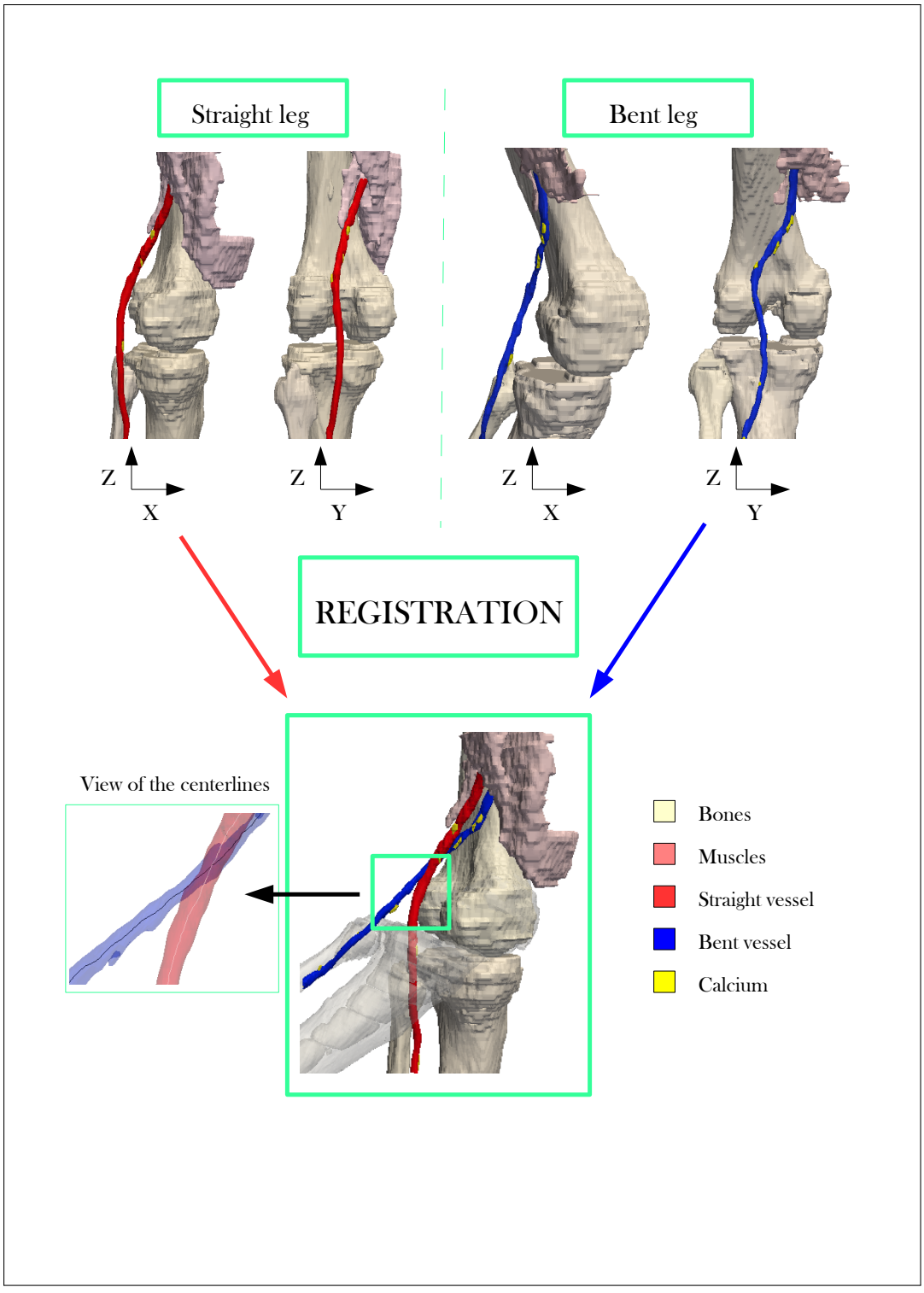

Figure 4.6: Scheme of the registration starting from the two cases of study, straight leg, on the left, and bent leg, on the right. On the bottom the result of the registration and on the left, a magnification of the centerlines.

the dataset is 2.5 mm. The data proposed are readable with the help of the colored legend, placed next to the figure. In the graphs, the X coordinate reports the values of the radius of the vessel expressed in [mm]. The Y one reports the centerline length expressed in [%]. The first two purple lines show the limits of the area of maximum radius, where the aneurysm is present. The third purple line shows the limit of the stent placement in the post configuration. The center subfigure permits to evaluate the dramatic increasing of the radius in the profile plot that possible leads to an aneurysm in the patient. This increasing is much less visible after the implantation of a covered stent. This is another proof of the past presence of an aneurysm.

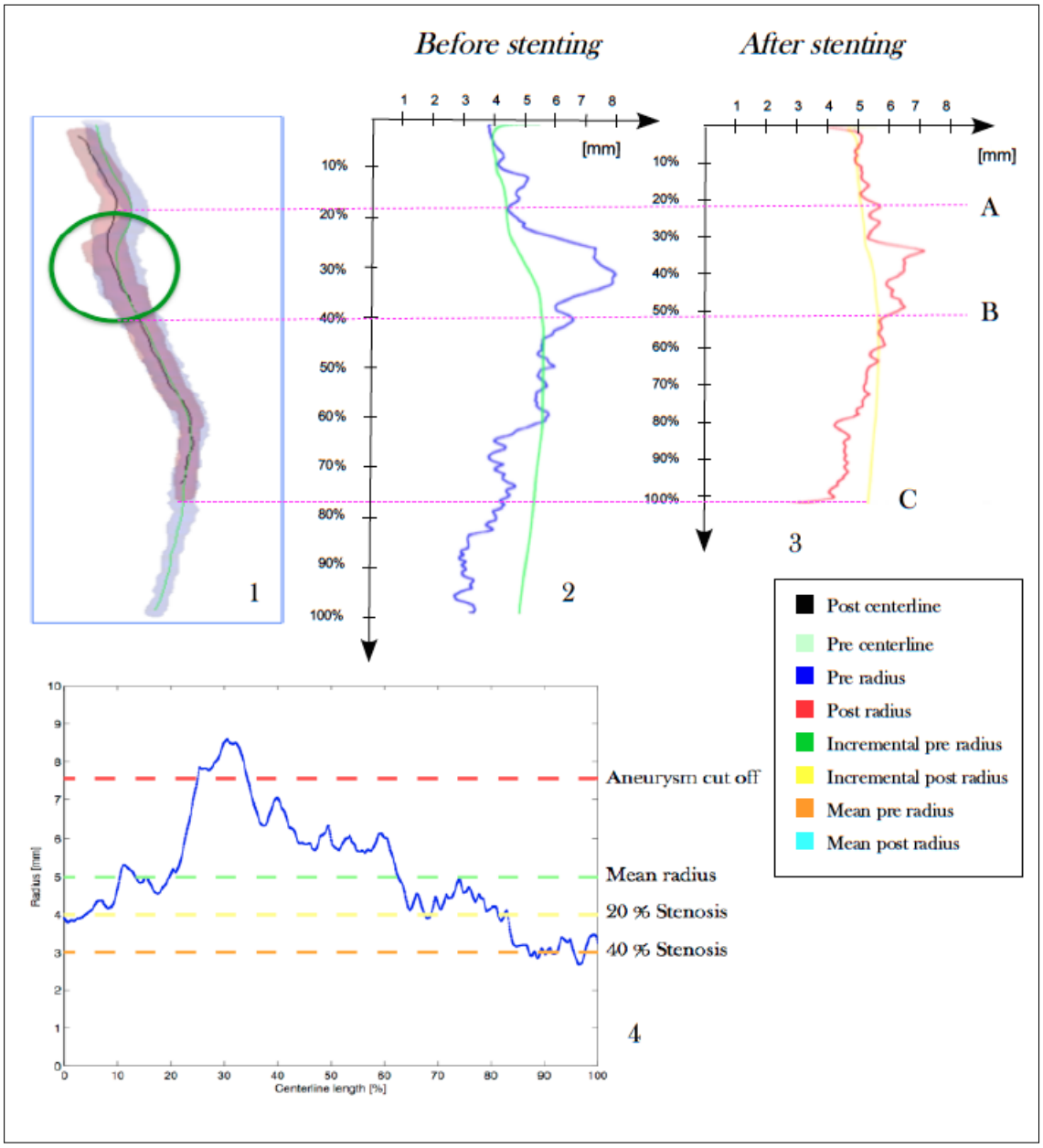

Figure 4.7: On the left part of the figure we show the evaluation of the radius profile for both configurations (before and after stenting). The violet borders (A-B) are the limits of the area where probably the aneurysm is more likely to be. The third line (C) is the limit of the stent implantation. The second subfigure on the right focuses on the previous configuration radius profile.

The evaluation of the aneurysm presence is easier isolating the subplot containing the radius profile as done in the right part of Figure 4.7. We know from literature that a correct mean value of radius for the popliteal artery is around 5 mm (Tarini (2010)). We consider as a value of coherent cut off for aneurisms an increment of at least the 50% of the radius of the vessel.

4.3.2 Evaluation of the curvature

As we already introduced in Chapter 3, the calculation of the curvature gave us some problems. The dataset of the centerline contains the curvature values for every nodes, but the measures are too much jagged to be utilized. For this reason, we calculate the values of the curvature with a method based on the regression curves. The method is fully described in the Appendix A.3. It permits us to detect the points of maximal and minimal curvature of the vessel. The points of maximal curvature, as said before, are the points where the probability of stent rupture is higher. They need to be detected. The coordinates of those points are easily obtainable with MatLab. In this paragraph we only report the results found with the script. When we get the coordinates, we put them into the visualization software Paraview, to see if they are always in the same position for both the vessel configurations. An interesting example of the utilization of this technique is reported in Figure 4.8. The results of the curvature method script is a vector containing the curvature of some sampled nodes of the centerline. The more the sampling is thick, the more the result plot is noisy. The Figure 4.8 wants to be the ideal conclusion of the work of centerline analysis. The user after the collection of the datasets and their elaboration wants to reach the knowledge of some results:

- the coordinates of the points of maximum and minimum radius; that are fundamental in case of presence of aneurysms for the first and stenoses for the second;
- the coordinates of the points of maximum and minimum curvature of the vessel; the point of maximum curvature is the more probable point where the stent rupture happens caused by fatigue;
- the radius profile of the two configurations, that is plotted in different graphs;

4.3.3 Shortening

The last main measurement we make on the vessel centerline is the shortening. From the calculation of the vessel length in the two cases of analysis, the calculation of the shortening is immediate. The shortening gives a clear measure of the changing in length of vessel, during the bending of the knee. It is expressed in percentage with a positive value when the second configuration has a lower length compared to the first one. To evaluate the robustness of our results we compared it with the measures of length and shortening found in literature, and introduced in Chapter 2. An exhaustive remark about the technical aspects of the shortening and the comparison with literature cases was done in Chapter 3.

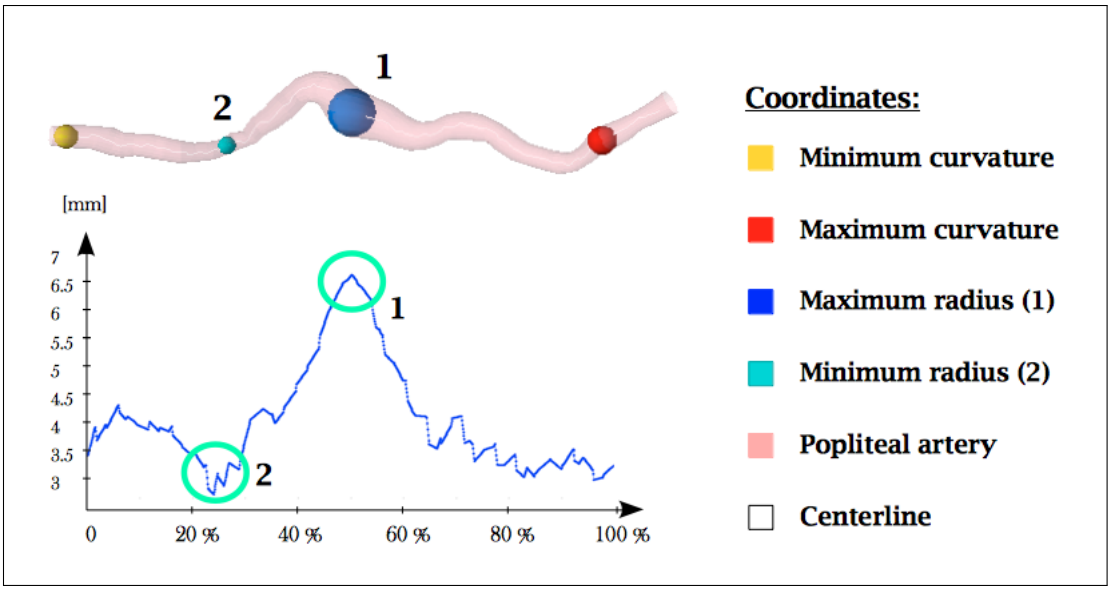

Figure 4.8: The figure tries to group all the important features of the centerline analysis, such as the points of maximum and minimum radius and curvature. Furthermore it reports a profile of the radius of the vessel showed in the top part of the figure. The graph expresses the relationship between the percentage of the vessel length and the radius in that point.

4.4 General remarks

This chapter is the first one completely dedicated to the explanation of some of our results. The weakness of this work is surely the small number of cases available. A good geometrical analysis of the features needs a bigger sample to get stronger results. However, the basic goal of this part of the work is not to find interesting results in patients, but more to create a steady workflow that permits the fast collection of data of further patients to make in the future a good database of the topic.

Chapter 5

Reconstruction of popliteal kinematics

The present chapter is dedicated to the explanation of our method of reconstruction of the popliteal kinematics during knee bending. The goal is to create a model that can be analyzed in terms of the kinematics. To do that, we have to import the vessel in a 3D FEA (Finite Element Analysis) software. The software we choose is Simulia Abaqus 6.12, of Dassault Systems, France.
Starting from the centerline it is possible to reconstruct the original vessel by the remeshing of it with techniques of sampling and interpolation. In this chapter we are going to describe the steps in order to get a good 3D FEA model of a vessel. The point of departure is its centerline.

5.1 From the centerline to the meshed vessel

The best software to use for the 3D reconstruction is MatLab. We prepared another interface, to automatize the steps that we are going to describe in the chapter. The GUI is completely described in Appendix C. Also this interface needs some graphics implementation to be used in real analysis. However, it is useful to make the data insertion easier. Furthermore it helps the visualization of the results.
This section is dedicated to the description of all the steps we need to get to the final input file result. The chapter will end with the explanation of each of them. Starting with the work, the first fundamental step is to convert the STL (or VTP) files, containing the centerline data, with a readable file for MatLab, such as a CSV (Comma Separated Values) file. This step was done with Paraview, the viewer software introduced in a previous chapter; however, it is possible to use lots of other softwares to do that.
Before the technical description of the steps, we want to explain in simple words the idea we applied. As we know the centerline is a line and the vessels have a structure cylindrical shape. Starting from the beginning of the centerline in the Z coordinates, we take the value of the vessel radius in that node. By the knowledge of the radius we create a discrete circumference of a fixed number of nodes that can be arbitrary set by the user. This circumference is placed around the first node of the centerline. Its orientation is the same as the centerline node one. Now that the first section of the new vessel is created, we move to the second node of the centerline. Here we do the same operation taking the correct value of the radius in that node, from the dataset. Now we have two different circumferences oriented in their correct direction in the space, and placed around the two first centerline nodes. We take a node of the first circumference and the relative

nearest node of the second one, and we connect them, creating an element. We make the same action for the n nodes of the circumference, and we finally get our first n-connecting element. Repeating these actions for all the sampled nodes of the centerline we get our new 3D vessel. This vessel is very smooth compared with the first model extrapolated from the CT. In Figure 5.2 is possible to appreciate the differences in smoothness between the two objects. Those actions lead to the realization of a model of vessel based on a real centerline. With this technique we are able to create a consistent new vessel for all new two configurations we need.
The problem now, that we have to face, is that the vessel needs to be tested with the insertion of a stent into it. In reality it is completely possible to insert a device into a bent vessel, or at least not linear one. This operation is not directly possible with a software. The problems born when the stent touches the vessel wall of the 3D model. In reality the stent would sweep on the vessel wall and go on into it. In the software situation this sweep is not immediate or even often not possible. It needs, when applicable, a huge definition of border conditions. To solve this problem we use an intelligent simplification of the case. We ideally pull the vessel until it becomes completely linear, when it reaches this position we are then able to place the stent into it. The linear model is created from the knowledge of the beginning and the ending node of the centerline. Taking the segment that connect this two nodes and dividing it in a fixed number m of intervals we find a fixed number *(m-1)* of internal nodes. The number *(m+1)* of nodes need to be equal to the number n of nodes taken with the sampling of the real vessel centerline. At the end of the setting of the parameters and of the writing of the input file we will have *4+p* different model instances of the centerline in analysis. Here below we report the models in the list, with some details that characterize them:

- *simple straight case* → this model has a fixed radius of 4 mm, or at least a bigger value compared with the measure of the stent radius. It is the very first model and we use it as point of departure of a test for a simple case of compression. In Chapter 7 the stent will be inserted into the remeshed vessel in this configuration;

- *crimped straight case* → model with a fixed radius of 0.85 mm. This model simulates the crimping of the stent, before the implantation into the real vessels. This action corresponds to the crimping that the stent is intended by the catheter before the implantation in the ill vessel. In this cases we are able to analyze the forces that acts on the inner surface of this cylinder shape;

- *simulation of the vessel in straight configuration* → with this model we reconstruct the vessel in the straight configuration. Using the technique of the sweep introduced above, we create an Abaqus readable input file of the vessel in the straight position. The radius this time, of course is variable. As explained above we take the data of the radius into the dataset from the medical partner;

- *intermediate configurations* → we create a variable number of p intermediate configurations, between the straight and the bent configurations in order to analyze in a deeper way and with more data, the results of the simulations;

- *simulation of the vessel in bent configuration* → the procedure of the definition of this instance is the same adopted in the straight configuration case;

We know that the list just presented above is not specific enough for the reader, so we report all the objects described in the list here below in Figure 5.1. In the figure, all the subfigure are marked with letters A and B, that are the points of beginning and ending of the popliteal artery. Furthermore, there is also a number in each subfigure that is the step number:

- *1* → simple straight case;

- *2* → crimped straight case;
- *3* → simulation of the vessel in straight configuration;
- *4-8* → intermediate configurations;
- *9* → simulation of the vessel in bent configuration;

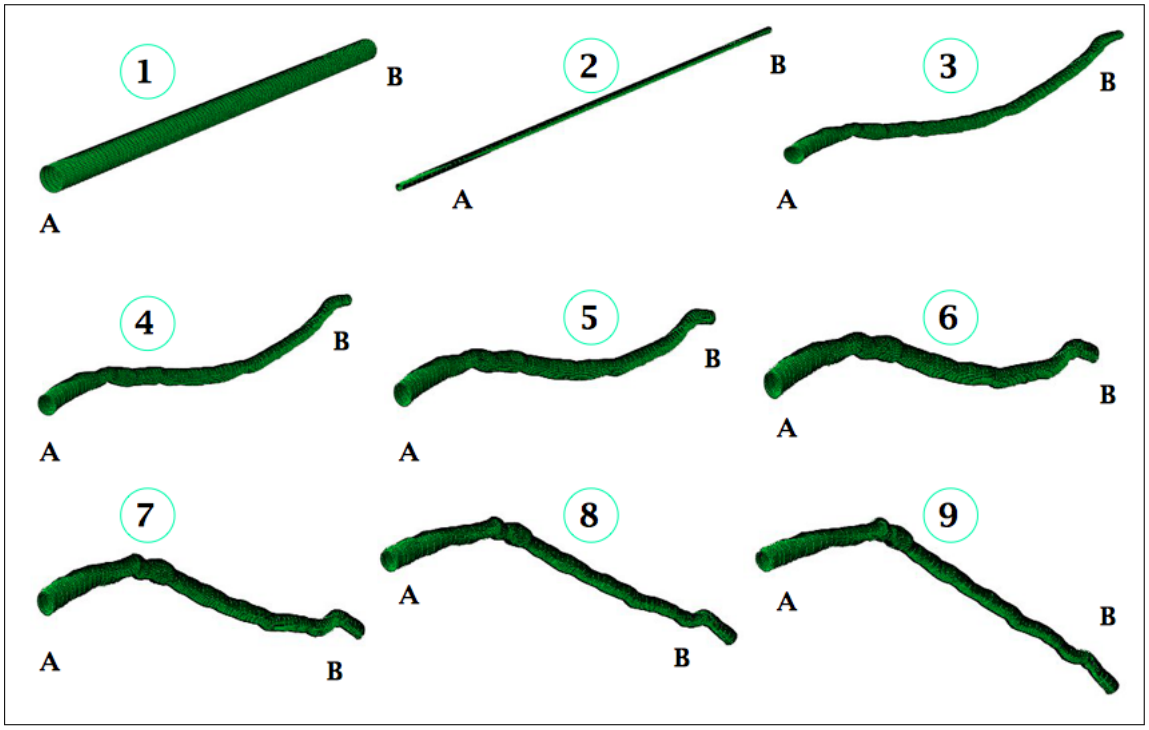

Figure 5.1: The figure shows examples of vessel remeshing. Here are reported all the configurations of the vessel that we are going to analyze, beginning from the simple straight case (1) to the simulation of the vessel in straight (3) and bent (9) configuration. The cases (4-8) are the intermediate configurations. Number (2) is the crimped straight case.

The method is based on the spatial orientation of the versors of the objects. As we said above we consider as object of interest the elaboration of the sections of the catheter defined by the meshes. Every sections need to be orientated correctly in space in according to the vessel reference coordinate. The idea is very simple: we consider the versor in the Z direction of the centerline as the reference for the sampling, and we apply this Z direction to the relative sampled circle of nodes. Then we take a generic point in space and we calculate its projection in the plane where the circle lies. The direction of the connection between the projection of the generic node and the center of the circle is defined by a versor that lies in the plane. With the scalar product between this new vector and the first one we found we get the second vector of the tern we are looking for. Now as we know from the simple geometry, the third versor is perpendicular to the other two of the base and is calculable with the scalar product of the two versor just defined. Now that we have the direction we can apply it to the object we want to rotate. With this technique it is possible to have 3D vessel instances, with a radius that changes in every node of the centerline according to the real data.

5.2 Vessel Design

If the script for the stent design is correct, it would create two main results: a testing catheter file and an input model for the analysis. The former is only a visualization object, that is useful to control that the vessel definition works correctly. The result is perceptible in Abaqus and consists in a simulation of the transition of the model into all the instances showed above, changing progressively its features and node positions. An example of a correctly remeshed vessel model is proposed in Figure 5.2. In Paraview, as said before, it is possible to directly match the results of the remeshing with the objects from the CT, simply overlapping the two instances. The second file created with the script is a input file ready for the simulations. This object is the one that will interact with the stent to simulate the implantation of the correction device. This topic is better explained in Chapter 7.

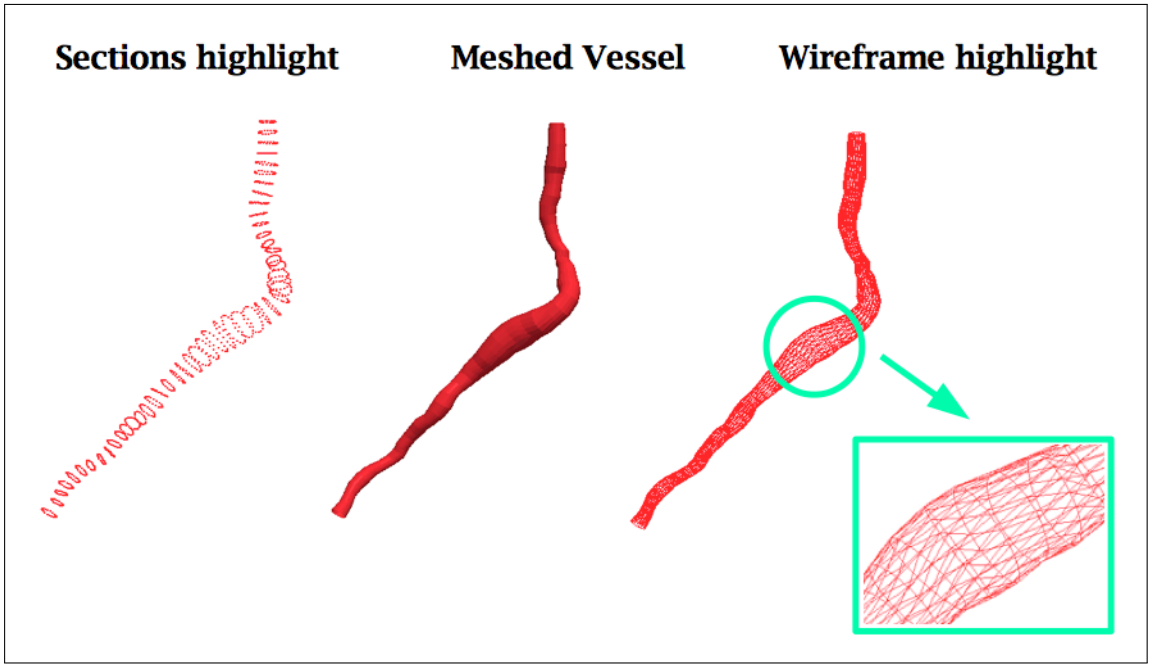

Figure 5.2: Presentation of the results of our remeshing method. Different visualization option of the STL results are shown.

5.3 Graphical User Interface (GUI)

Again for this routine we tried to make the job as automatic as possible. For this reason we created another very simple GUI, to automatize the necessary steps. The complete explanation of the interface is proposed in Appendix C. The generation of the mesh of the vessel is based, as presented above, on the redefinition of the mesh of the vessel by a technique of interpolation, that needs some parameters in order to work. Three are the parameters needed in order to make the GUI working properly:

- the number of nodes in the circumferential direction of every sections, from the radius;
- the number of nodes that composes the centerline, from the technique of interpolation;
- the number of intermediate steps, between the straight and the bent configuration, that gives the total number of frames of the simulation model;

The graphical part is easy to interpret, because it needs only these three parameter to start. However the work behind the graphical mask is quite relevant. The creation of the sections, that corresponds to the circumference explained above, is quite simple, but the calculation of each section orientation is delicate, as unfurled in the previous paragraph, it needs a lot of computational time.

5.4 Conclusion and evaluation of the quality increasing

The technique of remeshing described in the previous paragraphs, permits to get a smoother profile of the vessel studied. Indeed the main problem of the STL object got from the CT is the tortuosity of its superficial profile. The tortuosity is a consequence of the technique of 3D reconstruction, which is not able to connect in a linear way two different slice sections of the images. Obviously the remeshing could hide some peculiar features of the vessel profile, but in general it gives a brilliant result easier to use in the simulations. Furthermore also the mesh that comes out from the remeshed model is very smooth compared to the previous one. A complete comparison between the two kinds of meshes is proposed here below in Figure 5.3. The figure shows in blue the features regarding the model that we obtained directly from the CT, and in red the ones of the remeshed object.

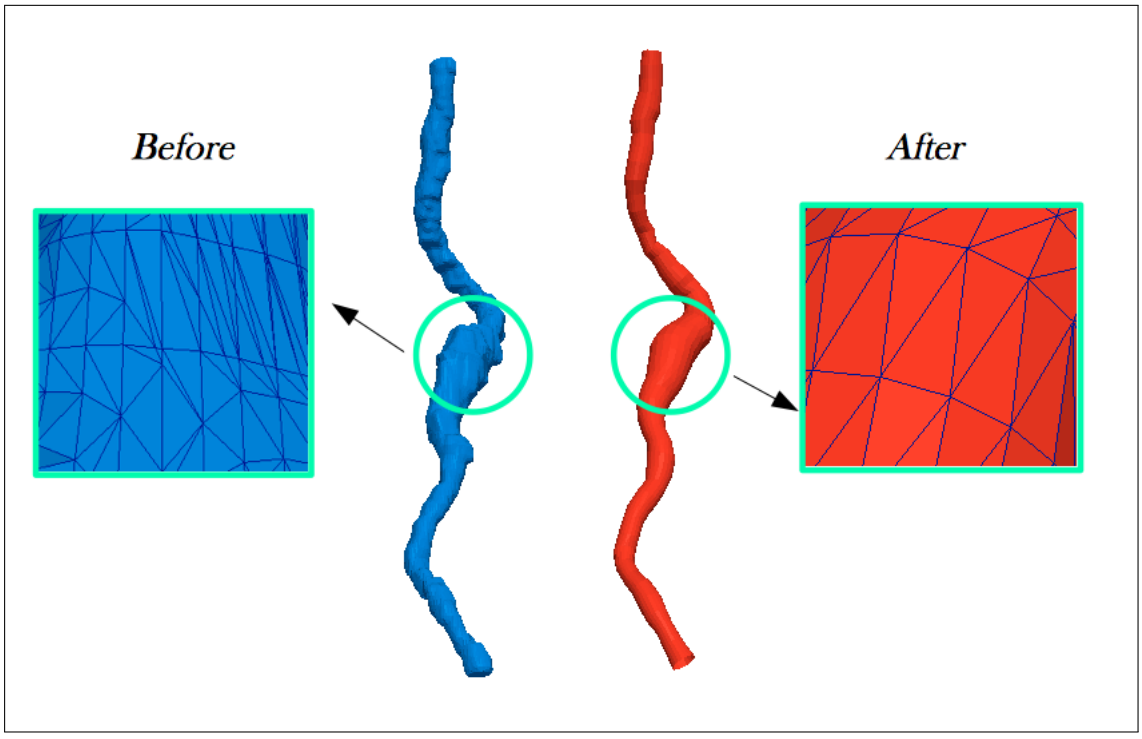

Figure 5.3: Comparison between the results from the 3D reconstruction of the CT in blue, and after the application of the remeshing filter in red. In the magnification boxes we can appreciate the mesh designs.

Chapter 6

Stent model

At this point of the work we have already applied the vessel model to the finite element software Simulia Abaqus 6.12. The step that follows the workflow reported in Chapter 3, is the design of the stent. Then the stent will be put into the vessel for the various simulations. Notice that the stent shape has been designed with MatLab. Our stent model aims at resembling the design features of the a read peripheral stent, i.e., the Viabahn of Gore. In this chapter we are going to describe all the actions that need to be done in order to get a proper input file containing one correct oriented stent, ready for the simulation. Firstly we are going to spend some words about the second generation stents, and in particular about the Viabahn, since it is our reference's model and, more precisely, about its mechanical properties which are the ones we want to reproduce later on.

6.1 Introduction to the stent

Catheters and balloons are the basis to be able to make an implant of stenting in the ill area of the body to heal. The first application of a coronary catheterizing in the modern age date back in 1929 by the doctor Werner Forssmann in Germany (Goerig (2008)). The intervention has been performed on his own antecubital veins in the right atrium. The first intervention on an awake patient has been performed in 1977 (Mueller (1995)).
The state of the art foresee now second generation stents but there are already projects about the improvement to the third generation ones. We will consider as point of reference the second generation one. We do not consider third generation stents because their development is still deeply in progress. To complete the description we are going to spend some words about the general characteristics of the stents we are going to use.

6.1.1 Muller-Hulsbeck results

This paragraph reports the results of the work of Muller-Hulsbeck et al. (2010) where the authors make a comparison between seven types of stents, available in the market. The goals is to understand which shape's model is more probably affected to chronicle stent rupture. Before discussing the technical aspects of the analysis is interesting to report immediately one of their results. They found that self-expanding stents do not show beneficial effect if the lesion is shorter than 5 cm. Unfortunately with longer stented segments the incidence of stent fractures appears to rise. Scheinert et al. (2005) report that the fracture rates for today's commercially available designs differ widely from 1.8% to 18%.
Many self-expanding stents share the same basic construction: the stents are laser-cut from a

nickel-titanium alloy tube, and the surface of the stent is electropolished, to make it smooth and corrosion-resistant. The basic stent design consists in a repeating pattern of zigzag units linked together. Some sketches of the device models reported also in the work of Muller-Hulsbeck et al. (2010) are depicted in Figure 6.1. The geometry of the zigzag or peak-valley design differs among models, as well as the bridges or transition zones connecting the zigzag elements. The cell size depends on the number of parallel peak-to-valley areas and the number of connections; fewer bridges between zigzags make the stent design more open and flexible. The authors make several fatigue tests, such as bending, compression and torsion to study the result of the various choices in commerce. The test is made both with the FEA and by fatigue testing. This aspect is very important because they are able to evaluate the differences between the results from the real models and the predictions of the FEA software.

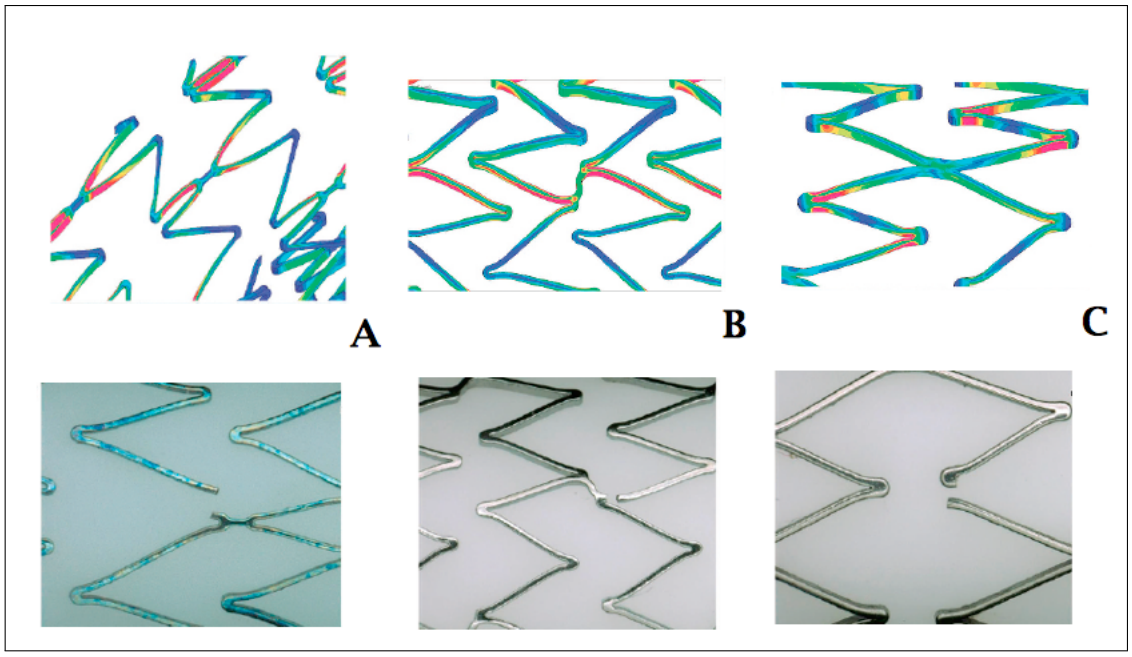

Figure 6.1: Comparison of different stent-unit shape, for each of the three models (A,B,C), the upper subfigure contains the FEA model of the real stent reported below. All the stents have been taking up to their rupture point.

6.1.2 The forces that interests the stent

The stent is a device that needs to be quite resistant, because it is subjected to forces of various nature. It is inserted into the vessel and so the first source of possible damage is surely the blood flow with its vorticity. Another problem is to take int account the muscles forces, that are surely another important aspect for the kinematics. However all the forces can be grouped into the main four stresses that are proposed in Figure 6.2.

6.1.3 The Viabahn of Gore

The stent we decide to reproduce for our analysis of the vessel kinematics, is the Viabahn of Gore Endoprosthesis, depicted in Figure 6.3. The GORE VIABAHN Endoprosthesis is constructed with a durable, reinforced, biocompatible, expanded polytetrafluoroethylene (ePTFE) linearly attached to an external nitinol stent structure. The flexibility of the GORE VIABAHN Endoprosthesis

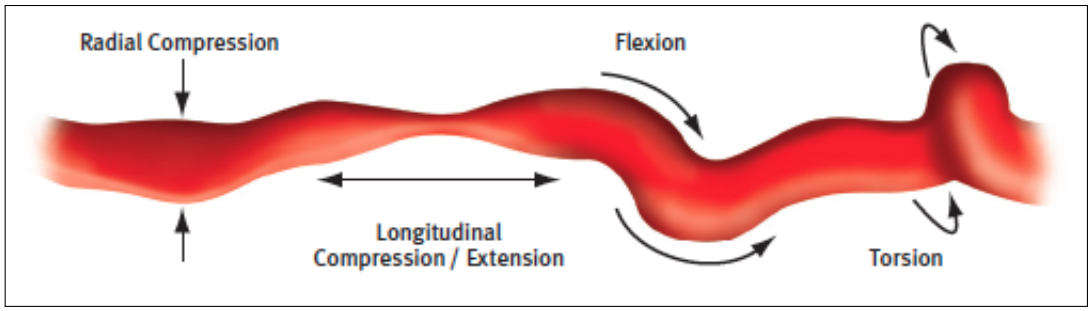

Figure 6.2: The sketch reports the four types of forces that can be applied to the stent: radial and longitudinal compression / extension, flexion and torsion.

enables it to traverse tortuous areas of the SFA and conform closely to the complex anatomy of the artery. W. L. Gore & Associates has now added a heparin-bonded surface to the GORE VIABAHN Endoprosthesis. The GORE VIABAHN Endoprosthesis with Heparin Bioactive Surface is the only device of its kind approved for both the SFA and iliac artery. The stent-graft features the addition of proprietary heparin-bonded technology to the proven combination of ePTFE and nitinol. End point covalent bonding keeps heparin anchored to the endoprosthesis surface, while the bioactive site remains free to interact with the blood. All those information has been taken from the website dedicated to the device (Gore (2014)).

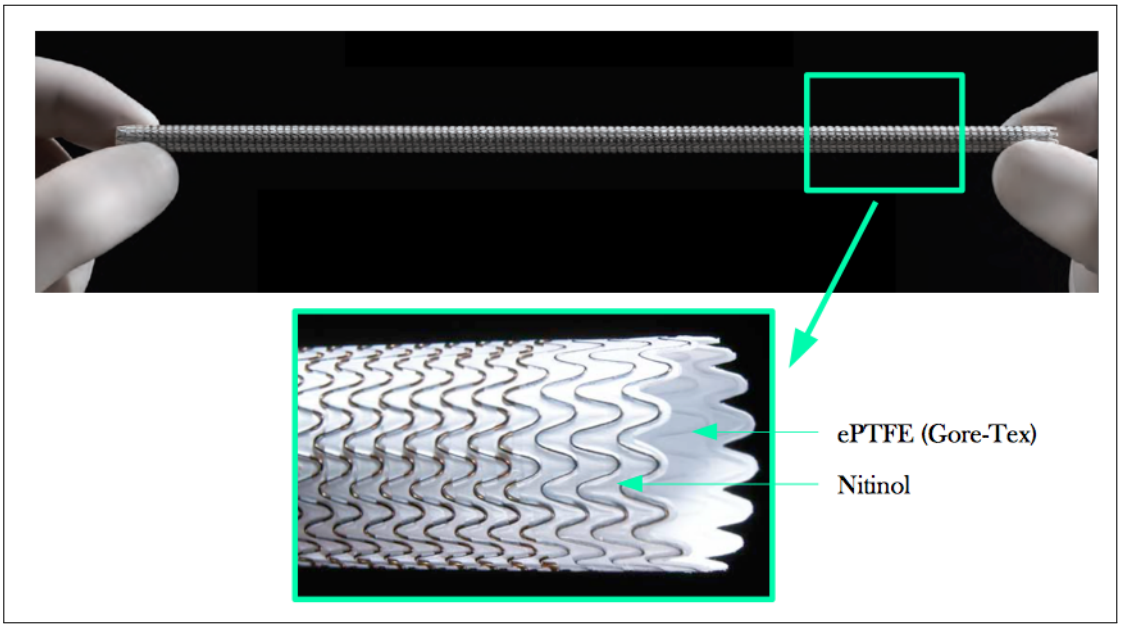

Figure 6.3: The Viabahn of Gore, in the magnification box its mesh profile.

6.1.4 The materials: ePTFE and NiTinol

The superficial layer that covers internally the stent is ePTFE also known as Gore-Tex, a waterproof/breathable fabric membrane, and a registered trademark of W. L. Gore and Associates (Wikipedia (2014)). Gore-Tex materials are typically based on thermo-mechanically expanded PTFE and other fluoropolymer products. They are used in a wide variety of applications such as high performance fabrics, medical implants, filter media, insulation for wires and cables, gaskets,

and sealants. However, Gore-Tex fabric is best known for its use in protective, yet breathable, rainwear. Gore-Tex is also used internally in medical applications, because it is nearly inert inside the body. In addition, the porosity of Gore-Tex permits the body's own tissue to grow through the material, integrating grafted material into the circulation system (Bowden (2013)).
The other material that compose the stent is Nitinol, a metal alloy which combines Nickel and Titanium (NIckel TItanium Naval Ordnance Laboratory), where the two elements are present in roughly equal atomic percentage.

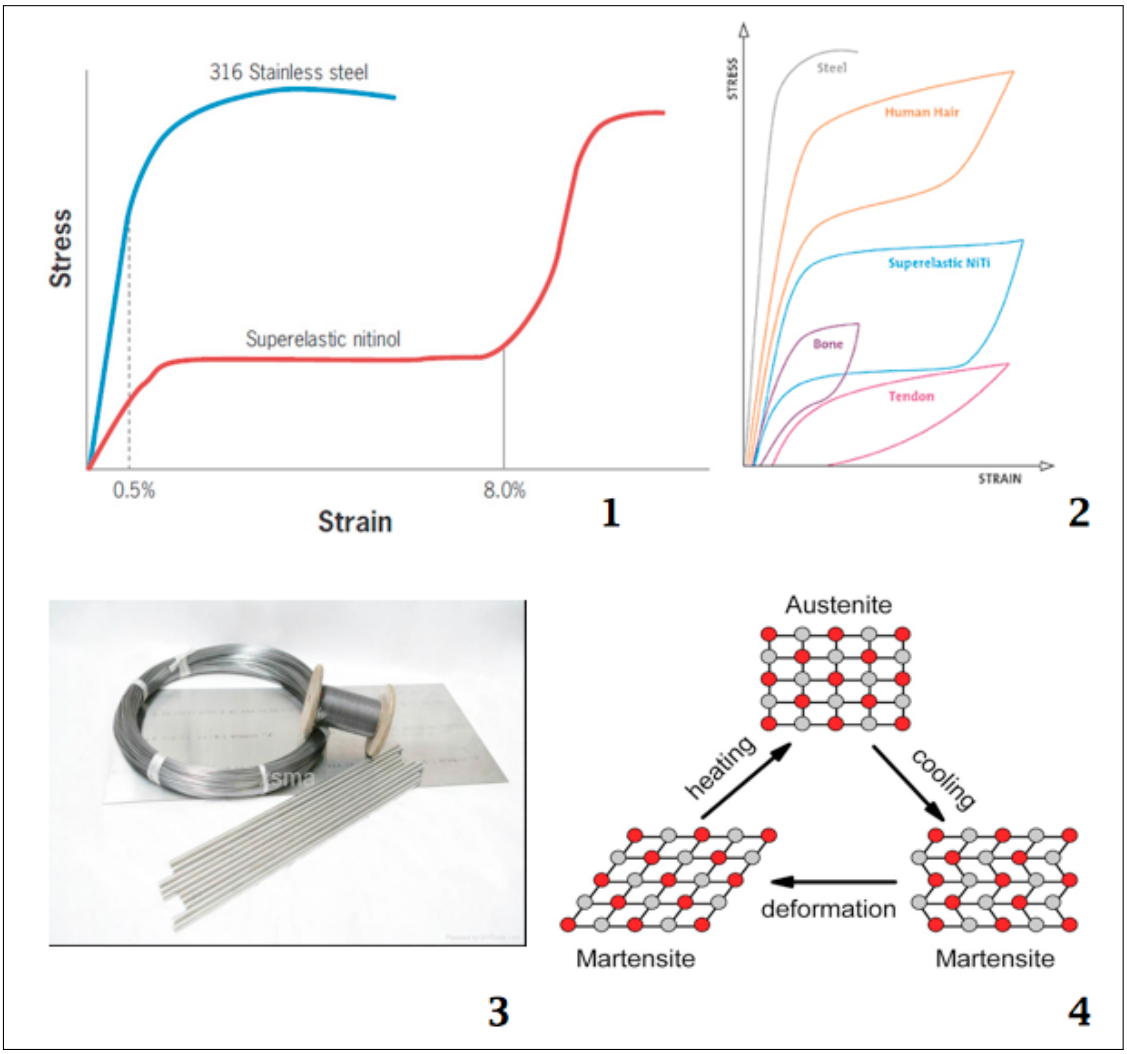

Figure 6.4: In this figure we have grouped some features of the Nitinol. From the top left (1), a plot of the curve Strain/Stress of the Nitinol compared to the 316 Stainless steel one; (2) the sale curve compared to other materials of the human body, the plot wants to stress the attention on the hysteresis characteristic of the material; (3) some examples of a common use of the material (courtesy of Design (2013)); (4) a schematic explanation of the transition of the material between Martensite and Austenite.

The number, that follows the specific name of the material, indicates the percentage of titanium of the composition (ex. Nitinol 60 is 40% made by nickel and 60% made of titanium). Nitinol alloys exhibit two unique properties that are closely related: shape memory and superelasticity, called also sometimes pseudoelasticity. The shape memory is the ability of a material to undergo

deformation at one temperature, then recover its original, undeformed shape upon heating above its transformation temperature. The superelasticity occurs at a narrow temperature range just above its transformation temperature. To get the superelasticy it is not necessary to warm the material to cause the deformation recovers. With this conditions the material exhibits enormous values of elasticity. The behavior of the material is shown below in Figure 6.4. At high temperatures, nitinol assumes an interpenetrating primitive cubic crystal structure, referred to as austenite. At low temperatures, nitinol spontaneously transforms to a more complicated monoclinic crystal structure, known as martensite (see the last plot of Figure 6.4). Important values to report about NiTinol are: its density, evaluated around 6.45 g/cm^3 and its elastic modulus of around 80 GPa for the Austenite and around 30-35 GPa for the Martensite, while the Poisson's ratio is 0.33.

6.2 The construction of our device model

Now that we have introduced stents and their general behavior, it is possible to better describe completely our model. Here in this section we are going to present all the steps needed to get the final result. Every important action will have a specific paragraph correlated, when available, with a figure. At the end of the chapter the stent is going to be ready for the contact simulation analysis with the catheter. In the Appendix C the automatization about the stent creating which was implemented also in a MatLab interface. The interface needs only two parameters to work, such as the stent length and the stent diameter. The diameter is set by the user manually. For the length we exploit the MatLab tool "ginput". It permits to choose the points in the plane with the cursor, and it gives back the coordinates of the points after their selection. In particular we need for our model two 3D points: those points are chosen on the plot of the vessel of the patient. The first point chosen is the point where the stent has to begin, after its placement. The second point is the inferior limit of the stent. Knowing these two points we deduce the exact length of the stent to insert. Here we have to specify that the measure of the length of the stent is not calculate by the simple subtraction of the coordinates of the two nodes. That calculation would be wrong, because it considers the vessel as a straight object. So for the calculation of the stent length we have to exploit the information contained in the centerline of the vessel to heal. Taking the starting point and end chosen with ginput, we evaluate which is the nearest node, of the centerline, to this selection. The calculation is now made on the centerline just selected by the evaluation of the distances of these two nodes. The measure is corrected in order to reach an integer number of ring of the mesh because the number of ring is calculated as the stent length in millimeter divided by 1.66.

6.2.1 Choice of the shape and creation of the stent

The choice of the unit shape is the first fundamental decision to make for the design. The unit shape is a characteristic basic configuration, that is going to be repeated lots of times in the stent mesh. We based our choice on the work of Muller-Hulsbeck et al. (2010). As starting point they described different stent shape and they predict what should be the best one. The hypothesis of the Muller-Hulsbeck et al. (2010) are in concordance with the shape of the Viabahn of Gore, a second generation stent that have been introduced in the previous section. The reason why we decided to create our personal stent along the line of the Viabahn is because it is the stent that has been implanted into the patient of Macchi Foundation, Varese. This is the only case where we have medical images of both before and after the stent implantation. So we want to compare the results, in terms of vessel kinematics, after the stenting, both in the real case and the FEA case. Because the explanation of the unit shape it is quite difficult, we reported below in Figure 6.5 all the characteristics of our model. The shape is based on the sinus function of a wave, where the

amplitude and the frequency in the unity space, of the wave, are set by the user. A fixed number of unity elements of the mesh, creates a ring. For example for a stent with a sagittal diameter of 6.5 mm, we put 9 unity elements. The stent is composed by a series of consecutively rings. The number of rings depend on the length of the stent. Also here we can report as an example, that a stent of 15 cm of length has 72 rings. The construction of the mesh is completely done in MatLab. At the end of the design, MatLab creates an input file suitable for Abaqus.

6.2.2 Merging of proximal elements

The problem we solve after the first input writing is the merging of the nodes defined in different part instances. The merge consist in a joint of the nodes that are nearer than a fixed distance decided by the user. Our stent in made of three different instances, called “Begin”, “Middle” and “End” that has some differences each other in terms of design. This difference is stressed in Figure 6.5.

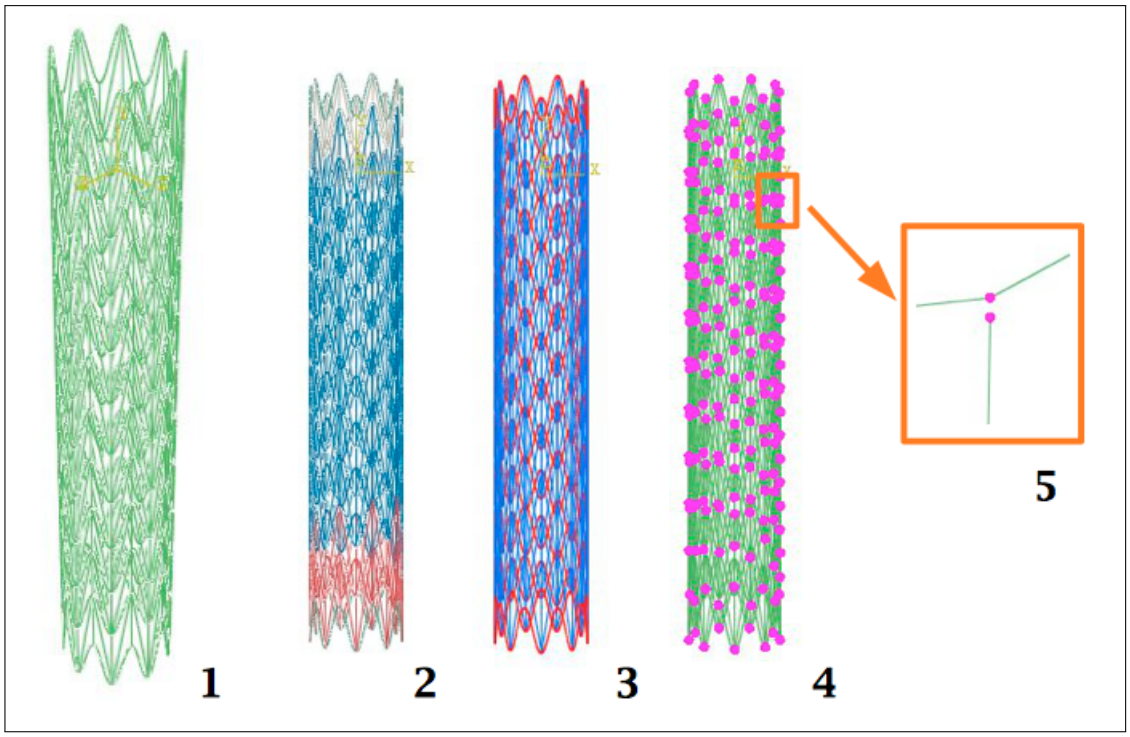

Figure 6.5: The motivations of the necessity of merging. (1) a short model of the stent, made of 10 rings; (2) evaluate the different instances showed in different colors; (3) evaluate the difference between truss elements in blue and beam ones in red. (4) the meshing step, with its zoom in (5).

The merging is possible to do directly in Abaqus, with a particular tool proposed by the software, that need as a parameter input only the maximal distance, between two nodes, where apply the merge. After that, we have another problem. The stent is made of two different element types that connect the nodes: beam elements and truss ones (fully described in Appendix A.5). The truss elements does not need any orientation. On the contrary the beam ones need an orientation tern for every different element. Abaqus permits to set the same orientation for all the elements, but the trusses need a particular orientation for every element that does not have the same spacial orientation. In particular, if we consider a case of a stent with 9 ring and 60 elements for every unit part, every ring would have 540 beam elements. Those elements would need the same orientation

in every rings, and so we must create 540 different sections with an orientation tern each. As we said, it is impossible to define more that one orientation tern in Abaqus, so we write the input of the merged stent and we open the new one in MatLab. Here we define all the orientation terns. Now we can move over to the next action concerning the stent.

6.2.3 Placement in the space

The next, and last problem that we need to solve in order to create an usable stent, is to correct position the device in the space according to the position of the vessel in space. Indeed we get the final orientation in 3D of the catheter and its position in space after the vessel remeshing. To be able to start the simulation we have to correctly insert the stent into the vessel before starting. It should be noticed that also this action is performed with a MatLab script. The method is based on the theory of the three orthogonal vectors that we can always define in space to create a base. The method has been explained in detailed in Chapter 5. The explanation is completely valid also for the stent orientation in space.

6.3 Final comments about the construction method

The method of stent design we have proposed through out the chapter might be improved by the substitution of some boring steps with their automatization. In this direction, the improvement of the interface potentiality is fundamental. It should be underlined that MatLab interfaces does not perform as much as other languages interfaces do. Nevertheless the method we defined permits to create ad hoc stent for every kind of patient with popliteal vessel diseases. These methods are also repeatable for eventually new design devices based on other stent existing in the market.

Chapter 7

Simulation

This chapter is the point of arrival of the thesis. We are going to put together all the things we explained in the previous chapters. In particular in this last chapter we expect to group all the results from Chapters 5 and 6. The goal here is to test the objects we have previously designed. It consists in two separated studies:

- stent tests, performed on the mechanical properties of the device presented in Chapter 6;
- contact analysis, a quick introduction on the forces that act during the interaction between the stent and the catheter, when the two objects are in contact;

The former tests consist on a group of simple stress tests: a uniaxial stress is applied to the device, in terms of fixed displacement, by boundary conditions. Those conditions need to be applied on a node set and impose the displacement of this set in the direction chosen. We need also to define another set, which is the fixed one. In this nodes the boundary conditions are always changeless. They consist on the forcing of the displacement to zero, in every direction. The graphical explanation of the imposition of the boundary conditions is depicted in Figure 7.1 which highlights the two node sets we need to define.

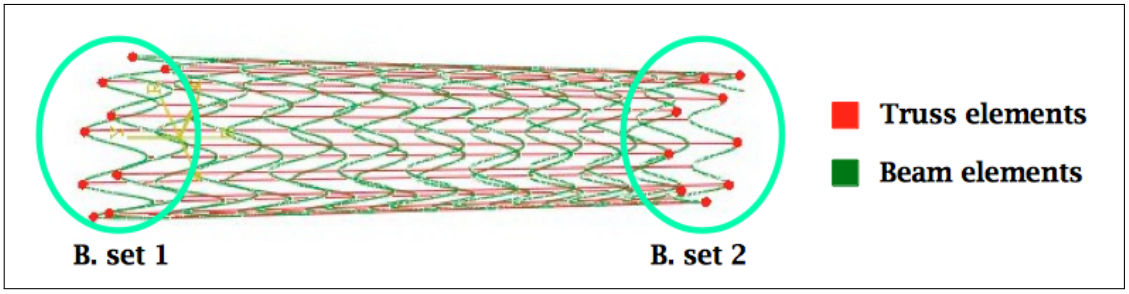

Figure 7.1: In the two green circles are depicted the two node sets. All the displacement of the nodes in 'B. Set 1' are fixed equal to zero. The colors of the stent show the presence of both beam and truss elements. The beams compose the rings of the cylindrical mesh. The trusses connect the rings together.

The second part of the chapter concerns the presentation of the contact simulation between the stent and the catheter. This operation mimics the closing of the stent before its implantation in the vessel made with the stent catheter by the surgeon. To perform it, we need to set several numbers of various conditions that are well explained in the relative sections.
At this point we should remark that all simulations are performed with the software Abaqus, version 6.12, by Simulia, Dassault Systems, France.

7.1 Stent tests

The evaluation of all mechanical properties of the stent is necessary for the second part of our simulation step. The goal is to understand if there are some mistakes, such as nodes or elements overlapping, in the stent design that do no permit its correct kinematics. On the contrary the catheter does not need a test because in the contact simulation it is imposed as the master undeformable surface. It needs to be noticed that the catheter is based on the reconstruction of medical images, from the medical partner.
In this very first part of the chapter, we are going to present different tests useful for better understanding of our analysis. They are all grouped in this list below:

- traction → according to the orientation of the stent, the traction is applied in the z direction of the cartesian coordinate system. The traction can be applied also in the cylindrical coordinate system, therefore in the Z direction;
- compression → it consists in a traction with a negative value of intensity;
- radial expansion → once more, considering the cylindrical system, it consists in a stress imposed in the r direction;
- torsion → it applies only to a system oriented it the cylindrical coordinate system. It consists in a displacement expressed as a stress imposed in the θ direction;

Figure 7.2 proposes a sketch that represents the conditions to apply all these stresses on the stent.

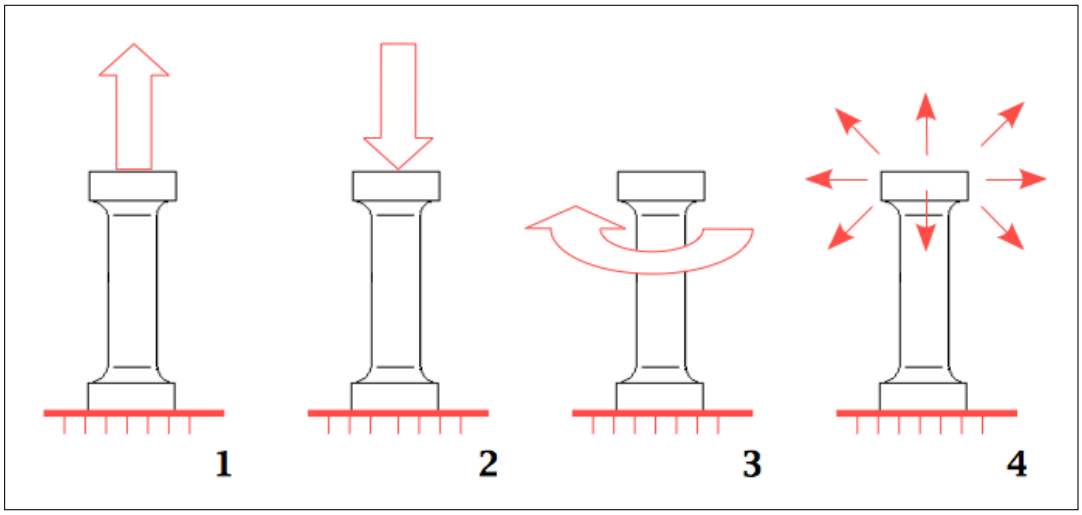

Figure 7.2: In the figure are shown the four tests just presented in the list above: traction (1), compression (2), torsion (3) and radial expansion (4).

Each test is presented in a separate paragraph. For a better understanding we report a clarifying figure of the situation for each test. As well as the evaluation of the correct design, these attempts want to analyze how the elements of the mesh change their shape if exposed to different stresses, both in macroscopical way and in numerical one. For the first two tests (traction and compression) we will report in terms of reaction forces the stress acting in the nodes of set 1 in order to evaluate the numerical response. The fundamental mechanical properties are principally the E of the elements and its ν. For this reason those are the only two properties set for our model. All their values are reported in Table 7.1.

	Beam elements	Truss elements
E	220 GPa	1 MPa
ν	0.33	0.33

Table 7.1: The table shows the principal mechanical properties of the two types of stent elements. The beam elements have properties similar to the steel.

After the evaluation of the stent design we change the mechanical properties presented in table 7.1 in order to analyze the differences in terms of stress responses compared with the situation of the beginning. In each test we modify only one parameter in order to understand which is the one with more influence in the kinematics. The results are compared in terms of reaction forces, in the nodes of the boundary set number 1. The graphs show the sum of reaction forces in every nodes of the set. The modified cases have the mechanical properties reported here in table 7.2.

Case	Mech. property	Coefficient	1° test	2° test
1	**Beam Young modulus**	**E**	220 GPa	440 GPa
2	**Truss Young modulus**	**E**	1 MPa	2 MPa
3	**Poisson ratio**	ν	0.33	0.25
4	**Poisson ratio**	ν	0.33	0.5

Table 7.2: The table shows the four cases we investigate in the reaction forces tests for each chosen design.

The modification of the parameters is made both on the stent with and without diagonal elements. We reported some graphics that compare the results regarding these two cases in the relative paragraph. The difference between stent with and without diagonal elements is well depicted in Figure 7.3. In the following graphs we use the same color line for the same parameter case.

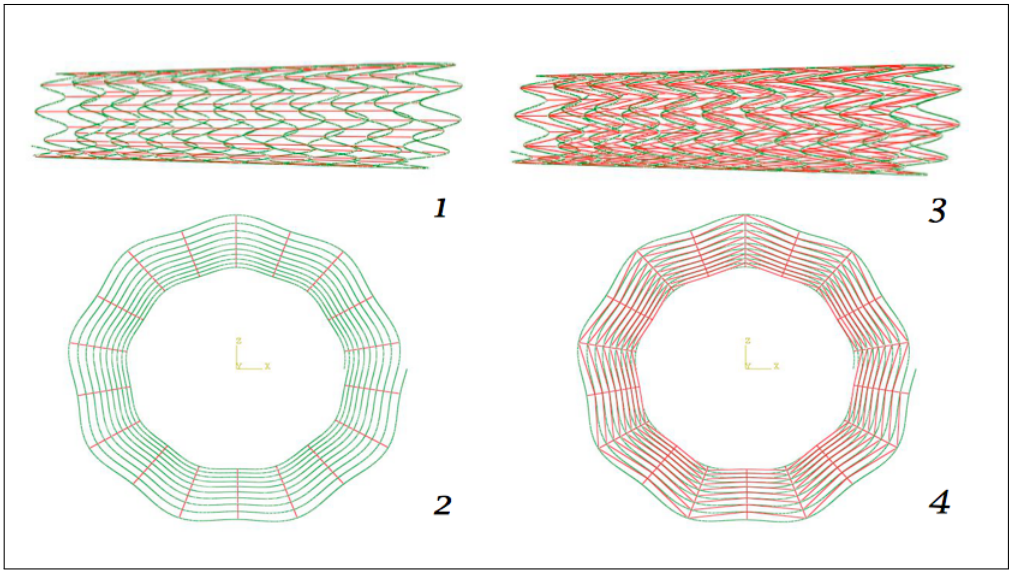

Figure 7.3: Comparison is sagittal plane and in horizontal one of the stent with and without diagonal truss elements.

As case of study, we consider in each test only a portion of the real stent size. Usually the length of a normal poplitea stent is between 15 and 20 cm, with a number of rings, in our design, between 50 and 80. We take as a sample a shorter design of 3 cm of length, made of 8 rings in order to be faster in the FE analysis and to get a better image of the object in its entirety.

7.1.1 Traction

The very first analysis we make is the test of simple traction of the stent. We take the stent in the initial configuration and we apply the boundary conditions. We apply to this object tractions of different intensity in terms of displacement. Three are the displacements given to the node of the second node set (see Figure 7.1):

- 0.3 cm $\rightarrow$ 10% of the stent length;
- 1 cm $\rightarrow$ 33% of the stent length;
- 2 cm $\rightarrow$ 70% of the stent length;

As Figure 7.4 shows, for every displacement the results of the traction tests consider the different design parameters explained in the previous paragraph, both for the stent with and without the diagonal truss elements. The mechanical effect we want to analyze here is the reaction force of the 10 nodes of the boundary set number 1, that remained steady. As depicted in Figure 7.4, increasing the of value of E causes an increment in the total reaction force that works on the 10 nodes specified (boundary set 1). In subfigure 1, 2 and 3 is briefly illustrated the evaluation of the reaction force with 3 different tractions value, comparing different value of the properties of the stent without the diagonal truss elements. On the other column, in the graphs number 4,5 and 6, is presented a similar analysis about the stent with the truss diagonal elements. This primer analysis wants to evaluate which one is the parameter that mostly influence the change in the radial force of the stent. One of the most interesting aspect is that doubling the E modulus of the truss elements causes a bigger reaction force rather that doubling the E modulus of the beam ones (see subfigure 4 of Figure 7.4). This phenomenon changes when the traction imposed gets closer to a value of increasing around the 25% of the stent length. At the bottom of Figure 7.4 it is possible to visualize what we have just said. This phenomenon does not happen in the stent without the diagonal elements. Indeed as showed in subfigure 1,2 and 3 the green line of beam E = 440GPa is always above the red one of truss E = 2MPa. Therefore the variation of the beam Young modulus is more influent in the variation of the total reaction force in boundary set 1. Another parameter that is worth to be studied is the ν of the elements. For the truss elements, variations from the beginning value of 0.33 of the ν does not cause any modifications in terms of reaction forces, while changes in the ν for the beam elements do. However, those differences are not appreciable in a traction test (see the magnification M1 in Figure 7.4). This because the ν is a value of the widening or of the narrowing of the material in the traversal direction, that it is not consistent in the traction case. However they are of some interests in the compression test as we will discuss in the next paragraph.

7.1.2 Compression

The second analysis we perform here is the so called compression. As explained in the Chapter 6, the beam elements are the ones used to simulate the interaction of the coating paper that the Viabahn has. For this reason the E module, of the truss elements, is tiny in terms of dimension (MPa). The compression is very small because of the proximity of the stent rings. Indeed with a little compression displacement the stent profile loses its linearity and assumes a bent shape

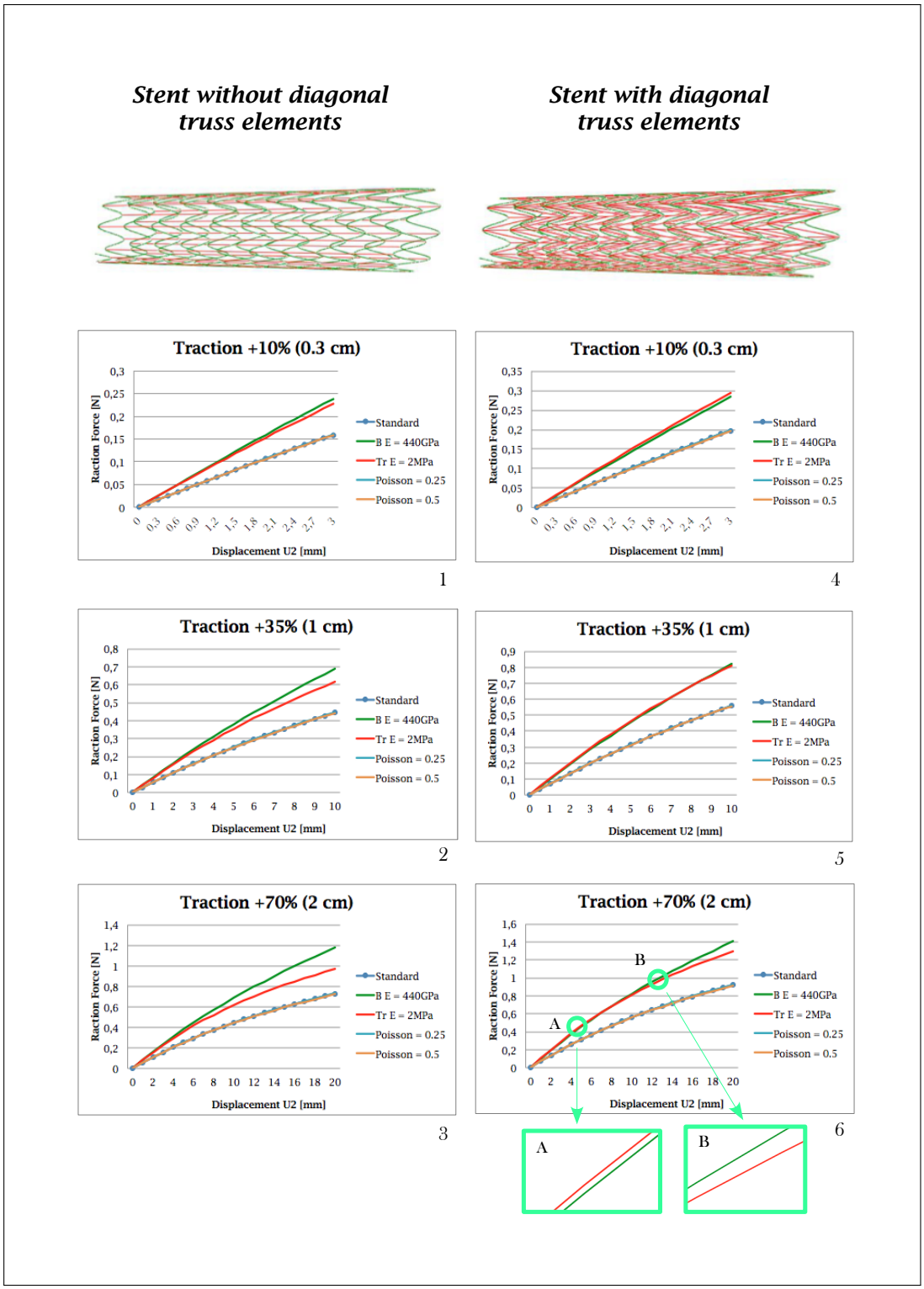

Figure 7.4: In the figure above are shown the results of the three cases of traction, comparing the different displacement-reaction force curves. Results from the stent without truss elements are shown in the left side and the results with truss elements are shown in the right part one.

profile.
Particularly in our compression test we apply a negative displacement in the U_2 direction (Z axis) of 0.3 cm, that is a shortening equal to the 10% of the total length (data reported in Figure 7.5). With bigger displacements the stent starts to lose its linearity in the shape profile. Also for the compression we analyze the reaction forces in the nodes of the steady boundary set. Observing the graphs, we can find an interesting variation in the displacement-reaction force curve. When even the stent loses its linearity in shape, the reaction force stops to increase proportionally together with the displacement (the changes of profile is stressed with the red arrows in Figure 7.5). Here we can also appreciate the different profiles of the curves that refer to the modified ν (in orange and cyan).

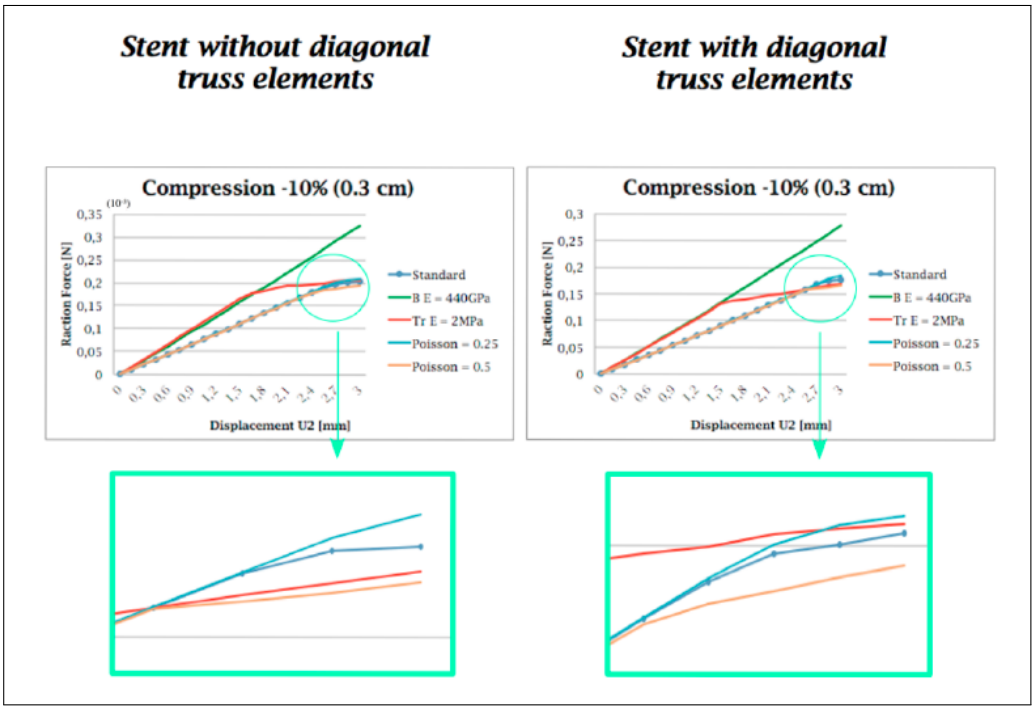

Figure 7.5: In the graphs we report the data about the compression of the stent by 0.3 cm of displacement. On the left the stent without diagonal element; on the right the one with diagonal elements. It is interesting to highlight that the amplification of the truss E causes a abrupt variation in the displacement/reaction force plane. The two magnification in the bottom of the figure shows the different profiles of the curves.

7.1.3 Radial expansion

The last interesting test that we should make on the stent still concerning the cylindrical coordinate system is its radial expansion. The radial expansion consists in the application of a positive value of displacement in the r direction (U_1) of the cylindrical coordinate system. This displacement can be applied to different node sets. If the displacement is applied only in the nodes of the boundary set 2, it gives a response in terms of displacement, different values for every node (see Figure 7.6 case 2). On the contrary if it is applied to all the nodes, the expansion is constant to all elements (see Figure 7.6 case 1).
Obviously the radial expansion with a value of displacement with negative value is traduced in a compression of the device. Figure 7.7 illustrates the comparison between the compression (case 1),

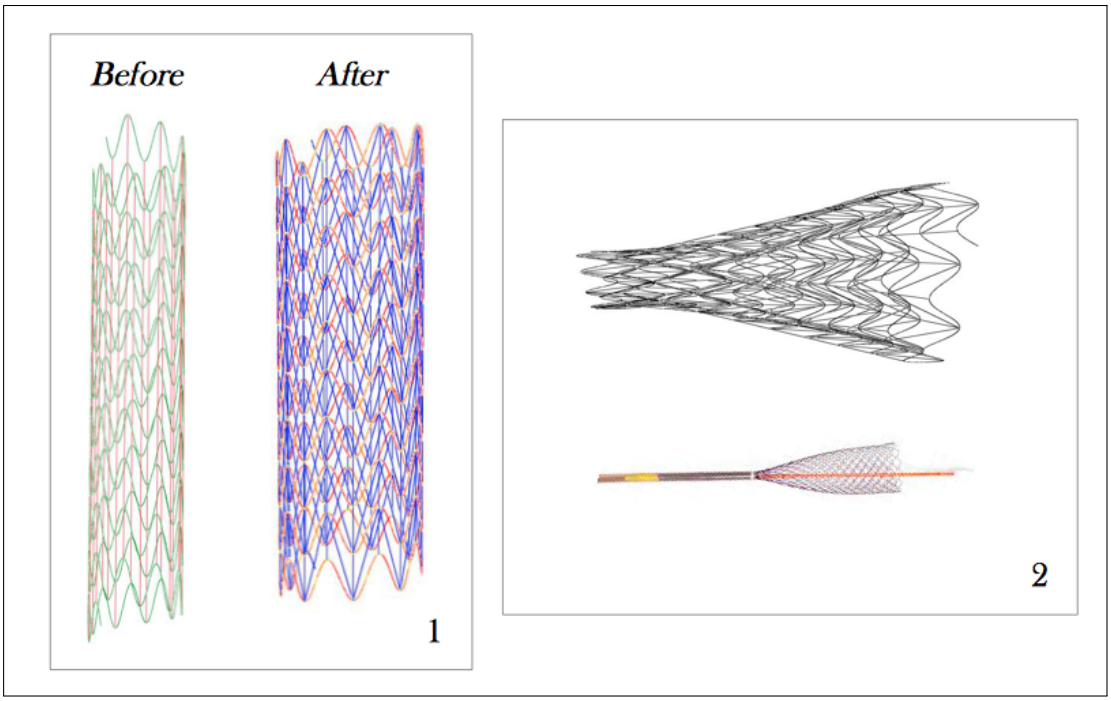

Figure 7.6: (1) radial expansion of a fixed value for every node; (2) radial expansion imposed only on peripheral nodes, with the comparison to the real case example performed on the wires tent.

the initial configuration (case 2) and the expansion (case 3) shown in the horizontal plane. The figure shows also that the truss elements are more urged to the displacement compared with the beam ones.

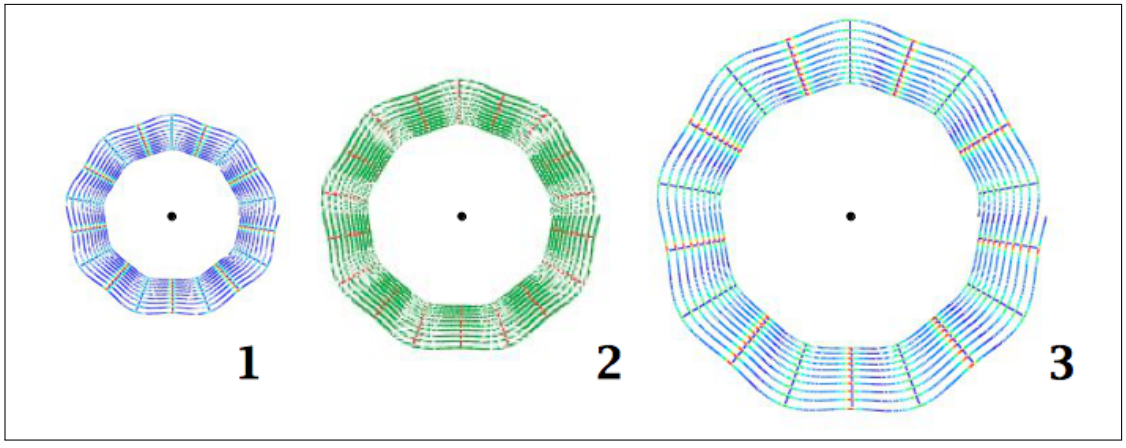

Figure 7.7: Comparison between the stent in design configuration (in the center) and its compressed (1) and expanded (3) forms.

7.1.4 Torsion

In this section we focus our attention on the torsion. However a correction needs to be done in order to differentiate this specific situation from the ones listed above. This is due to the fact that the stent has to be treated in a cylindrical coordinate system and not in the cartesian one. A cylindrical coordinate system is made up with by a bidimensional polar system, with the addition of a third coordinate, that measures the hight of a point from the basis plane. The system is in the form (r, θ, z). For a torsion test we impose a displacement in the U_2 coordinate of the cylindrical system, that is the θ. In our test we impose a rotation of different angles in the θ direction, of the nodes of boundary set number 2. In Figure 7.8 we depict what is the torsion result for our stent. We also show what happens to the device when the angle imposition is too big (case 3 and 4 in Figure 7.8). This situation starts to happen when the rotation is more than 1.5 radiants in the stent sample we tested (case 3 - 2 radiants, case 4 - 4 radiants). In the figure the results are shown in the horizontal plane to better appreciate changes of configuration.

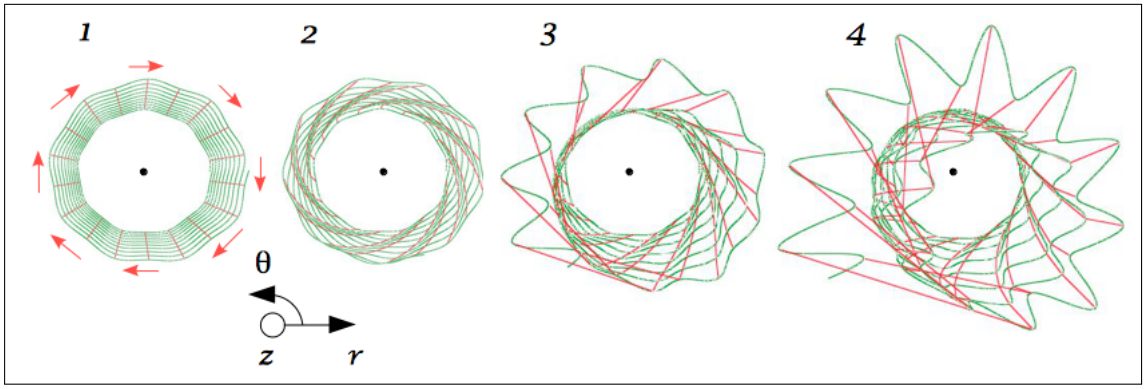

Figure 7.8: In the figure we present the torsion test. Stent is shown in horizontal plane to better demonstrate the torsion consequences. Beam elements are colored in green and truss ones in red. (1) displacement in terms of θ is applied to the stent in designed configuration. (2) the stent in deformed configuration after a displacement that does not reaches the limit of linear response of the elements. (3) and (4) stent configuration when the torsion imposed on the nodes is too high.

7.2 Contact analysis

Once we have tested the stent in all coordinate directions, we are now able to move our attention on the analysis of the contact. The contact analysis consists on the evaluation of the interaction between the stent (see Chapter 6) and the catheter (see Chapter 5) once they get closer one with the other. The goal is to calculate which one is the force that acts during the crimping of the stent, to understand how is the reaction of the stent to the crimping. The stent used here in the contact simulation is the one with the diagonal elements because it has demonstrated a better reaction to the stress imposed. In this section we are going to highlight all properties we set for the correct result of the simulation. The contact is caused by the crimping of the catheter, since it is placed around the stent in the negative radial (r) direction of the cylindrical coordinate system (r, θ, z). As done before in the stent tests, the displacement of the nodes of the catheter is fixed in terms of boundary condition displacements. The proper contact begins when the catheter nodes touch the stent nodes. At this point we are able to analyze some stresses that act on the stent and we are going to present them in the next paragraphs.

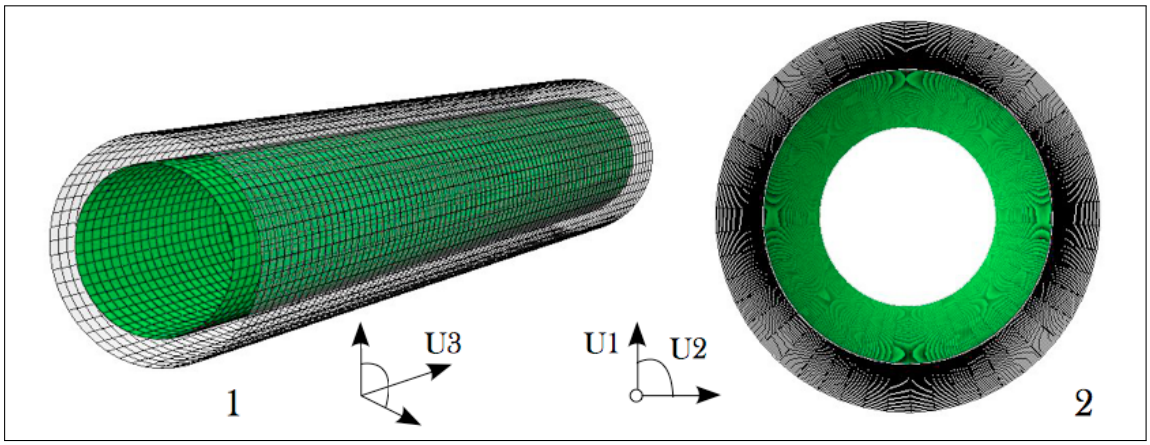

Figure 7.9: Graphical explanation of the procedure of catheter crimping, from custom view (1) and horizontal view (2).

7.2.1 Definition of the parameters of the model

For applying a correct contact simulation between the objects, some parameters has to be set:

- definition of the master and the slave surfaces → we choose as master surface the catheter, that we consider incompressible and perfectly smooth. The stent is set as the slave surface;
- the sliding formulation → we set finite sliding in stead of small sliding;
- slave adjustment → we do not set any slave adjustment between the available ones;
- definition of the interaction properties → the only property that we choose to impose in the tangent behavior of the elements that we considered as frictionless;

The definition of those parameters permits the correct implementation of the crimping in the FEA software, to get result as one depicted in Figure 7.10.

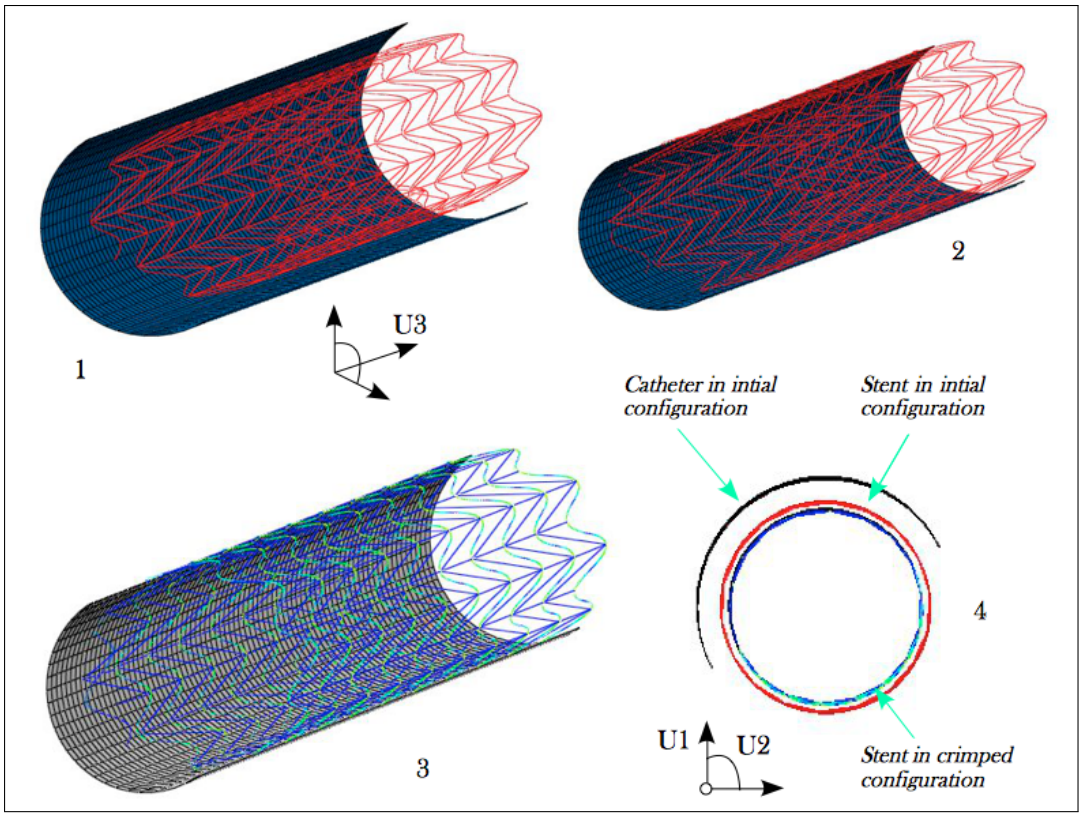

Figure 7.10: In the figure two different situations are depicted: the stent before (1) and after (2-3) the crimping of the catheter. Subfigure (4) shows in the horizontal plane the change in radius to the stent before and after the crimping test.

7.2.2 Numerical evaluation

The evaluation of the contact consist in the calculation of the stress that acts on a defined node of the mesh. Indeed the stress acting on that similar node positions should be comparable. For this reason it is also always possible to make the sum of all the stresses acting on every nodes, to get the total stress that acts on the object. In Figure 7.11 we report the values in [Pa] of the stress that acts on two particular node that we chose. Node 5660, reported in subfigure 1, is the terminal node of the upper ring of the stent mesh, as shown in the magnification box below the graph. Its response is linear because its only interaction is with the catheter and a beam element. The other subfigure (2) is about node 3443. It is a central node, where two truss elements are connecting together and with other beam elements (see magnification box number 2). We consider different property choices to evaluate the influence of each element type. Contrariwise from the stent traction and compression test, in this case the variation of the E of the truss elements does not influence much the value of the result. Also in this case the variation of the ν of the beam elements does not cause any differences. As it is detectable in the figure the stresses remain equal to zero until the catheter is in contact with the nodes of the stent.

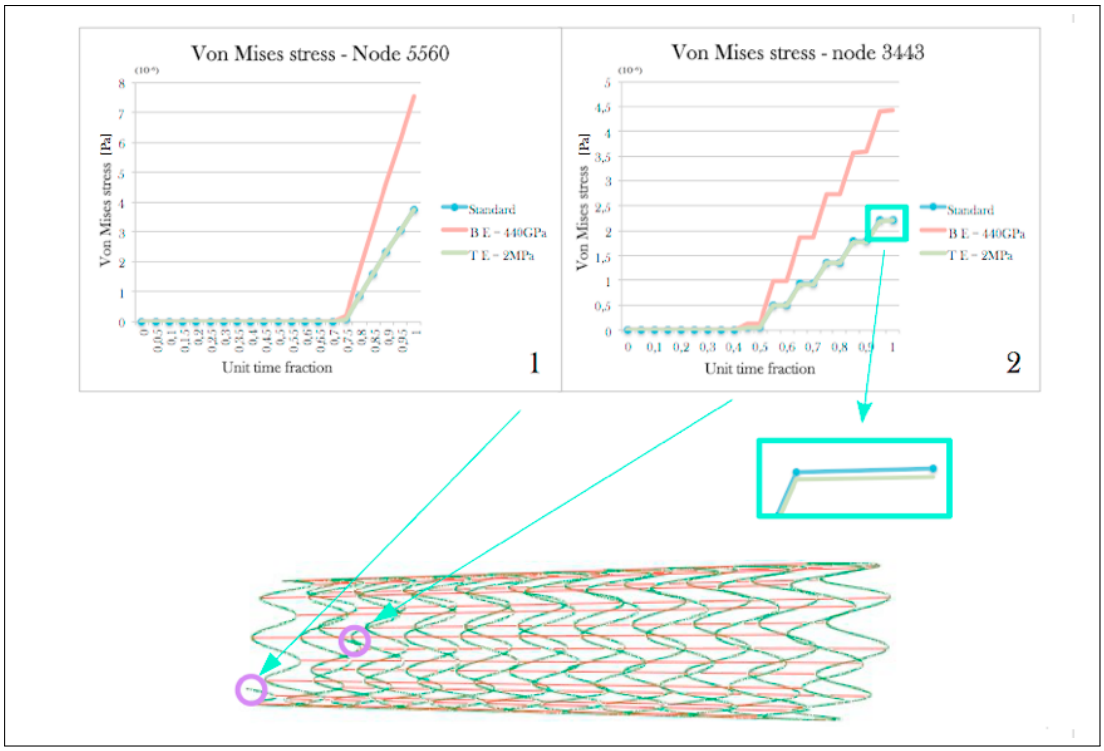

Figure 7.11: The time-Von Mises stress curve of two different nodes. The magnification shows that the Von Mises stress caused by the crimp is slightly proportionally inverse to the E of the truss elements.

7.2.3 Final remarks

As we introduced at the beginning of the chapter, we perform only a simple contact test based on the crimping of the catheter around the stent. The crimp permit us to evaluate only the stresses in radial direction. However similar analysis could be repeated to assess other stress components. The natural consequence of our analysis is the evaluation of the stent reaction when the vessel changes its configuration, from the straight configuration to the bent one, simulating the knee bending.

Chapter 8

Conclusions and further scenarios

Throughout this study work we presented the analysis of the kinematics of the popliteal artery. Starting from medical investigations obtained from our medical partners we built a FE model of the vessel in the different anatomical configurations of the leg. In parallel, using MatLab, we created a geometric model of endograft based on the Viabahn product of Gore. Subsequently we tested the two models described above through the Abaqus Simulia software. The stent testing consists in a series of mechanical tests done in order to evaluate its reaction force to a multiple series of stresses (traction, compression, torsion or radial expansion). Another testing that we did was to analyze the early interaction between the stent and the vessel. Thanks to a radial compression test we brought the vessel in contact with the stent, which got compressed in turn. In each test we changed some constitutive properties of the stent in order to evaluate which one would influence the most the results.
A possible further development of the project would be the complete simulation of a stent insertion into a vessel, from the beginning to end of the procedure. This would allow to evaluate the change in the vessel conformation before and after stent insertion. Such an advancement in the simulation would allow the doctor to understand in advance, during the operation, what will be the reaction of the vessel to the stenting procedure. The automatization of the simulation process would also overcome the lack of cases available for studying, which was one of the major problems that we encountered during this study work. In fact with the creation of a comprehensive database, the medical team would be able to better understand each specific case, comparing it with those handled by other teams.

Appendix A

Theory Explanations

A.1 VMTK Smoothing

The VMTK filter permits us to smooth the rough surfaces is based on the work of Taubin (1995). The method is innovative in case of smoothing piecewise linear shape of arbitrary dimension and topology. It consists on a linear low-pass filter that remove high curvature variations and avoid shrinkage.
The new smoothing algorithm consists on two consecutive Gaussian smoothing steps. Gaussian filter is a filter whose impulse response is a Gaussian function. The first Gaussian smoothing has a positive scale factor λ that is applied to all the vertices of the shape. The second one on the contrary has a negative scale factor μ, grater in magnitude to the first one. These two steps are repeated lots of times, consecutively alternating the positive and the negative Gaussian smoothing. The result, as said above is a low pass filter. Curve or surface curvature takes the place of frequency. The original non-smooth curve or surface is modeled as an underlying smooth curve or surface, plus a normal perturbation vector field. The underlying curve or surface is bounded above the curvature, and the perturbation that needs to be filtered out is regarded as zero mean high curvature noise. The two scale factors determine the pass - band and stop - band curvatures. For higher attenuation in the stop - band, the two Gaussian smoothing steps must be repeated alternating the two scale factors μ and λ. The amount of attenuation is then determined by the number of iterations N.

A.2 VMTK Registration

The explanation here below is taken by the work of Campanile (2012). The method "vmtkicpregistration" is included in the VMTK library as a python script. It is based on the ICP algorithm, that means iterative closest point. It registers a surface to another that is considered as reference. The algorithm is used to minimize the differences between two point clouds of the same object that comes from different scans. The first step of the algorithm is to find the correspondence between the points of the clouds. One of the clouds is considered as the reference, while the other is the target. Fig. A.1 shows in a very simple way the concept of iterative closest point.
This method is based on the hypothesis that the two closest points are also correspondent. Where the proximity is based on the concept of euclidean distance. Given a point of target t (X_t,Y_t,Z_t) and a point of reference r (X_r,Y_r,Z_r), the euclidean distance is defined as the segment that connects

the two points following the law here proposed:

$$d(t,r) = d(r,t) = \sqrt{(r_1 - t_1)^2 + \cdots + (r_n - t_n)^2} = \sqrt{\sum_{i=0}^{n} (r_i - t_i)^2} \tag{A.1}$$

Since we found the points that are realistically correspondent, it is necessary to define a function that is going to be minimized by the method of the least squares. The target surfaces, to be correctly aligned, needs to be translated and rotated. The transformation τ is going to be a function of roto-translation. Using the algebraic matrix, the rotation in 3D space, it is going to be represented as the product of matrix between the points x and the matrix of rotation R. However, the translation is going to be calculated by the vectorial sum of the of the points x and the vector of translation T. The formulation is something like this:

$$\tau(X_i^{source}) = RX_i^{source} + T \tag{A.2}$$

Then it is calculated the difference between the target and the reference after the transformation:

$$x_i target - \tau(x_i^{source}) = x_i^{target} - (Rx_i^{source} + T) \tag{A.3}$$

At the end we are able to calculate the total error in the following way:

$$argmin_{R,T} = \frac{1}{N} \sum_{i=0}^{n} x_i^{target} - (Rx_i^{source} + T) \tag{A.4}$$

The "vmtkicpregistration" permits us to register a rigid surface on another, that in our case are bones. It is possible to combine this tool with another called "vmtksurfacetransform" that permits to bring with the point cloud also other features of the body, such as the vessels or the soft tissue.

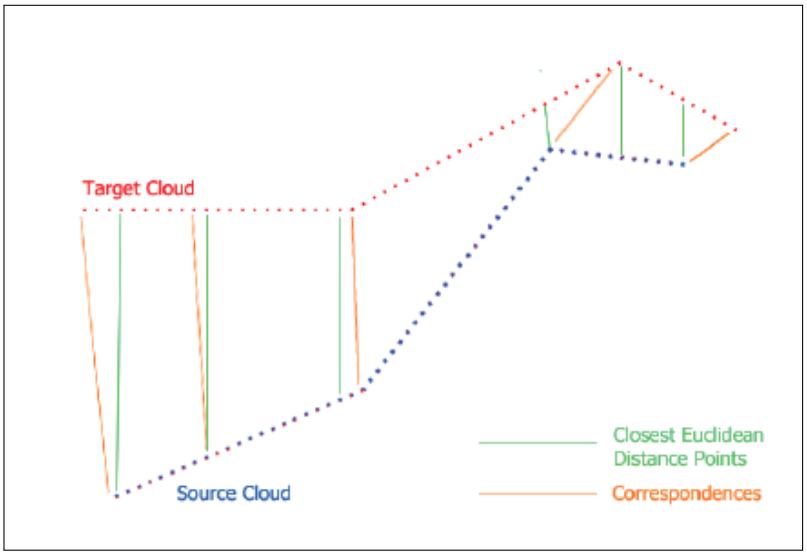

Figure A.1: Closest points between the target and the source, calculated with the euclidean distance, in comparison to the correspondent real points.

A.3 Curvature Method

As we introduced the curvature data taken from the centerline data were not useful, because affected of too much noise. To solve the problem we have elaborated the data containing the 3 coordinates of every node considered with an algorithm based on the polynomial regression.
The algorithm is based on the method of the ordinary least squares (Alberto (2005)). It gives an iterative method for generalize polynomial function of n degree. The idea is to base the evaluation of the curvature on the research of the parabolic function that better regress a number of point chosen by the user of the centerline that needs to be analyzed. As we know from elementary geometry, there is only one parabola that goes for three points in the space. If we choose as nodes for parabola three, we would find the noisy result we found before, because the curvature of every points of the parabola is exactly the value of curvature of every nodes. Now, the idea is to increase the number of points that passing through the parabola, or at least to regress to. Taking as first example four points, we would evaluate the curvature of all those points together getting as a result a value of curvature that is the mean of the values of the curvatures of the four nodes. The curvature is put in a new node that is called the centroid of the segment that connects the four nodes. We will now introduce the theory about our method.
We often can consider a variable y as the polynomial combination of another x:

$$y = A + Bx + Cx^2 + ... + Zx^n \tag{A.5}$$

That in a quadratic case is:

$$y = A + Bx + Cx^2 \tag{A.6}$$

If we know a series of value (x_i,y_i) with i =1,...N, for every value of x_i we can obtain y_i from the equation above. Now we consider that y is normal distributed. The probability of finding the values (y_1,...,y_n) is:

$$P(y_1, ..., y_n) \propto e^{\frac{-\chi^2}{2}} \tag{A.7}$$

where:

$$\chi^2 = \sum_{i=1}^{N} \frac{(y_i - A - Bx_i - Cx_i^2)^2}{\sigma_y^2} \tag{A.8}$$

Differentiating χ^2 between A,B,C and putting equal to 0 the derivates we obtain the members of the sum:

$$\begin{aligned} \sum y_i &= AN + B\sum x_i + C\sum x_i^2 \\ \sum x_i y_i &= A\sum x_i + B\sum x_i^2 + C\sum x_i^3 \\ \sum x_i^2 y_i &= A\sum x_i^2 + B\sum x_i^3 + C\sum x_i^4 \end{aligned} \tag{A.9}$$

The matrix obtained is the following (3x3):

$$\begin{bmatrix} N & \Sigma x_i & \Sigma x_i^2 \\ \Sigma x_i & \Sigma x_i^2 & \Sigma x_i^3 \\ \Sigma x_i^2 & \Sigma x_i^3 & \Sigma x_i^4 \end{bmatrix} \begin{bmatrix} I \\ J \\ K \end{bmatrix} = \begin{bmatrix} \Sigma y_i \\ \Sigma x_i y_i \\ \Sigma x_i^2 y_i \end{bmatrix} \tag{A.10}$$

That is of the simple form:

$$A \quad X \quad = \quad B \tag{A.11}$$

One simple resolution is the matrix resolution done by the inversion of A. However this method is not always applicable in fact if the matrix A is singular it is not possible to invert it. This

simple method permits to obtain an interpolating curve of degree 2. In general if we are looking forward to get a polynomial of n degree we would obtain (n+1) equation and (n+1) unknowns. The dimension of the matrix A would be (n+1)×(n+1) and the other matrix B and X would be (n+1)×(1). The components would be structured as follows:

$$\begin{bmatrix} N & \Sigma x_i & \Sigma x_i^2 & \cdots & \Sigma x_i^n \\ \Sigma x_i & \Sigma x_i^2 & \cdots & \cdots & \Sigma x_i^{n+1} \\ \Sigma x_i^2 & \Sigma x_i^3 & \cdots & \cdots & \Sigma x_i^{n+2} \\ \vdots & \vdots & \vdots & \ddots & \vdots \\ \Sigma x_i^n & \Sigma x_i^{n+1} & \cdots & \cdots & \Sigma x_i^{2n} \end{bmatrix} \begin{bmatrix} I \\ J \\ K \end{bmatrix} = \begin{bmatrix} \Sigma y_i \\ \Sigma x_i y_i \\ \Sigma x_i^2 y_i \end{bmatrix} \tag{A.12}$$

Also in this case the evaluation of the matrix A consists only in a sum of powers of the same elements. And the reversion of it is quite fast. Obviously the passage described here above has to be performed for all the three coordinates of the model (X,Y,Z) in order to get the curvature value in 3D.

A.3.1 Theoretical Reference

The resolution of the matrix that we have just described is the application of the model to a specific theoretical concept that connects the curvature to the 3D coordinates of the nodes of the model in the space (). After the preparation of the nodes for the elaboration, the first thing to do is to discretize the intervals calculating the distance between the nodes:

$$r(i) = x(i)\hat{i} + y(i)\hat{j} + z(t)\hat{k} \qquad \rightarrow \qquad s(i) = \|r(i) - r(i-1)\| \tag{A.13}$$

After that, it is the time to measure the vector unitary tangent, $\hat{T}$. The mathematical form of this vector are the following:

$$\hat{T}(s) = \frac{dr}{ds} = \frac{dr}{dt} \times \frac{dt}{ds} \tag{A.14}$$

$\hat{T}$ represents the velocity of the vector r multiplied by the length of the velocity vector. Moving ahead we report the differential form of the curvature that is:

$$K(s) = \|\frac{d\hat{T}}{ds}\| \tag{A.15}$$

The curvature represent the rapidity by which the vector T rotates. It is possible to calculate also the radius of curvature (ρ(s)) that is the inverse of the curvature value. To clarify the relation between these equations, we use a sketch, reported at the end of this paragraph that should be very easy to understand.

$$\hat{N}(s) = \frac{d\hat{T}}{ds} \times \frac{1}{K(s)} \tag{A.16}$$

$\hat{N}$ represents the unitary normal, and it is perpendicular to C, that is the direction of the curve that we are considering. Before the graphical explanation we need to introduce another concept that is the osculating plane that pass from r(s) and contains the vectors $\hat{T}$(s) and $\hat{N}$(s). The 3 dimensions always changes for each discrete point. In the osculating plane is always present the osculating circle that describes the behavior of C in the proximity of the point. It is worth to be noticed that if the curve that analyze C is a circumference, the osculating circle coincides with C. Here below in Fig.A.2 we report also the equation of the center of the osculating circle in red with

the other sizes of interest for this topic:

$$r_c(s) = r(s) + \rho(s)\hat{N}(s) \tag{A.17}$$

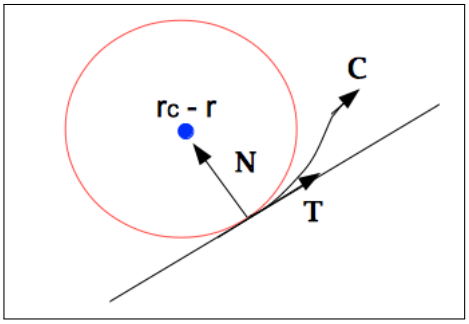

Figure A.2: Explanation of the relationship between the parameters introduced with the equations.

To test if the method just described is working correctly we applied it to simple cases of regular curves. The model is proposed in Fig. A.3. The initial shape that we want to calculate is composed by three tracts same in shape but different in scale connected one to the other. The result is a plot composed by three different horizontal constant segments of at the values of the curvature of the three tracts.

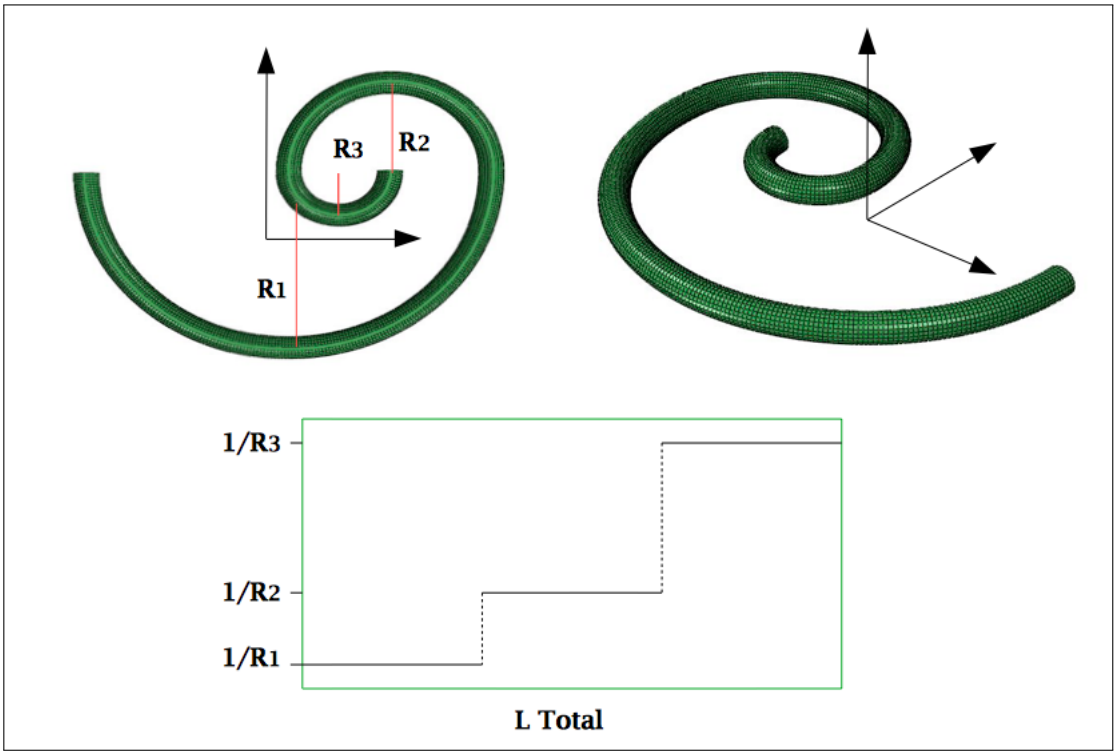

Figure A.3: Evaluation of the curvature of a simple geometry.

A.3.2 Literature reference: Piccinelli 2009

Next work that is going to be presented in the chapter has been redacted by italian authors, Piccinelli et al. (2009). It is slightly different from other works reported in the literature chapter, because it does not focus its attention on peripheral vessels as the others do, but the authors consider the cerebral vascular system, with the goal of detecting aneurysms, that is either a very common disease in the popliteal region. They discovered that the formation of intra-cranical aneurysms preferentially appears at bifurcations and sharp bends. However this work is interesting for the goal of our thesis. It gives a great description of how the authors got some key information as centerline or vessel curvature that we will fully investigated in this work of thesis. Another aspect in common to our work is the software used, that is VMTK, vascular modeling toolkit, an open source software. They divided the analysis in different consecutive steps. The first one has been the preparation of images with the segmentation of them got from the MRI. After that it has been the time of the computation of the centerlines; they also showed their result with the help of models based on the Voronoi diagrams. The last part that they performed has been the analysis of the bifurcations, that are the locations where complex flow has a chance to develop, and that several vascular diseases exhibit focal effects around them, as atherosclerosis and aneurysmal diseases. Therefore they have created a complete framework for robust characterization of the application of the framework to the case of cerebral aneurysms. Speaking in terms of mathematics and equations the treatment of the problems in this article is more detailed than what we actually need for our work, but it is interesting for its way to present the treatment. This scheme will be the same of the one of our work in some parts that will be stressed in the text with citations and references. Here below is reported an image that wants to show the most important passage of the definition of the maximal inscribed spheres in the vessel lumen. From the images the authors have found the radius of the vessel in every slice of tomography, showed in the first and second part of the image. They applied the sphere filter, that we also use in our treatment and we clarify in the relative chapter. The result is shown in the right part of the figure where is reported only the area of the sphere that is perpendicular to the vessel direction.

A.4 Color tool of ITK-Snap

The software ITK-Snap permits us to isolate the tissues of interest with a 3D reconstruction from the CT of the patient. We decided to write in the small paragraph where we want to describe the possible actions we could do with this software. The description is made with some explicative figures in order to help the reader. The strength of this software is that it permits to work together with all the set of CT. Our point of departure is the slice containing the beginning of the popliteal artery as shown in the first subfigure of Figure A.5. The first step to do is the regulation of the image contrast. The results are shown in subfigure number 2. As the reader can see the improvement in definition is sensible. Now we are ready for the image segmentation. We can use either automatic segmentation, made with a particular tool named “Snake ROI tool”, or manual one. The former is faster but is less precise; on the contrary the latest is more useful for the correction of the mistakes. We now start the description of the “Snake ROI tool”. The first step, is the definition of the intensity regions, reported in the third subfigure. The tool needs the picking of some spheres in the space. The spheres are the beginning of the segmentation regions. The software evaluates the values in intensity of grey of the pixels near to the limits of the spheres and into them. If the value is similar to a fixed value considered as the reference, the voxel is included in the segmentation. The beginning and the end of the work of this tool is reported in subfigure 4 and 5. In this example we want to make the segmentation of the femur and the patella of the left leg of the patient. We decided to consider only one leg because the problems about the popliteal artery concerned only

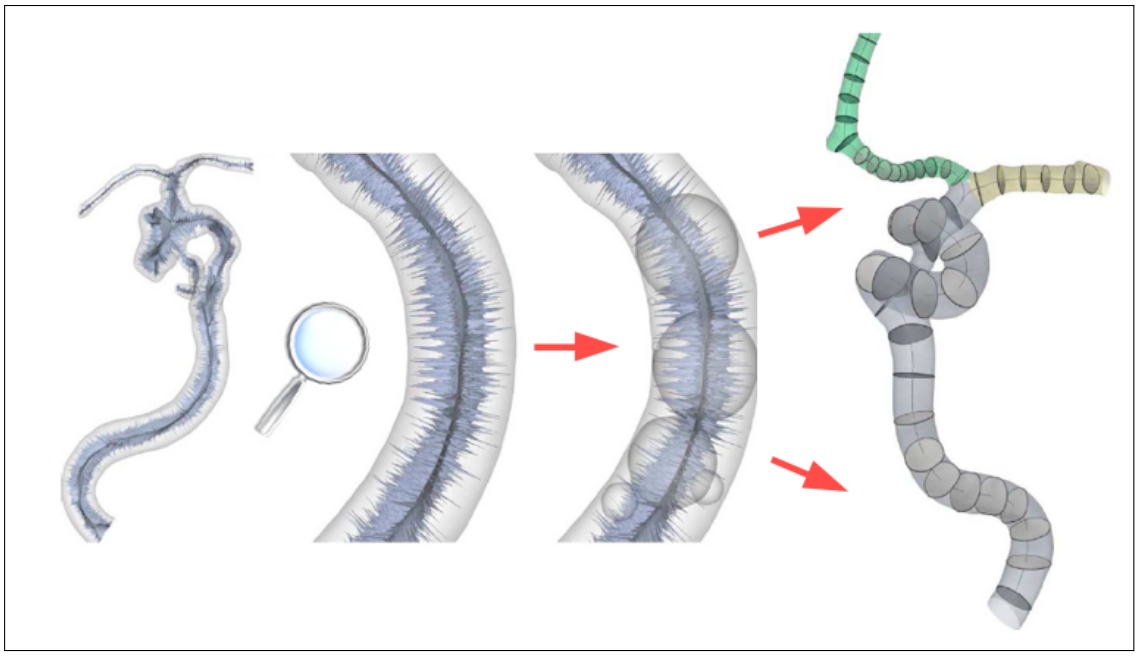

Figure A.4: The image shows the work-steps from the vessel image to the final 3D reconstruction (Piccinelli et al. (2009)). (1) vessel reconstruction after CT acquisition; (2-3) calculation of the maximal sphere inscribed in the vessel; (4) vessel remeshing from the sections found.

on the left one. Repeating the same steps for all other segmentation labels that the user want to create, we arrive to a result as the one proposed in subfigure 6. The exportation of this results is savable in different STL files, that can be visualized better with Paraview. Also ITK-Snap permits too the visualization, but the quality of the images proposed is not enough detailed to appreciate some features. Once we finish our work we can save separately or together the labels proposed in subfigure 6. From those files we can apply the other operations already described, such as for example the registration or centerline calculation.

A.5 Beam and truss elements

This section is dedicated to the explanation of the basic features of both the truss and the beam elements that compose our stent mesh. Truss elements are long and slender, have 2 nodes, and can be oriented anywhere in 3D space. Truss elements transmit force axially only and are 3 DOF elements which allow translation only and not rotation. A constant cross section area is assumed and they are used for linear elastic structural analysis. Truss elements are depicted in subfigure (1) of Figure A.6.
The beam element is a mathematical construct used to model beam-type structures. The typical beam element assumes all loading is discrete at the ends of the beam. These elements are either long and slender, have three nodes, and can be oriented anywhere in 3D space. Beam elements are 6 DOF elements allowing both translation and rotation at each end node. That is the primary difference between beam and truss elements. In the subfigure (2) of Figure A.6 the I J nodes define element geometry, the K node defines the cross sectional orientation. This is how you differentiate between the strong and weak axis of bending for a beam. A constant cross section area is assumed. In the image, the beam shape is shown only for visualization, the element is the dark blue rod. The I J axis runs from the near to far node. K is shown vertically above the I node or could be

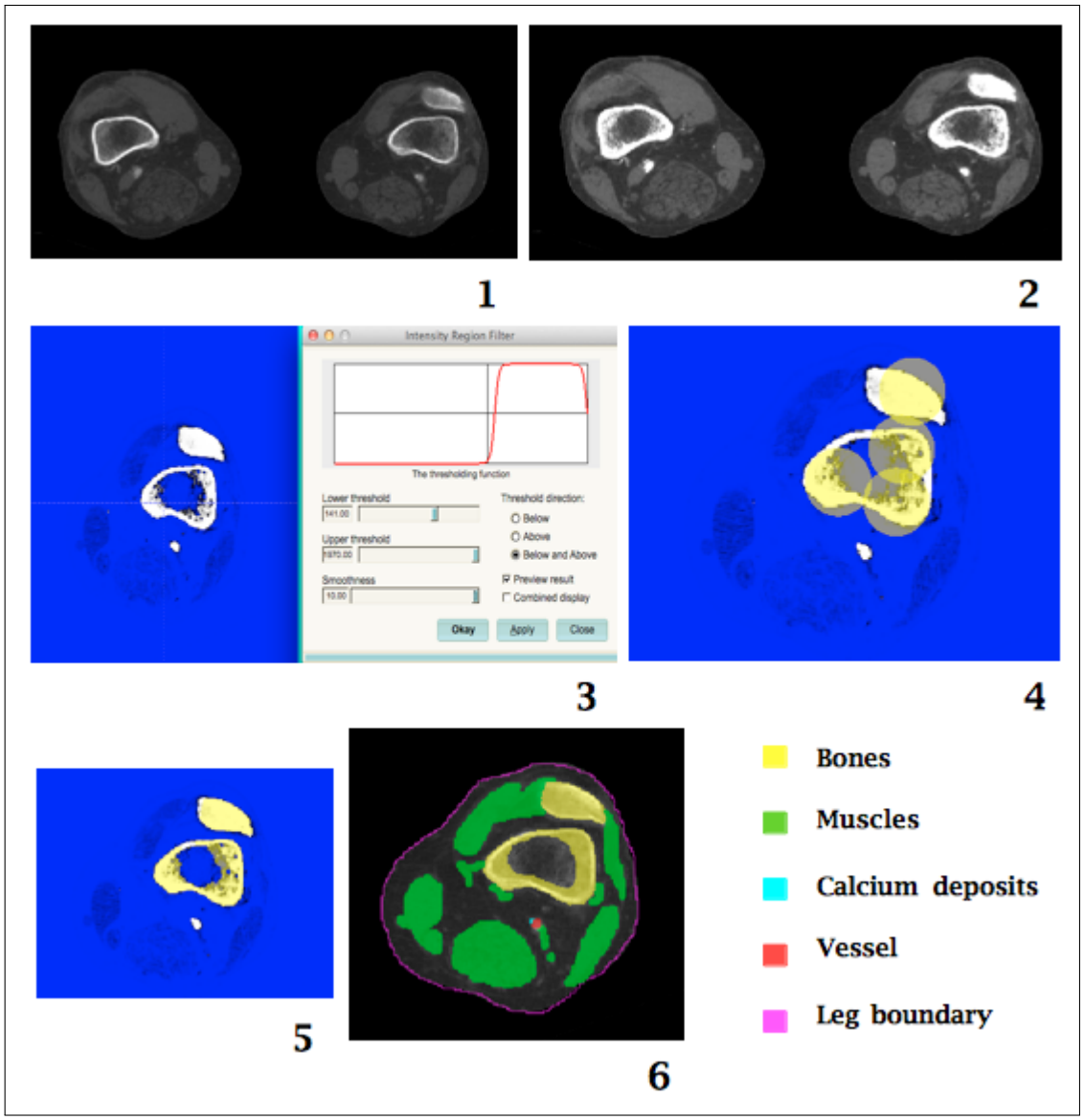

Figure A.5: Segmentation steps are shown from image (1) to (6). In order: CT opening (1), image contrast regulation (2), application of the intensity region filter (3), positioning of the spheres for the segmentation (4), primer result with one label (5), final segmentation result (6).

horizontally to the right of I.
Truss element does not need to be oriented in space because their 3 DOF do not allow the rotation. They are the better solution in problems where the rotation is not needed. Indeed the element orientation often gives problem in the definition. The orientation can be given both to each beam element taken separately or with the same versors for all the elements.

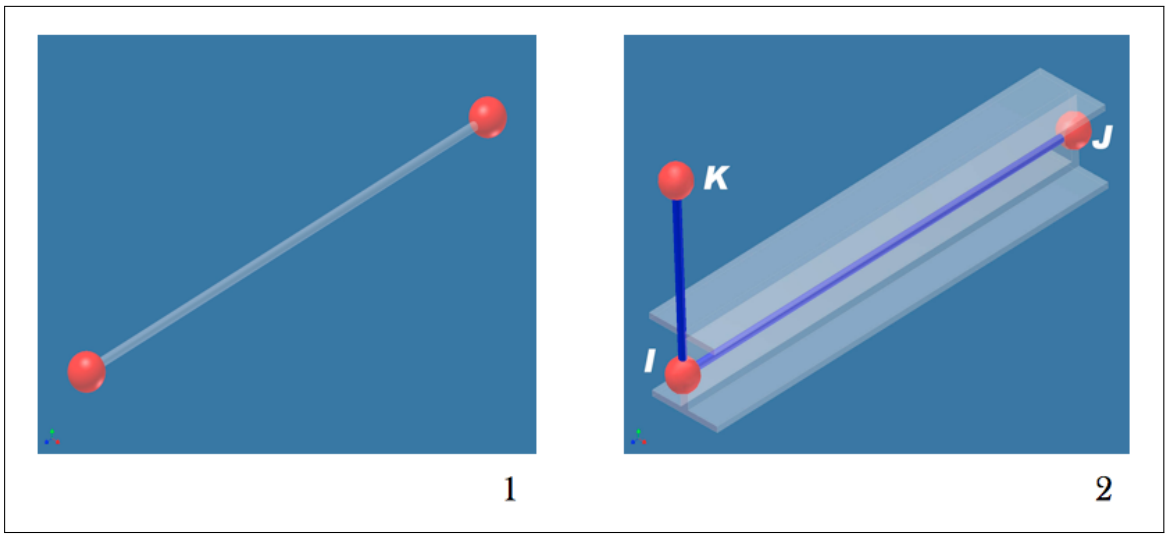

Figure A.6: (1) an example of truss element, (2) an example of beam element.

Appendix B

VMTK codes

Here below we report all the codes useful for the analysis in VMTK (Antiga (2014)). It should be noticed that the only limitation concerns the name of the file used with these methods and the space between the name of files.

Introduction that calls the source needed to get all the information used by WMTK:

source / Applications / vmtk.app / Contents / MacOS / vmtk

Registration
Basic registration of the input rigid feature on the reference rigid stl one:

vmtkicpregistration -ifile bone_input.stl -rfile bone_reference.stl -ofile bone_output.vtp

Registration of rigid feature and application of the matrix of transformation to other features of the body:

vmtkicpregistration -ifile bone_input.stl -rfile bone_reference.stl -ofile bone_output.vtp –pipe vmtksurfacetransform -ifile vessel_input.stl -ofile vessel_output.vtp

Centerline
Simple calculation of the centerline of a generic cylindrical like structure:

vmtkcenterlines -ifile vessel_input.stl - ofile vessel_centerine.vtp

Calculation of the centerline with the evaluation of some interesting geometrical features of the object considered:

vmtkcenterlines -ifile vessel_input.stl –pipe vmtkcenterlineresampling -length 0.1 –pipe vmtkcenterlinegeometry -ofile vessel_centerline.vtp

Smoothing
Appling the smoothing filter, based of the Taubin method, presented in the first part of the Appendix to the vessel:
vmtksurfacesmoothing -ifile vessel_input.stl -ofile vessel_smoothed.vtp

Applying the same method to the centerline:

vmtkcenterlinesmoothing -ifile vessel_centerline.stl -iterations 10000 -smoothingfactor 0.5 -ofile vessel_centerline_smoothed.vtp

Remeshing
vmtksurfaceremeshing -ifile vessel_input.stl -edgelength 0.001 -ofile vessel_remeshed.stl

Branching
Dividing the vessel into the branches that compose it:

vmtkbranchclipper -ifile vessel_input.stl -centerlinesfile vessel_centerline.vtp -groupidsarray GroupIds

Appendix C

Description of GUI (Graphical User Interface)

In some chapter of the thesis we referred about two interfaces that we made with the tool provided by MatLab called Guide. In this third appendix we are going to cover in a complete way all the advantages of this two software solutions that we designed. A MatLab script works behind both of the two interfaces. However if a specific botton is pushed, they both create also other format files such as TXT or INP, that are readable for example with a FEA software such as Abaqus Simulia.

C.1 Centerline analysis interface

In Chapter 4 we described an interface, reported in Fig. C.2, that is able to analyze all the important features for us of the centerline of 3D STL of a vessel, in both configuration, straight and bent, or pre and post the stent implantation. For both the cases the software works in the same way, showing the differences between the 2 configurations in terms of different measurements. The interface does not want to give any preliminary results before the choice of the patient, by the user. This is made by a confirmation button after the writing of the number of the patient in a specific editable white box in the left part of the interface, into the area named "patient choice". After the choice of the patient, and its confirmation, it will compare it in the panel next to the image of the hospital where the patient has been treated. Furthermore, the software will calculate some basic features of the STL files of the patients that it keeps in its archive; it will report the result in the proper panel in the left bottom part of the interface. This panel highlights the differences in terms of length between the two measurements reporting the shortening in percentage in the last editable area. Afterwards we will introduce the right part of the interface. This is dedicated to the plotting of two important measures of the vessels: the inner radius and the curvature. The first figure, in the top level, shows the variation of the stent radius compared to the vessel coordinate. On the contrary the second figure, below the radius one, shows the variation of the curvature of the stent compared to the vessel coordinate. The two plots want to analyze the differences between the two configurations that the vessel is giving. To do that the two plots corresponding to the two measures are reported in the same figure with two different colors.

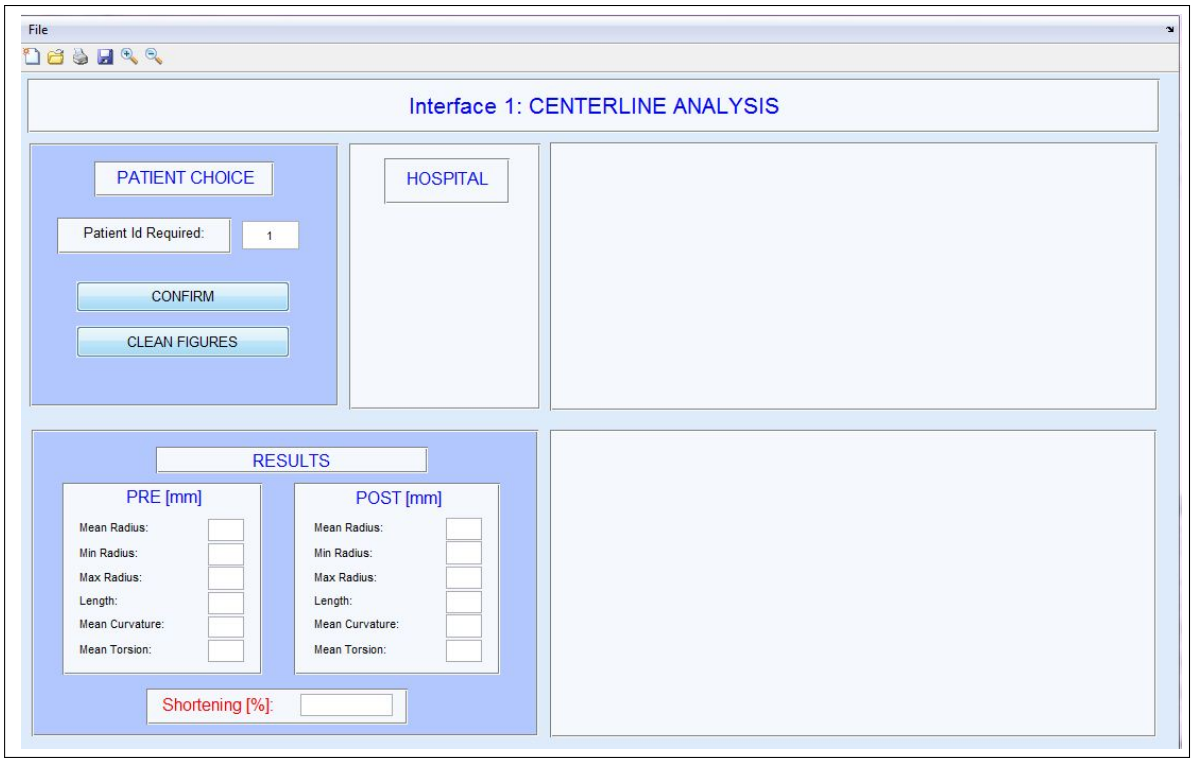

Figure C.1: Explanation of all the possible measures that can be taken from the STL data with the interface 1.

C.2 Kinematics analysis interface

The second interfaces groups the operations that are described in two different chapters: the reconstruction of the vessel for the FE analysis in chapter 5 and the stent design in chapter 6. The operations here are reported together because the results of the vessel reconstruction affects the choice of the stent to apply to the vessel for the simulation. In this paragraph we will present in parallel the parts of the interface with the actions that they perform. Starting from the top, in the left side of the interface there is a panel dedicated to the choice of the patient; it works exactly as in the other interface: the users has to choose one particular patient for the kinematics analysis and the software will load the data of that patient. The second step of the work is the fixing of the parameters necessary for the remeshing of the vessel. The user has to set three parameters: the number of circumferential nodes that forms the vessel mesh, the number of longitudinal nodes, and the number of intervals between the straight and the bent configuration of the vessel, to make the simulation more realistic. With the confirm button the user can upload to the software the data. It is also available a reset button if the user wants to rewrite the three parameters. After a few seconds in the right middle part of the interface, there will appear the results of the remeshing and of the sampling of the centerline nodes, for a deeper explanation of this aspects go to Chapter 5. The first plot shows the remeshed vessel in 3D. With the rotation tool available in toolbar at the top of the interface it is possible to better analyze the results. In the other plot in the right part of the interface the figure shows the image of the vessel in the .jpg format. Moving down to the inferior part of the interface, in the left side there is a panel dedicated to the measures of the stent that the user wants to implant in the patient. With the MatLab tool “ginput” the user can choose two nodes in the 3D figure. The software calculates the distance of the two nodes and gives it as a result. The distance will be the stent length for the construction. The other basic parameters of

the stent have to be set manually with the edit boxes. When the editing is completed the software starts after the user pushes a proper confirm button. If the length of the stent is similar to any model within the library of the software the confirmation switches on a checkbox next to the button, that tells the user that the selection of the stent is correct. If the selection is correct, also the other three button in the right part of the interface are disabled. Those buttons remains active when the stent has to be build from the beginning.
When the stent has to be build from the beginning it needs all of these 3 steps. With the first button the stent is written in the INP format that is readable with the FEA software. Now we have to open the file with ABQ and make the manual merging of the nodes. The merging consists in the collapsing in the same node of two or more nodes that are nearer than a fixed distance given by the user. After that the data has to come back to MatLab because we have to define the orientation of the beam elements of the mesh. Every section of the mesh need a specific orientation that cannot be calculable in ABQ, so it has to be calculated in MatLab. The user has to manually load back the data of the nodes and of the elements in different variables in MatLab and then pass them to the function dedicated to the calculation of the orientation. The effective departure of this function is decided by the user with the pushing of the second button called "beam orientation generation". At the end of the setting of the orientation, the INP of the stent has to be written again, taking in account the new information about the orientation. This passage is made with the third button.
So at the end of the utilization of this interface the user will have two results:

- an input file containing the different configurations of the vessel;
- an input file of the stent that he want to apply to the vessel for the simulation;

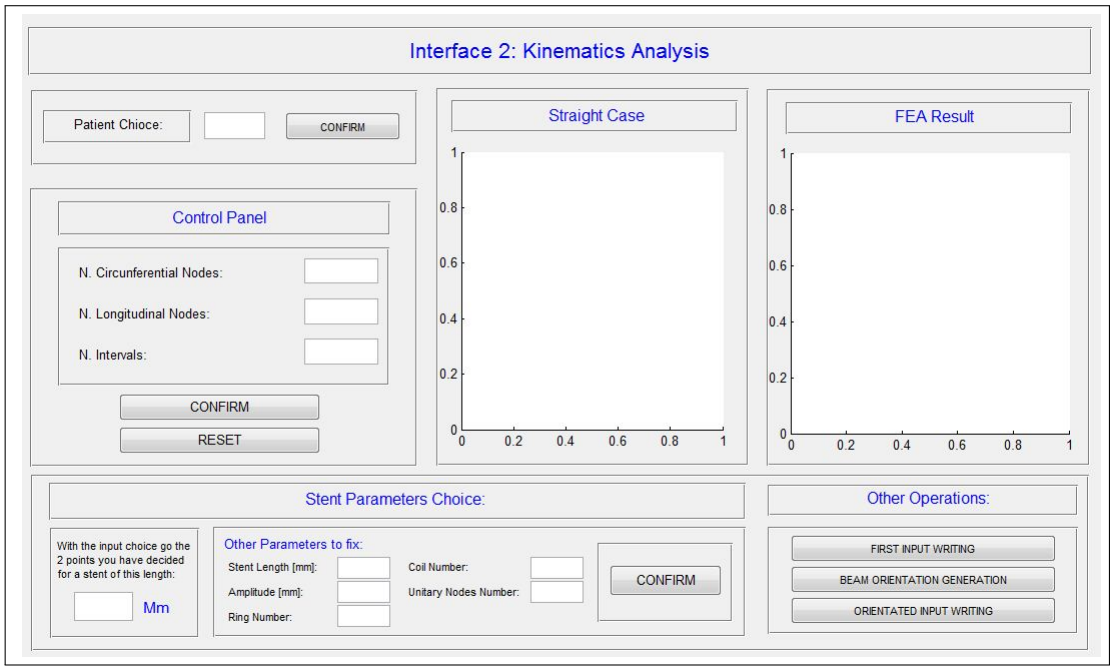

Figure C.2: Stent construction interface.

Appendix D

The device for the bending

For a people with the hight of 185 cm we assume those value for the measurement of the segments $\overline{AB}$ and $\overline{AC}$. We want to impose a bending of 45° and then of 90° of the knee. As we can easily see using the equation, if we put θ as 180°, $\overline{AC'}$ results as the sum of the other two segments.

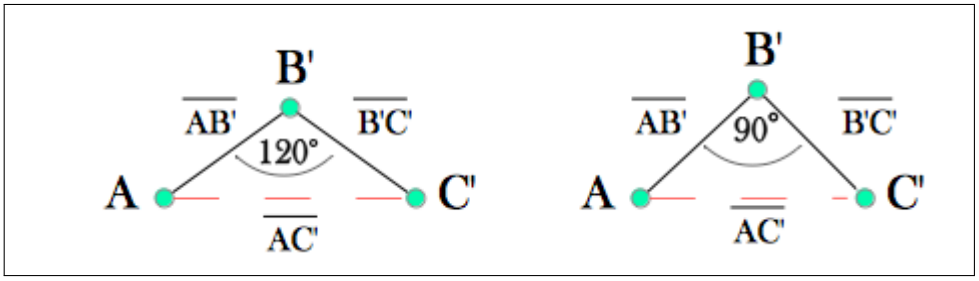

Figure D.1: Two examples of angle evaluation.

Those two example are put to clarify the concept that the most important data to evaluate is the angle made by the knee. As we can see from the results of the calculation proposed below, using the same length for the parts $\overline{AB}$ and $\overline{BC}$ we find different values of AC variating with the angle θ.

$$\begin{cases} \overline{AB} & = 55,2cm \\ \overline{BC} & = 44,9cm \rightarrow \overline{AC'} = 85,91cm \\ \theta & = 120° \end{cases}$$
$$\begin{cases} \overline{AB} & = 55,2cm \\ \overline{BC} & = 44,9cm \rightarrow \overline{AC'} = 70,44cm \\ \theta & = 90° \end{cases} \tag{D.1}$$

D.1 Preparation of the Device

In order to be precise in the preparation of the device that is going to be helpful for the bending of the knee of the patient, we have designed it with the Finite Element software Abaqus version 6.12. The leg easel is made of 2 different parts that are than placed together to produce a bending of 90° of the device. Here below are reported the exact measurement of the tool, that has been made in nylon.

- Horizontal length = 250 mm
- Vertical length = 300 mm
- Interval of Bending = 15° - 135°
- Radius of the hole in the middle = 5 mm
- Thickness = 15 mm

The idea with this two part is to build a sort of easel to keep the leg of the patient bent all over the imaging. To do that we have to practice an hole into the two parts and put something, like for example a thin rope, that connects them to keep in position during the loading of the leg on the device. Below i report this idea. The device has been created in nylon, as already said, in the Department of Mechanics, University of Pavia.

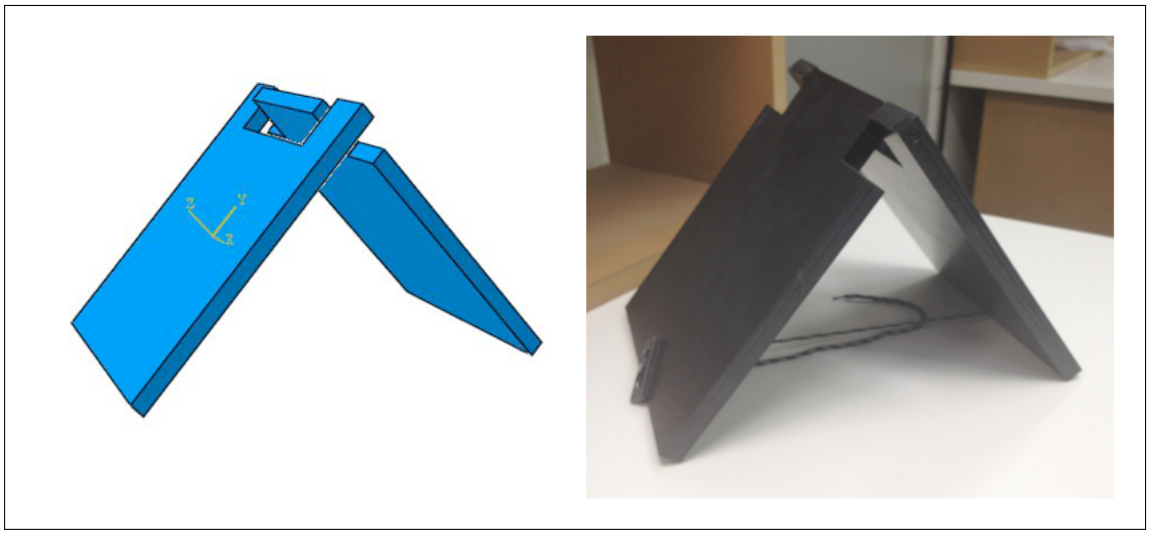

Figure D.2: On the left the primer FE model of the device used for knee bending; on the right its realization.

Appendix E

Table of Abbreviations and Softwares

In the table are reported in alphabetical order all the abbreviation used in the work; below them we report the software used in the thesis:

Abbreviation	**Significate**
3D	Three Dimensional
CAE	Computer Aided Engineering
CSV	Comma Separated Values
CT	Computed Tomography
DICOM	Digital Imaging and COmmunications in Medicine
DOF	Degree Of Freedom
E	Young modulus
FEA	Finite Element Analysis
GINPUT	Graphic INPUT from mouse or cursor
ICP	Iterative Closest Point
INP	INPut format
JPG	Joint Photographic experts Group
MRI	Magnetic Resonance Imaging
NITINOL	NIckel TItanium Naval Ordonance Laboratory
ν	Poisson ratio
STL	Surface Tessellation Language
VTK	Visualization ToolKit

Abbreviation	**Complete Name**
ABQ	Abaqus Simulia 6.12
ITK	ITK-Snap
LaTeX	LaTeX2ϵ
MatLaB	Matrix Laboratory
Paraview	Parallel Visualization application
VMTK	Vascular Modelling Toolkit

Bibliography

Alberto, D. (2005). Regressione polinomiale.

Antiga, L. (2014). The vascular modeling toolkit. OrobiX SRL.

Bowden, M. E. (2013). The cyborg transformed. *Chemical Heritage Foundation 22*.

Browse N. L., Y. A. E. (1979). The effect of bending on canine and human arterial walls and on the effect of bending on canine and human arterial walls and on the effect of bending on canine and human walls and on blood flow. *CardioVascular and Interventional Radiology 45*, 41–47.

Campanile, G. (2012). Studio della cinematica dell'arteria poplitea da immagini tac. Technical report.

Cheng, C. P., N. M. Wilson, R. L. Hallett, R. J. Herfkens, and C. A. Taylor (2006). In vivo {MR} angiographic quantification of axial and twisting deformations of the superficial femoral artery resulting from maximum hip and knee flexion. *Journal of Vascular and Interventional Radiology 17*(6), 979 – 987.

Cheng, D., J. Martin, H. Shennib, J. Dunning, C. Muneretto, and S. Schueler (2010). Endovascular aortic repair versus open surgical repair for descending thoracic aortic disease a systematic review and meta-analysis of comparative studies. *J Am Coll Cardiol 55*, 986–1001.

Choi, G., C. Cheng, N. Wilson, and C. Taylor (2009). Methods for quantifying three-dimensional deformation of arteries due to pulsatile and nonpulsatile forces: Implications for the design of stents and stent grafts. *Annals of Biomedical Engineering 37*(1), 14–33.

Design, M. (2013). http://medicaldesign.com/materials/precision-process-advances-nitinol-applications.

Diggery, R. G. T. D. (2012). *Catheters: Types, applications and potential complications (medical devices and equipment)*. Nova Biomedical.

Ganguly, A., J. Simons, A. Schneider, B. Keck, N. R. Bennett, and R. Fahrig (2011). In-vitro imaging of femoral artery nitinol stents for deformation analysis. *Journal of Vascular and Interventional Radiology 22*(2), 236 – 243.

Ghriallais, R. and M. Bruzzi (2013). Effects of knee flexion on the femoropopliteal artery: A computational study. *Medical Engineering & Physics 35*(11), 1620 – 1628.

Goerig, M. (2008). Werner forssmann: "the typical man before his time!" – self-experiment shows feasibility of cardiac catheterization. Agarwal Kamayni.

Gökgöl, C. and N. Diehm (2013, December). Quantification of popliteal artery deformation during quantification of popliteal artery deformation during leg flexion in subjects with peripheral artery disease: A pilot study. *Journal of Endovascular Therapy 20*(6), 828–835.

Gore, W. L. (2014). Gore® viabahn® endoprosthesis. http://www.goremedical.com/viabahn/.

Gray, H. (2009). *Gray's Anatomy*. Churchill Livingstone.

Jonker, F., F. Schlosser, F. Moll, and B. Muhs (2008). Dynamic forces in the sfa and popliteal artery during knee flexion. *Endovascular Today*, 53–58.

Mueller, R. S. T. (1995). The history of interventional cardiology. *Am Heart J*.

Muller-Hulsbeck, S., P. Schafer, N. Charalambous, H. Yagi, M. Heller, and T. Jahnke (2010). Comparison of second-generation stents for application in the superficial femoral artery: An in vitro evaluation focusing on stent design. *Journal of Endovascular Therapy 17*(6), 767–776.

Netter, F. H. (2014). *Atlas of Human Anatomy*. Saunder Elsevier.

Nikanorov, A. and M. Schillinger (2013, 9). Assessment of self-expanding nitinol stent deformation after assessment of self-expanding nitinol stent deformation after chronic implantation into the femoropopliteal arteries. *Eurointervention*, 8.

Nikanorov A., S. B. (2009). Fracture of self-expanding nitinol stents stressed fracture of self-expanding nitinol stents stressed in vitro under simulated intravascular conditions.

Piccinelli, M., A. Veneziani, D. Steinman, A. Remuzzi, and L. Antiga (2009). A framework for geometric analysis of vascular structures: Application to cerebral aneurysms. *IEEE transactions on medical imaging 28*(8), 1141–1155.

Scheinert, D., S. Scheinert, J. Sax, C. Piorkowski, S. Brunlich, M. Ulrich, G. Biamino, and A. Schmidt (2005). Prevalence and clinical impact of stent fractures after femoropopliteal stenting. *Journal of the American College of Cardiology 45*(2), 312 – 315.

Scheinert, D. Werner, M. (2013). Treatment of complex atherosclerotic popliteal artery disease with a new self-expanding interwoven nitinol stent. *Cardiovascular Interventions 6*(1).

Shulte, K. and I. Kralj (2012, December). One-year outcomes after implantation of the misago self-expanding nitinol stent in the superficial femoral and popliteal arteries of 744 patients. *Journal of Endovascular Therapy 19*(6), 774–784.

Smouse, H., A. Nikanorov, and D. LaFlash (2005). Biomechanical Forces in the Femoropopliteal Arterial Segment What happens during extremity movement and what is the effect on stenting? *Endovascular Today*, 60–66.

Tarini, F. (2010). Appunti di ecografia/ecocolor-doppler.

Taubin, G. (1995, 8). Curve and surface smoothing without shrinkage. *IEEE Transactions on Medical Imaging* (8).

Underwood, J. C. S. (2009). *General and Systematic Pathology*. Churchill Livingstone.

Wensing, P., F. Scholten, P. Buijs, M. Hartkamp, W. Mali, and B. Hillen (1995). Arterial tortuosity in the femoropopliteal region during knee flexion: a magnetic resonance angiographic study. *Journal of Anatomy 187*(1), 133–139.

Wikipedia, T. F. E. (2014). Gore-tex. http://en.wikipedia.org/wiki/gore-tex.

Young, M., M. Streicher, R. Beck, A. van den Bogert, A. Tajaddini, and B. Davis (2012). Simulation of lower limb axial arterial length change during locomotion. *Journal of Biomechanics 45*(8), 1485–1490.